

AD-A082 327

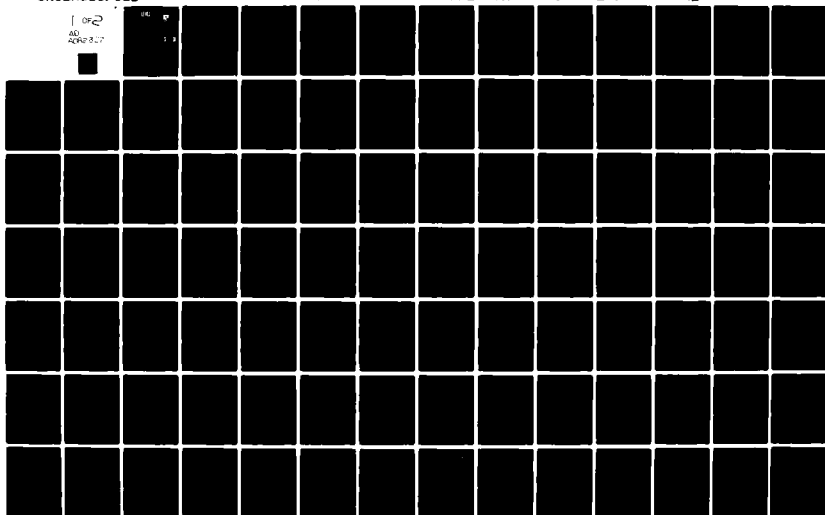
TEXAS A AND M UNIV COLLEGE STATION DEPT OF ELECTRICAL--ETC F/G 17/4  
LOW COST ANTI-JAM DIGITAL DATA-LINKS TECHNIQUES INVESTIGATIONS.--ETC(U)  
MAY 79 J H PAINTER, C J YOON F33615-75-C-1011

UNCLASSIFIED

AFAL -TR-77-104-VOL-2

NL

1 OF 2  
AD  
APR 8 1979



AD A 082327

**LEVEL** *III*

*1048181*

*2* *SE*



AFAL-TR-77-104  
VOLUME II

**LOW COST ANTI-JAM DIGITAL DATA-LINKS  
TECHNIQUES INVESTIGATIONS**

Telecommunication and Control Systems Laboratory  
Department of Electrical Engineering  
Texas A&M University  
College Station, Texas 77843

**DTIC**  
**ELECTE**  
**S D**  
**MAR 26 1980**  
**E**

Interim Report for Phase II  
Contract F 33615-75-C-1011  
For the period 1 October 1976 through 28 February 1978

Approved for public release; distribution unlimited.

MAY 1979

AVIONICS LABORATORY  
AIR FORCE WRIGHT AERONAUTICAL LABORATORIES  
AIR FORCE SYSTEMS COMMAND  
WRIGHT-PATTERSON AFB, OH 45433

NDC FILE COPY

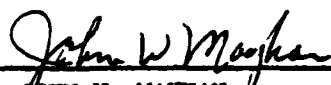
80 3 24 163

# NOTICE

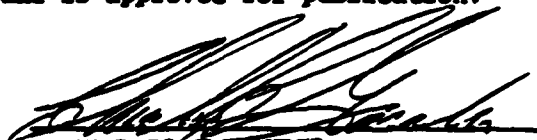
When Government drawings, specifications, or other data are used for any purpose other than in connection with a definitely related Government procurement operation, the United States Government thereby incurs no responsibility nor any obligation whatsoever; and the fact that the government may have formulated, furnished, or in any way supplied the said drawings, specifications, or other data, is not to be regarded by implication or otherwise as in any manner licensing the holder or any other person or corporation, or conveying any rights or permission to manufacture, use, or sell any patented invention that may in any way be related thereto.

This report has been reviewed by the Information Office (OI) and is releasable to the National Technical Information Service (NTIS). At NTIS, it will be available to the general public, including foreign nations.

This technical report has been reviewed and is approved for publication.

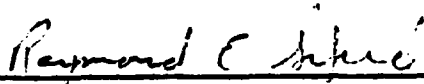


JOHN W. MAYHAN  
Project Engineer



CHARLES C. GAUDER  
Chief, Avionic Communications Branch  
Avionics Laboratory

FOR THE COMMANDER



RAYMOND E. SIFERD, COL, USAF  
Chief, System Avionics Division  
Avionics Laboratory

"If your address has changed, if you wish to be removed from our mailing list, or if the addressee is no longer employed by your organization please notify AFWAL/AAAD, W-PAFB, OH 45433 to help us maintain a current mailing list".

Copies of this report should not be returned unless return is required by security considerations, contractual obligations, or notice on a specific document.

19 REPORT DOCUMENTATION PAGE		READ INSTRUCTIONS BEFORE COMPLETING FORM	
18 1. REPORT NUMBER AFAL TR-77-184-Vol II-2	2 GOVT ACCESSION NO.	3 RECIPIENT'S CATALOG NUMBER	
6 4. TITLE (and Subtitle) LOW COST ANTI-JAM DIGITAL DATA-LINKS TECHNIQUES INVESTIGATIONS. Volume II.		5. TYPE OF REPORT & PERIOD COVERED Technical Interim rept. 1 Oct 76-28 Feb 78 ON Phase 2,	
10 7. AUTHOR(S) John H. Painter C. June Noon	15 8. CONTRACT OR GRANT NUMBER(s) F33615-75-C-1011		
9. PERFORMING ORGANIZATION NAME AND ADDRESS Texas A&M University Department of Electrical Engineering College Station, Texas 77843	16 10. PROGRAM ELEMENT, PROJECT, TASK AREA & WORK UNIT NUMBERS 2305 R3-01	17	
11. CONTROLLING OFFICE NAME AND ADDRESS Avionics Laboratory (AFWAL/AAAD) Air Force Wright Aeronautical Laboratories Wright-Patterson AFB, OH 45433	11 12. REPORT DATE May 1979	12	
14. MONITORING AGENCY NAME & ADDRESS (if different from Controlling Office)	13. NUMBER OF PAGES 157	14	
	15. SECURITY CLASS. (of this report) Unclassified		
	15a. DECLASSIFICATION/DOWNGRADING SCHEDULE		
16. DISTRIBUTION STATEMENT (of this Report)  Approved for public release; distribution unlimited.			
17. DISTRIBUTION STATEMENT (of the abstract entered in Block 20, if different from Report)			
18. SUPPLEMENTARY NOTES			
19. KEY WORDS (Continue on reverse side if necessary and identify by block number) Signal Processing Recursive Maximum Likelihood Demodulation Interference Cancellation Optimum Demodulation			
20. ABSTRACT (Continue on reverse side if necessary and identify by block number) This is a report on the second phase of an investigation into new techniques for communicating digital data between two terminals in an environment subject to multiplicative and additive colored noise and additive white noise. The recursive sampled-data detection technique, previously named Integrated Detection, Estimation, and Identification (IDEI), is extensively analyzed. The IDEI algorithms are shown to be robust, using both closed-form numerical, and Monte Carlo, analyses. Extensive results are given in graphical and tabular form.			

110214

Lrue

## ADDENDUM

### LOW COST ANTI-JAM DIGITAL DATA-LINKS TECHNIQUES INVESTIGATIONS

AFAL-TR-77-104, VOLUME II

MAY 1979

This addendum contains results which were completed too late for inclusion in the main part of the Interim Report. These results should properly have been included in Section IV., 1. However, the nature of the results is such that none of the findings or conclusions of the report are subject to change.

The Monte Carlo simulation routine, described in [1], was modified to include DPSK as a signal option, along with PSK and FSK. A random sequence of binary symbols was generated as usual. However, these symbols were then differentially encoded as per Table 1. At the receiver, several detectors were implemented. These included the standard detector for PSK and the IDEI detector for PSK. Also, the standard detector for DPSK was implemented, based on equations (78) - (83). Finally, an IDEI DPSK detector was implemented, using the IDEI-PSK detector and differential decoding.

Figure 49 shows the "calibration curve" for the various detectors. This graph serves the same purpose as Figure 7 and shows the Monte Carlo performances of the standard PSK detector, IDEI detector with differential decoding and standard DPSK detector, respectively, for white noise only. It is seen that the results appear the same as those in [10] and [13].

Figure 50 shows the results for multiplicative noise equal in strength to the desired signal, with a low-pass equivalent noise bandwidth of 275 Hz. This is the same "diffuse Doppler-spread multipath" disturbance as was used in Figure 9. The error rates for IDEI and standard detectors for PSK in Figure 50 fall upon those in Figure 9. The standard DPSK error rate is a little better than that for PSK, however the DPSK error rate is still saturated and unusable. The error rate for the IDEI detector using differential decoding is slightly worse than that for PSK, but this is to be expected.

The explanation for the poor performance of standard DPSK in this multiplicative noise environment is that the disturbance causes the received signal phase to violate the "slow-phase" restriction inherent in the derivation of the standard DPSK detection algorithm. Indeed, the phase-jitter process has a bandwidth of at least 275 Hz. which is not slow compared to the symbol rate of 2,500 BPS.

The performance of the IDEI detector is good, not because of the differential decoding, but because the equivalent phase disturbance on the received signal is being tracked out by the IDEI detector.

It should be recalled that the IDEI detector is being furnished with an unperturbed phase reference locked to that of the transmitted signal. However, it has been shown in a previous investigation [3] that the IDEI detector also tracks out phase reference perturbations due to the multiplicative noise effects on the carrier phase-locked loop, without an increase in error-rate. Thus the present IDEI results are valid for multiplicative noise with jittery phase reference.

Based on the above, two conclusions are clear. DPSK with a standard detector is unusable in diffuse aeronautical multipath due to violation of the "slow-phase" restriction on the standard DPSK detector. DPSK is unnecessary in diffuse aeronautical multipath if an IDEI detector is used, since PSK provides better performance.

Accession For	
NTIS GRA&I	<input checked="checked" type="checkbox"/>
DDC TAB	<input type="checkbox"/>
Unannounced	<input type="checkbox"/>
Justification	
By	
Distribution/	
Availability Codes	
Dist	Avail and/or special
A	

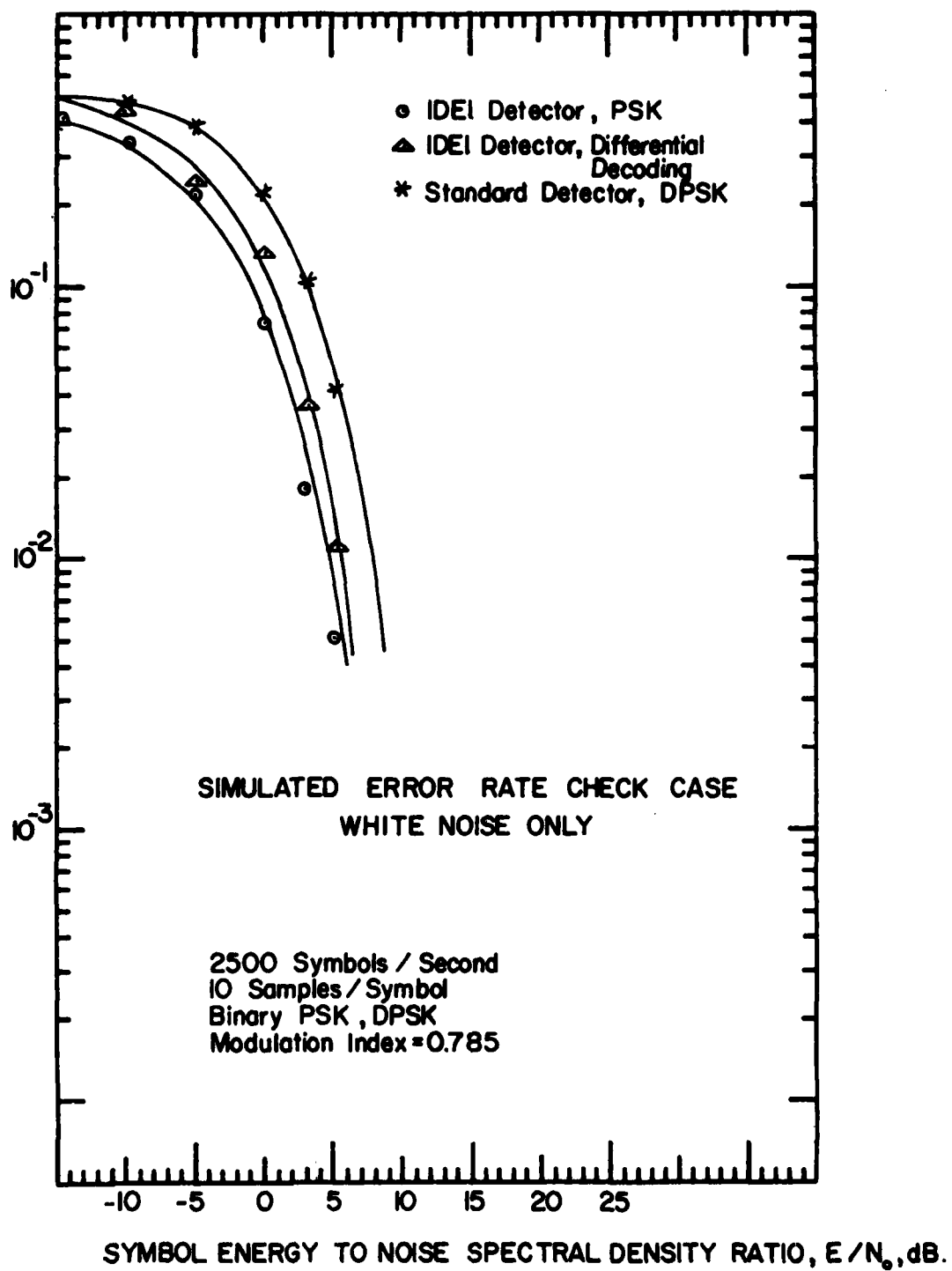


Figure 49. Simulated Error Rate Check Case for PSK, DPSK

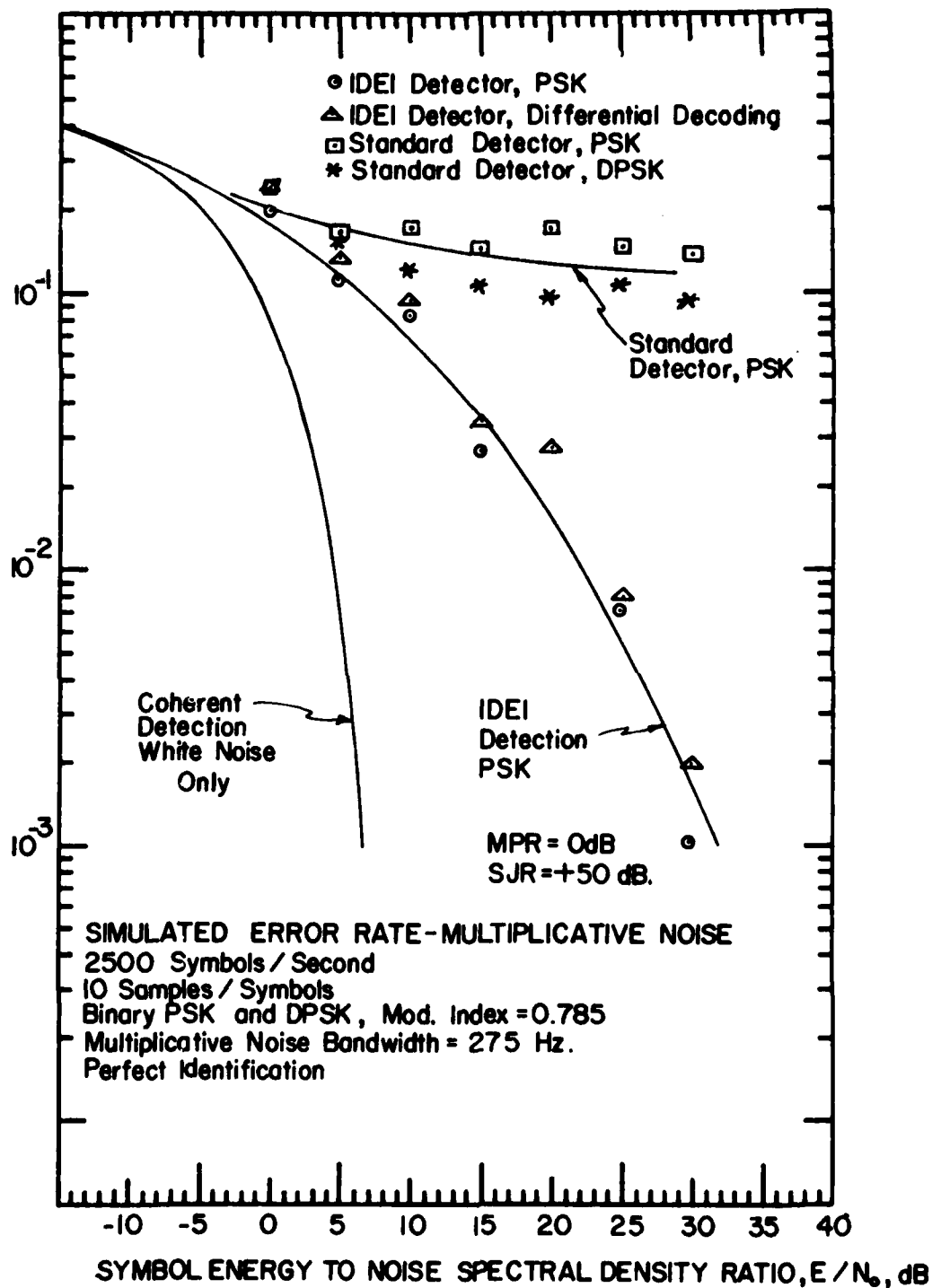


Figure 50. Simulated Error Rate for PSK and DPSK in Multiplicative Noise



## PREFACE

From 1971 through 1973, a new sampled-data processing technique for anti-multipath reception of aeronautical data-link signals was developed, and subsequently patented by the Principal Investigator, at NASA Langley Research Center. In 1974 a contract was issued by the Air Force Avionics Laboratory to determine if the same technique which provided processing gain against diffuse Doppler-spread multipath perturbations could be modified for use in anti-jam processing.

Anti-jam processing algorithms were produced under the 1974 contract, as well as a Monte Carlo simulation package for evaluating the performance of the algorithms. The contract was extended in 1976 for the purpose of making an exhaustive performance evaluation of the new processing algorithms. The present report gives the results of the performance evaluation conducted during the period from October 1976 through February 1978.

The results of the performance evaluation have been favorable toward continued development of the A-J processing technique. Further investigations have been identified and the contract has been extended for a further period. The present results have shown the A-J processing gain which is available through the new technique. Future efforts will be devoted to means for realizing this gain.

## LIST OF RESEARCH PERSONNEL

### NAME

Dr. John H. Painter	Principal Investigator
Mr. C. June Yoon	Research Assistant for i) Identification ii) Numerical Evaluation
Mr. Joel N. Holyoak	Research Associate for GFE Computer Facility
Ms. Lanette Dockall	Secretarial Assistant for Report Preparation
Mr. Paul Painter	Graphics

## TABLE OF CONTENTS

SECTION	PAGE
I. INTRODUCTION	1
II. ERROR RATE ANALYSES FOR INTEGRATED DETECTION, ESTIMATION AND IDENTIFICATION	4
1. Closed-Form Error Rate Under Mis-Identification	4
2. Spectral Analysis of the IDEI Detector with Perfect Identification	11
3. IDEI Detection of Differential Phase-Shift Keying	18
4. Closed-Form Error Rates for Standard Detectors	20
a. Coherent Detection	20
b. Non-coherent Detection	25
5. The Uniformly Most Powerful Property	29
III. MAXIMUM LIKELIHOOD IDENTIFICATION OF IN-PHASE/QUADRATURE VECTOR PROCESSES	35
1. The I-Q Canonical Model	35
2. Derivation of the Maximum Likelihood Algorithm	41
3. Estimation Performance of the M-L Identification Algorithms	50
IV. RESULTS	57
1. Simulation Versus Closed-Form Error-Rate Results for PSK and FSK	57
2. IDEI Closed-Form Performance for PSK in Colored Interference with Perfect Identification	71

## TABLE OF CONTENTS (Continued)

SECTION	PAGE
3. Error-Rate Sensitivity of IDEI Detector to Identification Error	91
4. Error-Rate Performance of the M-L Identification Algorithms	108
V. RECEIVER DESIGN AND PRACTICALITY EVALUATION	114
1. Basic Receiver System Design	114
2. Implementation of Identification	116
3. Hardware Practicality	117
VI. CONCLUSION	118
APPENDIX A. Derivation of the Pseudo-Innovations Autocovariance Function	120
APPENDIX B. Structure of the Pseudo-Innovations Autocovariance Function for a General In-Phase/Quadrature Process	128
REFERENCES	142

# LIST OF ILLUSTRATIONS

<u>Figure.</u>		<u>Page</u>
1	Data Generating Model.....	5
2	IDEI Detector.....	5
3	Spectral Relations.....	37
4	Partially Decoupled System.....	42
5	Identification Convergence for Transition Matrix.....	52
6	Identification Convergence for Gain and Innovations Variance.....	53
7	Simulated Error Rate Check Case.....	58
8	Minimization of Error Rate Versus Modulation Index....	59
9	Simulated PSK Error Rate - Multiplicative Noise.....	60
10	Simulated FSK Error Rate - Multiplicative Noise.....	61
11	Simulated PSK Error Rate - Colored Additive Interference.....	62
12	Simulated FSK Error Rate - Colored Additive Interference.....	63
13	Simulated and Closed-Form PSK Error Rate - Narrow-band Interference.....	65
14	Simulated and Closed-Form FSK Error Rate - Narrow-band Interference.....	66
15	IDEI and Standard Detector Error Rates for FSK in Colored Interference.....	67
16	Spectra of PSK and Full-band Colored Interference of the First Kind.....	68
17	Spectra of FSK and Full-band Colored Interference of the First Kind.....	69
18	Spectra of PSK and Full-band Colored Interference of the Second Kind.....	70
19	PSK and FSK Error Rates for the IDEI Detector in Full-band Colored Interference of the First Kind.....	72
20	IDEI and Standard Error Rates Versus Normalized Interference Bandwidth, With $E/N_0$ as Parameter.....	73
21	Spread-Spectrum Equivalence of IDEI Detection for Narrow-band Interference.....	75
22	Worst Case IDEI Performance and Optimum Interference Bandwidth.....	76

# LIST OF ILLUSTRATIONS (Continued)

Figure		Page
23	IDEI Performance for Colored Interference of the Second Kind - Aliased Results.....	78
24	Confirmation of Aliasing for Colored Interference Of the Second Kind.....	79
25	Comparison of Results for Both Kinds of Additive Colored Interference.....	80
26	IDEI and Standard Detector Performance Versus Ratio of Signal to Colored Interference Power.....	81
27	IDEI and Standard Detector Performance Versus SJR for $E/N_0 = 17$ dB.....	83
28	IDEI and Standard Detector Performance Versus SJR for $E/N_0 = 27$ dB.....	84
29	IDEI and Standard Detector Performance Versus SJR for $E/N_0 = 37$ dB.....	85
30	IDEI and Standard Detector Performance Versus SJR for $E/N_0 = 47$ dB.....	86
31	IDEI and Standard Detector Performance Versus SJR with $JT/N_0 = 70$ dB.....	87
32	IDEI and Standard Detector Performance for Interference of the Second Kind with $E/N_0 = 47$ dB.....	89
33	IDEI and Standard Detector Performance for Interference of the Second Kind with $JT/N_0 = 70$ dB.....	90
34	IDEI Error Rate Versus $E/N_0$ for RFI Strength Underestimated.....	93
35	IDEI Error Rate Versus $E/N_0$ for RFI Strength Overestimated.....	94
36	Variation of Detection Statistics Versus RFI Strength Identification Error, $E/N_0 = 25$ dB.....	95
37	Detection Loss Versus RFI Strength Identification Error, $E/N_0 = 25$ dB.....	96
38	IDEI Error Rate Versus SJR for RFI Strength Underestimated, $JT/N_0 = 60$ dB.....	97
39	IDEI Error Rate Versus SJR for RFI Strength Overestimated, $JT/N_0 = 60$ dB.....	98
40	Detection Loss Versus RFI Strength Identification Error, $JT/N_0 = 60$ dB.....	99

# LIST OF ILLUSTRATIONS (Continued)

<u>Figure</u>		<u>Page</u>
41	IDEI Error Rate Versus $E/N_0$ for RFI Bandwidth Underestimated.....	100
42	IDEI Error Rate Versus $E/N_0$ for RFI Bandwidth Overestimated.....	101
43	Variation of Detection Statistics Versus RFI Bandwidth Identification Error, $E/N_0 = 25$ dB.....	103
44	Detection Loss Versus RFI Bandwidth Identification Error, $E/N_0 = 25$ dB.....	104
45	IDEI Error Rate Versus SJR for RFI Bandwidth Underestimated.....	105
46	IDEI Error Rate Versus SJR for RFI Bandwidth Overestimated.....	106
47	Detection Loss Versus RFI Bandwidth Identification Error, $\frac{JT}{N_0} = 60$ dB.....	107
48	Basic Receiver Block Diagram.....	115
49	Simulated Error Rate Check Case for PSK, DPSK.....	v
50	Simulated Error Rate for PSK and DPSK in Multiplicative Noise.....	vi

# LIST OF TABLES

<u>Table</u>		<u>Page</u>
1	Truth-Table.....	19
2	Convergence of $\phi$ .....	55
3	Convergence of G and $V_{vv}$ .....	56
4	P(e) Invariance.....	88
5	Error Rate Performance of SJR = 0.....	109
6	Error-Rate Performance for SJR = -20 dB.....	113

## SECTION I

### INTRODUCTION

This is a report on the second phase of an investigation into new techniques for communicating digital data between two terminals in an environment subject to multiplicative and additive colored noise and additive white noise. The multiplicative noise is a model for non-frequency-selective fading due to Doppler-spreading such as caused by diffuse multipath reflections. The additive colored noise is a model for radio-frequency interference or jamming.

The communication technique being investigated is a receiver-based processing technique for standard signal modulations such as Phase-Shift-Keying, Frequency-Shift-Keying and Differential-Phase-Shift-Keying. The technique does not require the use of Spread-Spectrum modulations. The particular processing used is called Integrated Detection, Estimation, and Identification (IDEI). It is nearly optimum, under the minimum probability of error criterion, for M-ary signalling in additive and multiplicative Gaussian noise.

The results of the first phase of the investigation were documented in [1]. In that phase the optimum IDEI algorithms were derived and an elaborate Monte Carlo simulation package was written for testing the algorithms for PSK and FSK binary signals. The purposes of the second phase of effort were several. First, it was required to determine the best performance of the IDEI algorithms, operating with known bit timing and carrier phase references, and for perfect identification of the required statistics of the colored interfering processes. Second, it was required to determine the sensitivity of the detection algorithms to accuracy of the identification of the interference. Third, it was required to derive and validate optimum identification algorithms. Finally, it was required to form an initial estimate of receiver practicality.

The four requirements on the fourteen month investigation, described above, have been fulfilled and the results are documented below. During the course of the investigation a closed-form numerical expression was derived for evaluating the best performance and the sensitivity of the IDEI detector. Use of the closed-form for numerical computations was much more efficient, time-wise, than was use of the Monte Carlo simulation. Thus, more voluminous results were produced than might have been anticipated on a simulation basis only.



This report contains five main sections, excluding the Introduction and Conclusion. In Section II are presented all the mathematical analyses pertaining to the probability of error, or error rate, of the IDEI detector. These include the derivation of the closed-form error rate expression under mis-identification, a spectral analysis of the IDEI detector with perfect identification, the IDEI detection algorithms for DPSK, closed-form error rate determination for standard detectors, and the derivation of the Uniformly Most Powerful property of the IDEI detector.

In Section III are presented the mathematical derivations and results for Maximum-Likelihood Identification of In-Phase/Quadrature Vector Processes. These include derivation of a minimum canonical form for the I-Q generator model, derivation of the M-L identification algorithms, and validation results for the estimation performance of the MLI algorithms.

In Section IV are presented all the numerical results obtained in the present investigation, either by Monte Carlo methods or by closed-form numerical evaluation. These include a comparison of Monte Carlo versus closed-form error-rate results for PSK and FSK, IDEI error-rate with perfect identification, IDEI error-rate sensitivity to identification error, and error-rate performance of the MLI algorithms.

Section V contains the receiver design and practicality evaluation. Section VII contains the appendices.

The outcome of this second phase of the investigation may be summarized as follows. It will be shown below that the IDEI detection algorithms are reasonably robust (insensitive) to error in identification of the colored interference process statistics, provided the errors are made in a particular way. If the tracking filters are synthesized to match an identified disturbance process which is of different bandwidth and/or strength from the true process, then the algorithms' performance changes smoothly, proportional to the bandwidth or strength errors. If, however, the filter parameters are directly identified from the received signals using an optimum stochastic (maximum-likelihood) technique, rather than synthesized in a deterministic manner, the detector performance is highly sensitive to identification error. Thus it appears that the practicality of the IDEI algorithm hinges on the exact method by which identification is implemented. Further work is suggested in this area.

It is also shown below that the best performance (perfect identification) of the IDEI detector is orders of magnitude better than that of standard matched filter detectors in an environment of heavy additive colored noise. The IDEI detector provides gain against narrow-band interference equivalent to spectrum-spreading factors of the order of  $10^3$  to  $10^4$ . It is also shown that the amount of gain is a function not only of the interference to signal ratio, but also of the degree of similarity between signal spectrum and interference spectrum.

Suggested steps toward reducing the present theoretical results to practice are outlined in Section VI.

## SECTION II

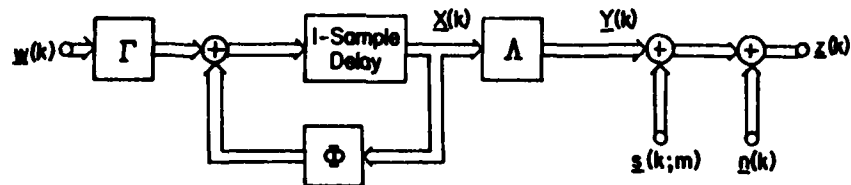
### ERROR RATE ANALYSES FOR INTEGRATED DETECTION, ESTIMATION, AND IDENTIFICATION

#### 1. CLOSED-FORM ERROR RATE UNDER MIS-IDENTIFICATION

The emphasis of the work being presently reported was on the performance of the new disturbance-tracking IDEI coherent detection algorithms for binary signals subject to additive colored plus white noise. The colored noise represents a jamming signal while the white noise represents receiver-generated interference. Thus, the analytical results presented in this section are based on a simplification of the more general multipath and jamming model treated in [1]. It is assumed that the received data is in In-phase/Quadrature (I-Q) form, resulting from a standard coherent product demodulation of the band-pass radio-frequency signal. A vector-Markov data generating model is hypothesized, as in Figure 1. The data model has been obviously simplified, such as by deleting any vector-multiplicative noise as might result from impure phase references in the I-Q demodulator. Such effects have been treated elsewhere [1, 2, 3]. The simple model will suffice for the present investigation.

In Figure 1, the I-Q data,  $\underline{z}(k)$ , is in sampled-data 2-vector form, where  $k$  is sample number.  $\underline{\Delta}(k;m)$  is a 2-vector waveform representing the low-pass I-Q components of the transmitted signal.  $m$  is the transmitted symbol, taken here as a member of the binary alphabet,  $\{0, 1\}$ . Given the value of  $m$ , the waveform of  $\underline{\Delta}(k;m)$  is known for all  $k = 1, 2, \dots$ . It is assumed that the signals,  $\underline{\Delta}(k;m = 0)$  and  $\underline{\Delta}(k;m = 1)$ , are A Priori equally likely and have equal energy on the symbol period. Likewise,  $\underline{n}(k)$  is the I-Q 2-vector of additive white Gaussian noise.  $\underline{n}(k)$  is taken as zero-mean with known diagonal variance matrix,  $V_{nn}$ .

In Figure 1, the additive colored noise is generated as  $\underline{y}(k)$ . The 2-vector,  $\underline{y}(k)$ , is obtained from a 2N-vector,  $\underline{x}(k)$ , through the output 2 by 2N matrix,  $\Lambda$ . The transition matrix,  $\Phi$ , is 2N x 2N. The filter which produces  $\underline{y}(k)$  is excited by a white, zero-mean, unit-variance Gaussian input 2-vector,  $\underline{w}(k)$ . The input matrix,  $\Gamma$ , is 2N x 2. By choosing the constant filter structure,  $\{\Gamma, \Phi, \Lambda, N\}$ , properly, the filter will, in the steady-state, generate a stationary, zero-mean  $\underline{y}(k)$ , having a prescribed covariance matrix,  $V_{yy}(j)$  for  $j = 0, 1, 2, \dots$ . Using a suitable sampling



Data Generating Model

Figure 1. Data Generating Model

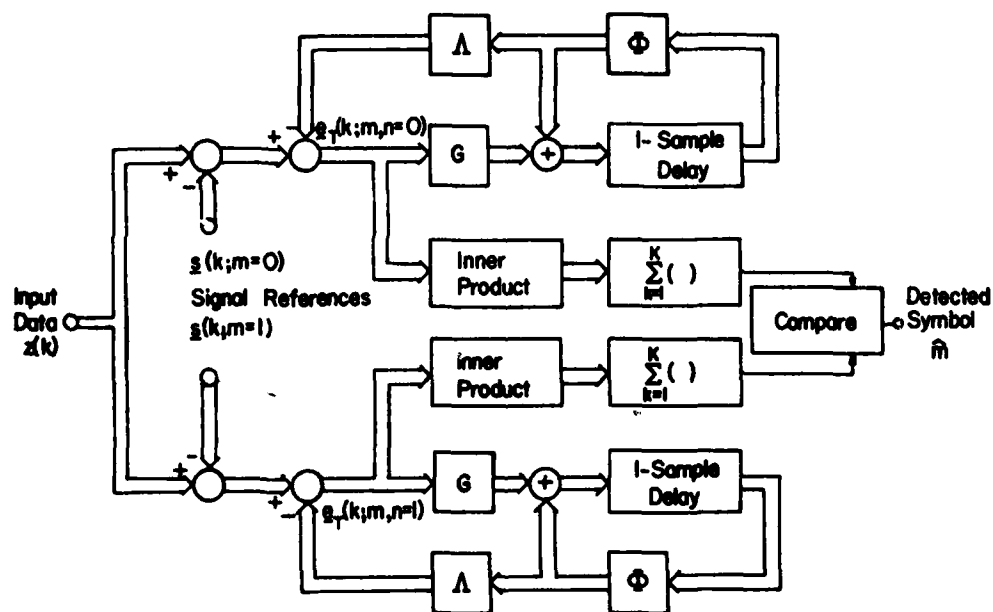


Figure 2. IDEI Detector

model, the covariance matrix,  $V_{yy}(j)$  may be related to the continuous-time power spectrum of the additive colored interference. The equations governing the data generator are:

$$\begin{aligned}\underline{x}(k+1) &= \Phi \underline{x}(k) + \Gamma \underline{w}(k); & \underline{x}(0) \text{ prescribed} \\ \underline{y}(k) &= \Lambda \underline{x}(k) \\ \underline{z}(k) &= \underline{a}(k;m) + \underline{y}(k) + \underline{n}(k); & E\{\underline{y}(k)\} = E\{\underline{n}(k)\} = 0 \\ & & m = 0, 1 \\ V_{yy}(j) &= \lim_{k \rightarrow \infty} E\{\underline{y}(k+j) \underline{y}^T(k)\}; & k = 1, 2, \dots \\ & & j = 0, 1, 2, \dots \\ V_{nn}(k-j) &= E\{\underline{n}(k) \underline{n}^T(j)\} = V_{nn} \cdot \delta_{jk}\end{aligned}$$

$\delta_{jk}$  is Kroneker delta

$$V_{nn} = \sigma_n^2 I_{2 \times 2} \quad (1)$$

With the data modeled as discussed above, the IDEI detector takes the form of Figure 2, which is a special case of the more general receiver for multiplicative and additive noise, treated in [1]. This version of the IDEI detector is the decision-directed approximation to the optimum detector under the Maximum A Posteriori Probability (or Maximum Likelihood, or Minimum Probability of Error) criterion. The detector operates as follows.

From each incoming data sample in the upper branch is subtracted the corresponding sample of the signal reference waveform for the symbol  $m = 0$ . In the lower branch, the reference waveform for  $m = 1$  is subtracted from the data. Following the signal subtraction is a filter which attempts to track the colored additive noise,  $\underline{y}(k)$ , in the presence of the white noise,  $\underline{n}(k)$ . The filter is linear and is in the canonical form of a Kalman filter with gain,  $G$ . Under the stationarity assumption the gain  $G$  is constant and the steady-state Kalman filter is just a particular form of the Wiener filter [4]. Note that the requirement for an exact signal reference

waveform implies identifying the level or strength of the desired signal component in the received data. This implication was commented upon in [1]. However, it turns out that the IDEI algorithms possess the Uniformly Most Powerful [5] property with respect to the strength of the desired signal component. This property is derived in a following section. The effect of this property upon identification is detailed below.

The feedback tracking error waveform in each filter is designated  $e_T(k;m;n)$ . The argument  $n$  denotes the assumed symbol (and filter). The argument  $m$  denotes the symbol actually present in the data.  $e_T(\ )$  is a 2-vector. The tracking error waveforms from each filter are processed in a quadratic form which essentially squares and averages the waveforms over the  $K$  samples per signal symbol. The sum-squared tracking errors for each filter are then compared at the end of each symbol period. The filter displaying the least sum-squared tracking error is assumed to have been using the "correct" signal reference and the symbol decision is made accordingly.

The tracking filters are operated with decision direction. At the end of a symbol period, after decision has been made, the state vector of the "wrong" filter is reset to the state of the "correct" filter. In the case of a correct previous decision, both filters start the subsequent symbol period "locked" to the colored additive interference,  $y(k)$ . In the case of an incorrect decision, both filters are incorrectly initialized for the following symbol period.

Monte Carlo simulations have been used to evaluate the performance of the IDEI detection algorithms. These results are given below. The algorithms were exercised with colored multiplicative noise or colored additive noise, individually, along with white additive noise. The simulated error rates were compared with those of standard detectors for both binary PSK and FSK modulations. It was found that for white noise only, the new detection algorithms gave exactly the same errors, symbol for symbol, as the standard algorithms. However, in the presence of colored additive or multiplicative noise the IDEI algorithms always yielded better performance than did the standard receiver.

Naturally, it is desirable to have closed-form expressions for the error rate performance, to back up and extend the simulation results. Such expressions are readily obtained, provided one more assumption is

made. The probability of error for a particular symbol is easily formulated under the assumption that the tracking filters were correctly initialized or, equivalently, that the previous decision was correct. This assumption becomes increasingly good as the error rate becomes smaller, provided the errors do not cluster. Error rate curves based on the assumption will be lower bounds for the practical IDEI error rate performance. A comparison with Monte Carlo results for clustered errors will show the usefulness of the lower bound.

Under the assumption of a correct prior decision, the general detection statistic of [1] may be written as

$$S = \sum_{k=1}^K \underline{e}_T^T(k;m;n=0) V_{II}^{-1} \underline{e}_T(k;m;n=0) - \underline{e}_T^T(k;m;n=1) \cdot V_{II}^{-1} \underline{e}_T(k;m;n=1) \quad (2)$$

where  $\underline{e}_T(k;m;n)$  is the filter's total transient tracking error waveform and  $V_{II}$  is the assumed Innovations variance. From Figure 2 it may be seen that the total transient tracking error may be partitioned into a response due to the zero-mean Gaussian noises (colored and white) and a response due to the desired signal and reference terms. Thus, define

$$\underline{e}_T(k;m;n) = \underline{\xi}(k) + \underline{e}_\Delta(k;m;n) \quad (3)$$

where  $\underline{\xi}(k)$  is the (pseudo-Innovations) response due to zero-mean stochastic input and  $\underline{e}_\Delta(k;m;n)$  is the filter's transient response to a driving function

$$\underline{\mu}(k) = \underline{\Delta}(k;m) - \hat{a}\underline{\Delta}(k;n) \quad (4)$$

In (4)  $\hat{a}$  is the identification estimate of the desired signal level, which is unity for perfect identification. Because of the Uniformly Most Powerful property of the IDEI algorithms,  $\hat{a}$  may just be set to unity. When identification is perfect, including the filter parameters, then  $\underline{\xi}(k)$  is identically  $\underline{v}(k)$ , the Innovations process, and  $\underline{\mu}(k)$  is identically zero

when  $m = n$ . Thus,

$$\begin{aligned} \underline{e}_\delta(k; m; n) &= \underline{0} & \forall k ; m = n \\ \underline{e}_\delta(k; m; n) &\neq \underline{0} & \forall k ; m \neq n \end{aligned}$$

$$\begin{aligned} \underline{\xi}(k) &= \underline{v}(k) \\ V_{II} &= V_{vv} \end{aligned} ; \quad \text{Perfect Identification} \quad (5)$$

Substituting (3) into (2) yields

$$\begin{aligned} S &= \sum_{k=1}^K \{ 2 \underline{\xi}^T(k) V_{II}^{-1} [\underline{e}_\delta(k; m; n = 0) - \underline{e}_\delta(k; m; n = 1) + \\ &\quad \underline{e}_\delta^T(k; m; n = 0) V_{II}^{-1} \underline{e}_\delta(k; m; n = 0) - \underline{e}_\delta^T(k; m; n = 1) \\ &\quad V_{II}^{-1} \underline{e}_\delta(k; m; n = 1)] \} \end{aligned} \quad (6)$$

The process,  $\underline{\xi}(k)$ , is zero-mean, Gaussian and, conditioned on  $m$  the  $\underline{e}_\delta(\cdot)$  are deterministic. Thus  $S$  is conditionally Gaussian and is described by the following means and variances.

$$\begin{aligned} E\{S|m=0\} &= \sum_{k=1}^K [\underline{e}_\delta^T(k; m=0; n=0) V_{II}^{-1} \underline{e}_\delta(k; m=0; n=0) + \\ &\quad - \underline{e}_\delta^T(k; m=0; n=1) V_{II}^{-1} \underline{e}_\delta(k; m=0; n=1)] \triangleq -\mu \\ E\{S|m=1\} &= \sum_{k=1}^K [\underline{e}_\delta^T(k; m=1; n=0) V_{II}^{-1} \underline{e}_\delta(k; m=1; n=0) + \\ &\quad - \underline{e}_\delta^T(k; m=1; n=1) V_{II}^{-1} \underline{e}_\delta(k; m=1; n=1)] \triangleq \mu \end{aligned} \quad (7)$$

In (7) the assumption has been employed that (equal energy) the sum-squared tracking errors are equal. The conditional variances are



$$\text{var}\{S|m=0\} = \text{var}\{S|m=1\} =$$

$$4 \sum_{j=1}^K \sum_{k=1}^K [\underline{e}_\delta(j;m=0;n=0) - \underline{e}_\delta(j;m=0;n=1)]^T V_{II}^{-1} \cdot$$

$$V_{\xi\xi}(j-k) V_{II}^{-1} [\underline{e}_\delta(k;m=0;n=0) - \underline{e}_\delta(k;m=0;n=1)] \triangleq \sigma^2 \quad (8)$$

where  $V_{\xi\xi}(j-k)$  is the auto-covariance function of the process,  $\underline{\xi}(k)$ , which is in general colored.

It is shown in Appendix A that the auto-covariance function of the pseudo-innovations,  $\underline{\xi}(k)$  is given by

$$\begin{aligned} V_{\xi\xi}(\ell) &= \Lambda [\Phi^*(I - G^*\Lambda)]^{\ell-1} \Phi^* [V_{xx}^{\sim\sim\sim T} - G^*(\Lambda V_{xx}^{\sim\sim\sim T} + V_{nn})] \\ &\quad + \Lambda \sum_{i=1}^{\ell} [\Phi^*(I - G^*\Lambda)]^{\ell-1-i} \cdot \Delta\Phi \cdot \Phi^{\ell-i} V_{xx}^{\sim\sim\sim T}; \quad 0 < \ell \\ &= \Lambda V_{xx}^{\sim\sim\sim T} + V_{nn}; \quad 0 = \ell \end{aligned} \quad (9)$$

where  $\Phi^*$  and  $G^*$  are the values of the identified (or assumed) transition matrix and Kalman gain respectively.  $\Phi^*$  and  $\Phi$  are related by

$$\Phi^* = \Phi - \Delta\Phi \quad (10)$$

The quantity  $V_{xx}^{\sim\sim\sim}$  is the actual predicted state estimation error variance matrix. The quantity  $V_{xx}^{\sim}$  is the cross-variance between the state and state prediction error. Both  $V_{xx}^{\sim\sim\sim}$  and  $V_{xx}^{\sim}$  are obtained as solutions to appropriate discrete-time Ricatti difference equations, which are derived in Appendix A. The method of solution used is to propagate the equations numerically until steady state is reached, according to a Cauchy test on succeeding stages. The quantity,  $V_{nn}$ , is the variance matrix for the white additive noise,  $\underline{n}(k)$ .

With  $\mu$  and  $\sigma$  defined by (7) and (8), respectively, the error rate or probability of error is given by

$$P(e) = \frac{1}{2} [1 - \operatorname{erf}(\frac{\mu}{\sqrt{2}\sigma})] \quad (11)$$

where "erf" denotes "error function". For the case where identification is perfect, (7) and (8) simplify and (11) becomes

$$P(e) = \frac{1}{2} [1 - \operatorname{erf}(\frac{\mu}{\sqrt{2}\sigma})] =$$

$$= \frac{1}{2} \left[ 1 - \operatorname{erf} \left( \frac{1}{\sqrt{2}} \sqrt{\frac{1}{2} \sum_{k=1}^K \mathbf{e}_\delta^T(k; m=1; n=0) V_{vv}^{-1} \mathbf{e}_\delta(k; m=1; n=0)} \right) \right] \quad (12)$$

where  $V_{vv}$  is the true Innovations variance.

## 2. SPECTRAL ANALYSIS OF THE IDEI DETECTOR WITH PERFECT IDENTIFICATION

It has been observed lately by Schwartz [6] ... "that the discrete-time formulation may provide insight into constructive techniques for realizing, or approximating, the rather general (and sometimes abstract) results that have appeared for the continuous-time versions." ... of receivers containing estimators. The observation certainly proved true for the IDEI receiver wherein the disturbance tracking feature was a direct result of the discrete-time sequential formulation of the detection statistic. However, the present formulation of the error rate probability on a discrete-time basis yields even more insight into the detection problem.

For instance, equation (12) shows that the effective noise in the detection problem is evidently the Innovations process, since its variance,  $V_{vv}$ , plays the part of  $\sigma^2$  in the error function argument. Thus the error rate is controlled, not by the total power of the additive colored interference, but rather by the power in the untracked portion of the colored interference, plus the white noise power. Secondly, the Innovations variance is minimized, and consequently the error rate is minimized when the filter is "matched" to the colored interference waveform in the Wiener sense.

Equation (12) also shows that the effective signal power is proportional to the sum of the squares of the deterministic tracking error waveform of the "matched" filter when driven by the difference of the two possible versions of the transmitted signal. There are two obvious ways to maximize this effective signal power and thus minimize the error rate. One is to maximize the distance between the two signal vectors,  $\underline{s}(k;m=0)$  and  $\underline{s}(k;m=1)$ . The maximum distance is obtained when the two possible transmitted signals are anti-correlated. Optimization may also be obtained by designing the signal waveform so as to maximize the tracking error at each sampling instant. Note that the deterministic transient error response of the "matched" filter will only approach zero identically when the filter bandwidth (and, hence, the bandwidth of the colored interference) is orders of magnitude greater than the transmitted signal bandwidth.

While the formulation of (12) lends itself to some qualitative observations about the behavior of the detector, it is desired to translate the parameter,  $\mu/\sqrt{2}\sigma$ , into a different form. In his treatment of the optimum continuous-time detection of known binary signals in colored noise, Blachman [7] was able to relate detector performance to the spectra of signals and noise. The present discrete-time problem may be examined similarly by assuming arbitrarily fast sampling and transforming to continuous-time.

A continuous-time version of the sampled-data detector may be set up by assuming that the symbol interval is the closed interval,  $[-T/2, T/2]$ . The continuous decision statistic is then

$$S = \int_{-T/2}^{T/2} [\underline{e}_T^T(t;m;n=0) \underline{e}_T(t;m;n=0) - \underline{e}_T^T(t;m;n=1) \underline{e}_T(t;m;n=1)] dt \quad (13)$$

The mean and variance of the statistic are then

$$\begin{aligned} \mu &= \int_{-T/2}^{T/2} \underline{e}_\delta^T(t;m=1;n=0) \underline{e}_\delta(t;m=1;n=0) dt \\ \sigma^2 &= 4 \int_{-T/2}^{T/2} \int_{-T/2}^{T/2} \underline{e}_\delta^T(t;m=0;n=1) V_{\xi\xi}(t-t') \underline{e}_\delta(t;m=0;n=1) dt dt' \end{aligned} \quad (14)$$

Now define

$$\begin{aligned} \pi(t) &= 1; & t \in [-T/2, T/2] \\ &= 0; & \text{otherwise} \end{aligned} \quad (15)$$

and define

$$\underline{x}(t) = \pi(t) \cdot \underline{e}_\Delta(t; m=0; n=1) \quad (16)$$

Then (14) may be written as

$$\begin{aligned} \mu &= \int_{-\infty}^{\infty} \underline{x}^T(t) \underline{x}(t) dt \\ \sigma^2 &= 4 \int_{-\infty}^{\infty} \int_{-\infty}^{\infty} \underline{x}^T(t) V_{\xi\xi}(t-t') \underline{x}(t') dt dt' \end{aligned} \quad (17)$$

By Parseval's Theorem, then,

$$\mu = \frac{1}{2\pi} \int_{-\infty}^{\infty} \underline{X}^T(\omega) \underline{X}^*(\omega) d\omega \quad (18)$$

where  $\underline{X}(\omega)$  is the Fourier Transform of  $\underline{x}(t)$ , and  $()^*$  denotes complex conjugate.

Next observe that

$$\int_{-\infty}^{\infty} V_{\xi\xi}(t-t') \underline{x}(t') dt' = V_{\xi\xi}(t) * \underline{x}(t) \triangleq \underline{q}(t) \quad (19)$$

where  $()*(t)$  denotes convolution. Thus

$$\begin{aligned} \sigma^2 &= 4 \int_{-\infty}^{\infty} \underline{x}^T(t) \underline{q}(t) dt \\ &= 4 \left[ \frac{1}{2\pi} \int_{-\infty}^{\infty} \underline{X}^T(\omega) \underline{Q}^*(\omega) d\omega \right] \\ &= 4 \left[ \frac{1}{2\pi} \int_{-\infty}^{\infty} \underline{X}^T(\omega) [S_{\xi\xi}(\omega) \underline{X}(\omega)]^* d\omega \right] \end{aligned} \quad (20)$$

where  $S_{\xi\xi}(\omega)$  is the Fourier Transform of the auto-covariance matrix function of the pseudo-innovations.

Now,  $\underline{X}(\omega)$  is

$$\underline{X}(\omega) = [T \operatorname{sinc}(\frac{\omega T}{2\pi})] * \underline{E}_\delta(\omega) \quad (21)$$

where  $\underline{E}_\delta(\omega)$  is the Fourier Transform of the transient error waveform,  $\underline{e}_\delta(t; m=1; n=0)$ , and  $\operatorname{sinc}(\ )$  is the function

$$\operatorname{sinc}(x) = \frac{\sin(\pi x)}{\pi x} \quad (22)$$

Thus, the argument of the probability of error function,  $P(e)$ , is

$$\frac{\mu}{\sqrt{2}\sigma} = \frac{1}{2\sqrt{2}} \cdot \frac{\frac{1}{2\pi} \int_{-\infty}^{\infty} [T \operatorname{sinc}(\frac{\omega T}{2\pi}) * \underline{E}_\delta(\omega)]^T [T \operatorname{sinc}(\frac{\omega T}{2\pi}) * \underline{E}_\delta(\omega)] * d\omega}{\sqrt{\frac{1}{2\pi} \int_{-\infty}^{\infty} [T \operatorname{sinc}(\frac{\omega T}{2\pi}) * \underline{E}_\delta(\omega)]^T S_{\xi\xi}^*(\omega) [T \operatorname{sinc}(\frac{\omega T}{2\pi}) * \underline{E}_\delta(\omega)] * d\omega}} \quad (23)$$

Now, assume perfect identification and also that the bandpass spectrum of the additive colored interference is even-symmetric with respect to the carrier frequency of the transmitted signal. Then,  $\underline{\xi}(t)$  is the true innovations and is white. Thus,  $S_{\xi\xi}(\omega)$  is diagonal and constant, with

$$S_{\xi\xi}(\omega) = \eta \begin{bmatrix} 1 & 0 \\ 0 & 1 \end{bmatrix} \quad (24)$$

where  $\eta$  is the white noise spectral density for each I and Q component of the white noise. Note that the bandpass white noise density is  $\eta/2$ .

Then (23) becomes

$$\frac{\mu}{\sqrt{2}\sigma} = \sqrt{\frac{1}{2\pi} \int_{-\infty}^{\infty} \frac{1}{8\eta} [T \operatorname{sinc}(\frac{\omega T}{2\pi}) * \underline{E}_\delta^T(\omega)] [T \operatorname{sinc}(\frac{\omega T}{2\pi}) * \underline{E}_\delta^*(\omega)] d\omega} \quad (25)$$

Since the additive colored interfering process spectrum is even-symmetric with respect to carrier frequency, the I and Q portions of the Wiener filter are not cross-coupled. Then

$$\underline{E}_\delta(\omega) = H_e(\omega) \begin{bmatrix} S_{\delta I}(\omega) \\ S_{\delta Q}(\omega) \end{bmatrix} = \begin{bmatrix} H_e(\omega) S_{\delta I}(\omega) \\ H_e(\omega) S_{\delta Q}(\omega) \end{bmatrix} \quad (26)$$

where  $H_e(\omega)$  is the Wiener filter transfer function from input to error point, for either the I or the Q filter.  $S_{\delta I}(\omega)$  and  $S_{\delta Q}(\omega)$  are the Fourier transform of the differences of the two possible I and Q signal components, respectively.

Now  $H_e(\omega)$  is a whitening filter for the sum of additive colored interference plus white noise. The transfer function is such that

$$|H_e(\omega)|^2 \cdot [S_{yy}(\omega) + \eta] = \eta \quad (27)$$

where  $S_{yy}(\omega)$  is the spectral density of either the I or Q component of the colored interference. To minimize the error rate,  $P(e)$ , requires maximization of  $\frac{\mu}{\sqrt{2}\sigma}$ , as given in (25). This requires maximizing the integral of the convolution of  $T \cdot \text{sinc}(\frac{\omega T}{2\pi})$  with the whitened  $S_{\delta I}(\omega)$  and  $S_{\delta Q}(\omega)$ .

To obtain more visibility into the problem, assume that the length  $T$  of the detection interval is much greater than the reciprocal of the highest frequency present in the whitened difference signal spectrum. This would occur if the symbols were being detected in blocks (block-coding). Then the convolution with  $T \cdot \text{sinc}(\frac{\omega T}{2\pi})$  approximates convolution with a delta function, which just reproduces  $\underline{E}_\delta(\omega)$ . Then (25) becomes

$$\begin{aligned} \frac{\mu}{\sqrt{2}\sigma} &= \sqrt{\frac{1}{2\pi} \int_{-\infty}^{\infty} \frac{1}{8\eta} \underline{E}_\delta^T(\omega) \cdot \underline{E}_\delta^*(\omega) d\omega} \\ &= \sqrt{\frac{1}{2\pi} \int_{-\infty}^{\infty} \frac{1}{8\eta} |H_e(\omega)|^2 \cdot [|S_{\delta I}(\omega)|^2 + |S_{\delta Q}(\omega)|^2] d\omega} \\ &= \sqrt{\frac{1}{2\pi} \int_{-\infty}^{\infty} \frac{1}{8} \frac{|S_{\delta I}(\omega)|^2 + |S_{\delta Q}(\omega)|^2}{S_{yy}(\omega) + \eta} d\omega} \quad (28) \end{aligned}$$

In terms of the band-pass parameters, (28) is

$$\frac{\mu}{\sqrt{2}\sigma} = \sqrt{\frac{1}{2\pi} \int_{-\infty}^{\infty} \frac{1}{4} \frac{|S_{\delta}(\omega)|^2}{S_{yy}(\omega) + n} d\omega} \quad (29)$$

The limiting case of (29) as  $n \rightarrow 0$  is the classical whitening filter result, given by Blachman [7].

In the form of (29) it is clear why some signals should outperform others for a fixed interfering spectrum. Suppose the spectrum,  $S_{yy}(\omega)$ , decreases as  $\frac{1}{\omega^N}$  for increasing  $\omega$  and the spectrum  $|S_{\delta}(\omega)|^2$ , decreases as  $\frac{1}{\omega^M}$ . For  $M < N$ , as white noise level,  $n$ , goes to zero, the integrand approaches  $k\omega^{N-M}$  and the infinite integral becomes arbitrarily large. This would be a singular detection problem. In practice, however,  $n$  will remain finite and the integrand will approach  $\frac{K}{\omega^M}$ . For  $1 < M$ , singular detection will not occur.

As Blachman commented, it is clear that the spectrum  $|S_{\delta}(\omega)|^2$  should be made large where the spectrum  $S_{yy}(\omega)$  is small and vice versa, in order to minimize  $P(e)$ . Failing this, the tails of the spectrum  $|S_{\delta}(\omega)|^2$  should be made to decay at a rate less than that of  $S_{yy}(\omega)$ , at least in the frequency range over which the detector responds.

#### Example: PSK Versus FSK

(28) will be evaluated for PSK and FSK signalling waveforms. The In-phase and Quadrature low-pass waveforms are

$$s_I(t;m) = A \cos\phi(t;m) \quad (30)$$

$$s_Q(t;m) = A \sin\phi(t;m)$$

$$\begin{aligned} \text{where } \phi(t;m) &= \Delta\phi c(m) ; & \text{PSK} \\ &= \Delta\omega t \cdot c(m); & \text{FSK} \end{aligned} \quad (31)$$

$$\begin{aligned} \text{and } c(m) &= 1 : m = 0 \\ &= -1 : m = 1 \end{aligned} \quad (32)$$

where  $\Delta\phi$  and  $\Delta\omega$  are the modulation index and frequency deviation, respectively. Then,

$$\begin{aligned}
\delta_I(t;m) &= A \cos(\Delta\phi c(m)) = A \cos(\Delta\phi) & : \text{PSK} \\
\delta_Q(t;m) &= A \sin(\Delta\phi c(m)) = A c(m) \sin(\Delta\phi) \\
\delta_I(t;m) &= A \cos(\Delta\omega t \cdot c(m)) = A \cos(\Delta\omega t) & : \text{FSK} \\
\delta_Q(t;m) &= A \sin(\Delta\omega t \cdot c(m)) = A c(m) \sin(\Delta\omega t) & (33)
\end{aligned}$$

and

$$\begin{aligned}
\delta_{\Delta I}(t) &= \delta_I(t;m=0) - \delta_I(t;m=1) \\
&= 0 \\
\delta_{\Delta Q}(t) &= \delta_Q(t;m=0) - \delta_Q(t;m=1) \\
&= 2A \sin(\Delta\phi) \pi_T(t) & : \text{PSK} & (34)
\end{aligned}$$

$$\begin{aligned}
\delta_{\Delta I} &= \delta_I(t;m=0) - \delta_I(t;m=1) \\
&= 0 \\
\delta_{\Delta Q} &= \delta_Q(t;m=0) - \delta_Q(t;m=1) \\
&= 2A \sin(\Delta\omega t) \pi_T(t) & : \text{FSK} & (35)
\end{aligned}$$

The Fourier Transforms are

$$\begin{aligned}
S_{\Delta I}(\omega) &= 0 & : \text{PSK or FSK} \\
S_{\Delta Q}(\omega) &= 2A T \sin(\Delta\phi) \frac{\sin(\frac{\omega T}{2})}{(\frac{\omega T}{2})} & : \text{PSK} \\
S_{\Delta Q}(\omega) &= \int_{-T/2}^{T/2} 2A \sin(\Delta\omega t) e^{-j\omega t} dt & : \text{FSK} & (36)
\end{aligned}$$

Then, the numerator of the argument in (28) is

$$\begin{aligned}
|S_{\Delta Q}(\omega)|^2 &= (2AT \sin(\Delta\phi))^2 \frac{\sin^2(\frac{\omega T}{2})}{(\frac{\omega T}{2})^2} & : \text{PSK} \\
&= \left| \int_{-T/2}^{T/2} A \sin(\Delta\omega t) e^{-j\omega t} dt \right|^2 & : \text{FSK}
\end{aligned}$$



The FSK result may be shown to be

$$|S_{\Delta Q}(\omega)|^2 = 4A^2 \left[ \frac{1}{\omega + \Delta\omega} \sin(\omega + \Delta\omega) \frac{T}{2} - \frac{1}{\omega - \Delta\omega} \sin(\omega - \Delta\omega) \frac{T}{2} \right]^2 \quad : \text{FSK} \quad (38)$$

It can be shown that both the PSK and FSK spectra decay as  $\frac{1}{\omega^2}$  for large  $\omega$ . Thus, any difference in performance (as observed in the following section) is not due to the high frequency behavior of the spectra. Or such is the conclusion to be drawn from the simplification of (28). Therefore the performance difference must be explained by the detailed behavior of (25) in the frequency region of the main bodies of the signal spectra.

### 3. IDEI DETECTION OF DIFFERENTIAL PHASE SHIFT KEYING

Another type of signal modulation for which comparisons between IDEI and standard detectors were desired is the Differential Phase-Shift-Keyed (DPSK) signal. DPSK was first described as a technique used in the Collins Kineplex system [8, 9, 10]. Kineplex actually embodied techniques which later were analyzed and characterized as DPSK, Quadri-phase, and L-Orthogonal Signalling [11].

DPSK was an ad hoc development to circumvent channel perturbations of the phase reference required for coherent detection of PSK. It was based on the premise of a slowly varying phase disturbance process with a time constant (inverse bandwidth) much greater than one symbol period. Under this assumption, the next previous symbol may be used as the phase reference for detection of the present symbol. The channel which best fits this model is the HF channel, for which Kineplex was designed. Many channels do not fit the model, such as the aeronautical data-link channel, subject to Earth-reflective multipath.

The DPSK signalling scheme is to reverse the signal phase between previous and present symbol if the present symbol is a "1" and not to reverse if the present symbol is a "0". Let  $m(j)$  denote the signalling symbol (waveform) on the  $j$ th time period and  $n(j)$  denote the information symbol (bit) on the  $j$ th time-period. Consider the truth table of Table 1.

TABLE 1  
TRUTH-TABLE

$m(j-1)$	$m(j)$	Reversal	$n(j)$	$m(j-1) \oplus m(j)$
0	0	No	0	0
0	1	Yes	1	1
1	0	Yes	1	1
1	1	No	0	0

Table 1 shows that the classic DPSK signalling scheme is identical to differential encoding of the signalling symbols. That is, for DPSK it is true that

$$n(j) = m(j) \oplus m(j-1) \quad (39)$$

Since (39) describes classic DPSK, it is obvious that DPSK may be detected either coherently or non-coherently. When detected non-coherently, the detection algorithm must consider data over two signal symbol intervals in order to make the decision as to whether or not a phase transition occurred. When detected coherently, each signalling symbol may be detected individually and the information symbol decoded from (39). In terms of sampled-data processing, it is obvious that coherent detection of DPSK may be implemented recursively. Non-coherent detection may need to store all the data samples from the preceding signalling interval and may or may not be implemented as a recursive process.

The question of whether to implement coherent or non-coherent detection for DPSK depends on the type of channel involved and the performance of the detector in that channel. For a standard DPSK detector, a non-coherent scheme should be used since DPSK was invented to overcome the short-comings of the standard coherent PSK detector. For the IDEI detector in its present stage of development, detection must be coherent. This is because the present IDEI detection algorithms are coherent algorithms.

It was not a task of the present contract to derive IDEI algorithms on a non-coherent basis.

It has been shown [12], and will be documented below, that the coherent IDEI detector for PSK operates well under heavy aeronautical multipath conditions. It was previously shown in a NASA investigation of the IDEI detector [3] that using a very unstable phase reference derived from the multipath channel does not change the error rate from that caused by the multiplicative noise effect on the data itself. This is because the phase rotation process is itself a vector multiplicative noise and is absorbed in the multipath multiplicative noise model. What this all means is that the IDEI error rate for DPSK can be obtained using coherent symbol by symbol detection and decoding according to (39).

It should be noted that a single isolated error in detecting one signalling symbol,  $m(j)$ , produces a pair of errors in the information symbols,  $n(j)$  and  $n(j+1)$ . If it is assumed that IDEI detection errors for PSK occur independently and singly, then

$$P_{\text{DPSK}}(e) = 2 P_{\text{PSK}}(e) \quad : \text{ IDEI detection} \quad (40)$$

The goodness of this assumption is tested below in the section on performance results.

#### 4. CLOSED-FORM ERROR RATES FOR STANDARD DETECTORS

##### a. Coherent Detection

In the course of the analyses of the error rate performance of the IDEI detector, it was desired to make comparative analyses between it and standard detectors, designed for white noise interference only. It was desired to make these comparisons not only by Monte Carlo simulations, but also by numerical solution of closed-form expressions for the standard error rate.

For binary phase-shift-keying, PSK, there is only one standard detection technique, which is a coherent one. This detection scheme is characterized as a "Correlation Receiver," or "Matched Filter". It is loosely referred to as an "Integrate and Dump" detector. For binary frequency-shift-keying, FSK, there are two standard detectors, one coherent and the other non-coherent. The coherent scheme is used when there is no

difficulty in deriving a carrier phase reference. If carrier phase is not assumed derivable, then the incoherent FSK detector is used.

For high signal to noise ratios (low error rates) the performance of the coherent detector is about 2.5 dB better than that of the non-coherent detector [11]. For purposes of comparing the IDEI performance to standard detector performance for FSK, the best standard detector is chosen, which is the coherent one.

From [1], the sufficient statistic for coherent detection is

$$u = \sum_{k=1}^K \underline{z}^T(k) [\underline{\Delta}(k;0) - \underline{\Delta}(k;1)] \quad (41)$$

where  $\underline{z}(k)$  and  $\underline{\Delta}(k;m)$  are as defined in (1). The decision rule is

$$u \underset{m=0}{\overset{m=1}{\geq}} 0 \quad (42)$$

The probability of error,  $P(e)$ , for coherent detection is

$$\begin{aligned} P(e) &= \Pr\{0 < u, m=1\} \cup \{u \leq 0, m=0\} \approx \\ &= \frac{1}{2} \left[ \int_0^{\infty} p(u|m=1) du + \int_{-\infty}^0 p(u|m=0) du \right] \end{aligned} \quad (43)$$

assuming that the occurrences of  $m=1$  and  $m=0$  are equally likely. The density,  $p(u|m)$ , is Gaussian and is described by the  $K$ -sample conditional means and variances of  $u$ .

Substituting the defining relation for  $\underline{z}(k)$ , of (1), into (41) yields

$$u = \sum_{k=1}^K [\underline{\Delta}(k;m) + \underline{y}(k) + \underline{n}(k)]^T [\underline{\Delta}(k;0) - \underline{\Delta}(k;1)] \quad (44)$$

Since  $\underline{y}(k)$  and  $\underline{n}(k)$  are zero-mean, then

$$E\{u|m\} = \sum_{k=1}^K \underline{\Delta}^T(k;m) [\underline{\Delta}(k;0) - \underline{\Delta}(k;1)] \quad (45)$$

It is assumed that the "energy" of  $\underline{\Delta}(k;1)$  and  $\underline{\Delta}(k;0)$  are equal so that

$$\sum_{k=1}^K \underline{\Delta}^T(k;0) \underline{\Delta}(k;0) = \sum_{k=1}^K \underline{\Delta}^T(k;1) \underline{\Delta}(k;1) \quad (46)$$

Then

$$E\{u|m=0\} = -E\{u|m=1\} \triangleq \mu \quad (47)$$

The variance is given by

$$\begin{aligned} \text{var}\{u|m\} = & \sum_{j=1}^K \sum_{k=1}^K [\underline{\Delta}(k;0) - \underline{\Delta}(k;1)]^T E\{[\underline{y}(k) + \underline{n}(k)][\underline{y}(j) + \underline{n}(j)]^T\} \cdot \\ & [\underline{\Delta}(j;0) - \underline{\Delta}(j;1)] \end{aligned} \quad (48)$$

Thus, it is seen that

$$\text{var}\{u|m=0\} = \text{var}\{u|m=1\} \triangleq \sigma^2 \quad (49)$$

In (48), the expectation is the 2 x 2 autocovariance of the sum of the I-Q vectors of white noise and colored noise. Since  $\underline{y}(k)$  and  $\underline{n}(k)$  are zero-mean and independent, (48) may be rewritten as

$$\begin{aligned} \text{var}\{u|m\} = & \sum_{j=1}^K \sum_{k=1}^K [\underline{\Delta}(k;0) - \underline{\Delta}(k;1)]^T [V_{yy}(k-j) + V_{nn}(k-j)] \cdot \\ & [\underline{\Delta}(j;0) - \underline{\Delta}(j;1)] \end{aligned} \quad (50)$$

where  $V_{nn}(k-j)$  is the 2 x 2 white-noise variance given in (1). Assuming that  $\underline{y}(k)$  is the low-pass I-Q vector resulting from a stationary band-pass process, then  $V_{yy}(\ )$  has the form

$$V_{yy}(\ ) = \begin{bmatrix} V_{ii}(\ ) & V_{iq}(\ ) \\ -V_{iq}(\ ) & V_{ii}(\ ) \end{bmatrix} \quad (51)$$

If the continuous-time bandpass process has a power spectrum which is even-symmetric about the signal carrier frequency (demodulation reference

frequency) then  $V_{iq}(\cdot) \equiv 0$ , identically. See Section IV for details.

From the above, then, the probability of error for coherent detection is given as

$$P(e) = \frac{1}{2} \left[ 1 - \operatorname{erf} \left( \frac{\mu}{\sqrt{2}\sigma} \right) \right] \quad (52)$$

where  $\operatorname{erf}(\cdot)$  is the tabulated "error function". It is desirable to write  $P(e)$  in terms of the ratio  $E/N_0$  where  $E$  is the energy of the continuous time signal waveform in one symbol period and  $N_0$  is the spectral density of the continuous-time white noise,  $n(t)$ . The continuous-time version of (52) is

$$P(e) = \frac{1}{2} \left[ 1 - \operatorname{erf} \left[ \sqrt{\frac{E(1-\rho)}{2N_0}} \right] \right] \quad (53)$$

where  $\rho$  is the correlation coefficient between the two possible signal waveforms. For PSK,  $\rho = -1$ . For FSK,  $\rho = 0.043$  for  $\Delta\phi = 0.785$ . Thus,  $\rho \approx 0$ . These results may be obtained from the defining integrals,  $\rho = E^{-1} \int_0^T \underline{\Delta}^T(t; m=1) \underline{\Delta}(t; m=0) dt$ , where  $E = \int_0^T \underline{\Delta}^T(t; m=1) \underline{\Delta}(t; m=1) dt$  and the  $\underline{\Delta}(t; m)$  are given in equation (33).

In order to tabulate results for  $P(e)$  as a function of  $E/N_0$ , the identity is made

$$\frac{E(1-\rho)}{2N_0} = \frac{\mu}{\sqrt{2}\sigma} \quad (54)$$

This leads to setting the level,  $\sigma_n^2$ , of the white noise variance,  $V_{nn}$ , according to

$$\sigma_n^2 = \frac{S \cdot L(\Delta\phi) \cdot K}{E/N_0} \quad (55)$$

where  $S$  is total carrier power,  $K$  is number of samples per symbol, and  $L(\Delta\phi)$  is a modulation loss factor of the modulation index,  $\Delta\phi$ .

$$\begin{aligned} L(\Delta\phi) &= \sin^2(\Delta\phi) && \text{:PSK} \\ &= 2 \sum_{k=1}^K \sin^2 \left( \frac{2\pi}{K} \left( k - \frac{1}{2} \right) \Delta\phi \right) && \text{:FSK} \end{aligned} \quad (56)$$

Note that by using (55),  $E/N_0$  becomes the ratio for the actual signalling energy which, for low index modulation, does not include the energy left in the residual unmodulated carrier. Comparison of performance between differing modulation types (PSK or FSK) is done on the basis of equal symbol  $E/N_0$ . Thus, the white noise variances,  $\sigma_n^2$ , may not be equal, if the modulation loss factors differ.

Letting  $J$  denote the power of the colored process  $y(k)$  (in band-pass form) and  $B_J$  the one-sided equivalent noise bandwidth of the low-pass I-Q process,  $y(k)$ , an equivalent white spectral density,  $N_J$ , for the colored process is defined by

$$J = N_J \cdot 2 B_J \quad (57)$$

Then the total equivalent white noise spectral density for the standard detector is

$$N_T = N_0 + N_J \quad (58)$$

where  $N_0$  is the usual white noise density.

The total signal power  $S$  is related to symbol energy,  $E$ , and symbol period  $T$  by

$$E = S \cdot T \cdot L(\Delta\phi) \quad (59)$$

where  $L(\Delta\phi)$  is modulation loss factor, defined in (56).

Thus

$$S = \frac{E}{L(\Delta\phi) \cdot T} \quad (60)$$

and

$$\frac{S}{J} = \frac{E}{L(\Delta\phi) \cdot T \cdot N_J \cdot 2 B_J} \quad (61)$$

Now,

$$\left(\frac{E}{N_0}\right) N_0 = E = \left(\frac{S}{J}\right) \cdot L(\Delta\phi) \cdot \left(2 \frac{B_J}{R}\right) N_J \quad (62)$$

where  $R$  is symbol rate. Thus

$$N_J = \frac{(E/N_0)}{L(\Delta\phi) \cdot (\frac{S}{J})} \cdot (\frac{R}{2B_J}) \cdot N_0 \quad (63)$$

and

$$\begin{aligned} N_T &= N_0 + N_J \\ &= \left[ 1 + \frac{(E/N_0)}{L(\Delta\phi) \cdot (\frac{S}{J})} \cdot (\frac{R}{2B_J}) \right] N_0 \end{aligned} \quad (64)$$

Thus

$$\frac{E}{N_T} = \frac{F}{1 + \frac{F}{(E/N_0)}} ; \quad F = L(\Delta\phi) \cdot (\frac{S}{J}) \cdot (2 \frac{B_J}{R}) \quad (65)$$

Knowing all the quantities in  $F$ , (65) may be substituted for  $E/N_0$  in (53) to compute the standard coherent detector error rate when the colored noise process is of much greater bandwidth than the desired signal.

#### b. Non-coherent Detection

In order to have a fair comparison between the IDEI and standard detectors for DPSK, it is desirable to use a non-coherent version of the standard detector. Thus, it must be determined whether a closed-form error rate expression can be obtained for the sampled-data, non-coherent, DPSK standard detector.

The model for the received data,  $\underline{z}(k)$ , is somewhat different than that of (1). Here, the data is described by

$$\underline{z}(k) = H_0 \underline{s}(k;m) + \underline{y}(k) + \underline{n}(k) \quad (67)$$

where  $\underline{y}(k)$  and  $\underline{n}(k)$  are the noise terms of (1). The term  $H_0$  is a two-by-two rotation matrix given by

$$H_0 = \begin{bmatrix} \cos\phi_0 & \sin\phi_0 \\ -\sin\phi_0 & \cos\phi_0 \end{bmatrix} \quad (68)$$



where  $\phi$  is taken to be a uniformly distributed random phase angle due either to the channel or to a completely unknown detection phase reference. The modeling of  $\phi_0$  as a uniformly distributed random constant results from the physical assumption that the phase perturbation on the received I-Q signal components is very slowly time-varying with respect to the symbol period.

For DPSK, the signal vector is given specifically by

$$\underline{d}(k;m) = \begin{bmatrix} \cos[c(k;m)\Delta\phi] \\ \sin[c(k;m)\Delta\phi] \end{bmatrix} = \begin{bmatrix} \cos(\Delta\phi) \\ c(k;m) \cdot \sin(\Delta\phi) \end{bmatrix} \quad (69)$$

where  $\Delta\phi$  is carrier phase deviation in radians and  $c(k;m)$  is the value of the square modulating waveform, given as

$$\begin{aligned} c(k;m) &= -1 & : & & m = 0 \\ &= +1 & : & & m = 1 \end{aligned} \quad (70)$$

Letting  $j$  denote the present symbol number (or period) and  $j-1$  denote the previous symbol number, it is seen that

$$\begin{aligned} [H_0 \underline{d}_{j-1}(k;m)]^T [H_0 \underline{d}_j(k;m)] &= \\ &= \cos^2(\Delta\phi) + c_{j-1}(k;m)c_j(k;m)\sin^2(\Delta\phi) \end{aligned} \quad (71)$$

For the case of no residual carrier where  $\Delta\phi = \pi/2$ , it can be seen that the expression of (71) has the value +1 when there is no phase transition between symbols and the value -1 when there is a phase transition. Thus, it can be seen that DPSK can be detected non-coherently on a sampled-data basis by forming the sufficient statistic

$$v = \frac{1}{K} \sum_{k=1}^K \underline{z}_{j-1}^T(k) \underline{z}_j(k) \quad (72)$$

where  $\underline{z}_{j-1}(k)$  are the data-samples (2-vectors) from the previous symbol interval and  $\underline{z}_j(k)$  are the data-samples from the present symbol interval. The decision rule is

$$v = \begin{cases} n(j)=0 \\ \geq T \\ n(j)=1 \end{cases} \quad (73)$$

where  $T$  is the decision threshold given by

$$T = \cos^2(\Delta\phi) \quad (74)$$

Unfortunately, the statistic  $v$  is not Gaussian, due to the cross products between the noises  $y(k)$  and  $n(k)$  on the previous and present periods. The probability of detection error for the non-coherent DPSK problem has only been solved exactly for the continuous-time formulation with uncorrelated (white) noise [8, 10]. The exact closed-form solution for colored noise, as  $y(k)$  generally is, on a sampled-data basis is not to be dealt with, further, here. Thus, the obvious precision approach is to simulate non-coherent detection algorithms and obtain the exact error rate performance of the standard detector empirically.

Also unfortunately, the non-coherent detector defined by the algorithms (72) and (73) is not recursive. It requires storage of received data points for an entire symbol period. A recursive algorithm may be implemented which requires storing only one statistic from period to period. This is the angle-estimating algorithm, based on [13]. From (67) - (69), it follows that in the absence of noise

$$\underline{z}(k) = \begin{bmatrix} z_i(k) \\ z_q(k) \end{bmatrix} = \begin{bmatrix} \cos[\Delta\phi \cdot c(k;m) - \phi_0] \\ \sin[\Delta\phi \cdot c(k;m) - \phi_0] \end{bmatrix} \quad (75)$$

where use has been made of the fact that

$$\begin{aligned} \sin[\Delta\phi \cdot c(k;m)] &= c(k;m) \sin(\Delta\phi) \\ \cos[\Delta\phi \cdot c(k;m)] &= \cos(\Delta\phi) \end{aligned} \quad (76)$$

Thus, without noise

$$\frac{z_q(k)}{z_i(k)} = \tan[\Delta\phi \cdot c(k;m) - \phi_0] \quad (77)$$

Now define the discrete-time version of an "integrate-and-dump" matched filter as

$$\begin{aligned} M_i(K) &= \frac{1}{K} \sum_{k=1}^K z_i(k) \\ M_q(K) &= \frac{1}{K} \sum_{k=1}^K z_q(k) \end{aligned} \quad (78)$$

Define a statistic for the  $j$ th symbol interval as

$$S(j) = \arctan \left[ \frac{M_q(K)}{M_i(K)} \right]_j \quad (79)$$

where  $\left[ \right]_j$  denotes that  $M_i(\ )$  and  $M_q(\ )$  are computed during the  $j$ th interval. In the noiseless case

$$S(j) = \Delta\phi \cdot c_j(k;m) - \phi_0 \quad : \quad \text{No noise} \quad (80)$$

Assuming  $\phi_0$  is constant over two symbol periods

$$\begin{aligned} S(j) - S(j-1) &= \Delta\phi [c_j(k;m) - c_{j-1}(k;m)] \\ &= 2\Delta\phi \quad : \quad c_j(k;m) \approx 1, c_{j-1}(k;m) = -1 \\ &= -2\Delta\phi \quad : \quad c_j(k;m) \approx -1, c_{j-1}(k;m) = 1 \\ &= 0 \quad : \quad c_j(k;m) \approx c_{j-1}(k;m) = \pm 1 \end{aligned} \quad (81)$$

Thus, denote a test statistic over two periods as

$$S = |S(j) - S(j-1)| - \Delta\phi \quad (82)$$

The decision rule is

$$\begin{aligned} n(j) &= 1 \\ S &\geq 0 \\ n(j) &= 0 \end{aligned} \quad (83)$$

## 5. THE UNIFORMLY MOST POWERFUL PROPERTY

In this section it will be shown that for a broad set of conditions it is not necessary to identify the strength, or scale, of the received signal,  $\underline{\Delta}(k;m)$ . From (1), the received data is

$$\underline{z}(k) = \underline{\Delta}(k;m) + \underline{y}(k) + \underline{n}(k) \quad (84)$$

where  $\underline{\Delta}(k;m)$  is desired signal,  $\underline{y}(k)$  is colored noise, and  $\underline{n}(k)$  is white noise. Now, the scale, or amplitude, of  $\underline{\Delta}(k;m)$  is not known, A Priori. Only the possible waveforms of  $\underline{\Delta}(k;m)$  for  $m = 0, 1$ , are known exactly. Thus, the reference signals for the optimum receiver of Figure 2 should generally be  $\hat{a}\underline{\Delta}(k;0)$  and  $\hat{a}\underline{\Delta}(k;1)$  where  $\hat{a}$  is the estimate of received signal strength. It is shown below under what conditions the probability of error is independent of  $\hat{a}$ .

From (11) the probability of error for the IDEI detector is given by

$$P(e) = \frac{1}{2} [1 - \text{erf}(\frac{\mu}{\sqrt{2}\sigma})] \quad (85)$$

From Lemmas 2 and 3 of Appendix B it may be shown that the mean,  $\mu$ , and variance,  $\sigma^2$ , given in (7) and (8) and used in (85), may be written as

$$\begin{aligned} \mu &= b \sum_{k=1}^K [\underline{e}_{\Delta}^T(k;m=0, n=1) \underline{e}_{\Delta}(k;m=0, n=1) \\ &\quad - \underline{e}_{\Delta}^T(k;m=0, n=0) \underline{e}_{\Delta}(k;m=0, n=0)] \\ \sigma^2 &= 4(b^2 + (b')^2) \sum_{j=1}^K \sum_{k=1}^K v_{\xi\xi}(j-k) [\underline{e}_{\Delta}(j;m=0, n=0) \\ &\quad - \underline{e}_{\Delta}(j;m=0, n=1)]^T [\underline{e}_{\Delta}(k;m=0, n=0) - \underline{e}_{\Delta}(k;m=0, n=1)] \end{aligned} \quad (86)$$

In (86)  $b$  and  $b'$  are the diagonal term and super diagonal term, respectively, of the  $2 \times 2$  inverse variance matrix of the identified Innovations process ( $V_{II}^{-1}$  in (8)).  $v_{\xi\xi}(j-k)$  is the diagonal term of the  $2 \times 2$  pseudo-innovations autocovariance matrix.  $v_{\xi\xi}(j-k)$  is a scalar function.

The quantities,  $\underline{e}_{\Delta}(k;m=i, n=j)$  are the transient error response (error residuals) of the Kalman (Wiener) filter to a driving signal

$$\underline{s}_{ij}(k) = \underline{s}(k; m=i) - \hat{a}\underline{s}(k; n=j) : \quad i, j \in \{0, 1\} \quad (87)$$

Now denote

$$\underline{e}_{\Delta}(k; m=i, n=j) \triangleq \underline{e}_{ij}(k) \quad (88)$$

The steady-state Kalman filter, which is just a particular canonical form of the Wiener filter is described by

$$\begin{aligned} \hat{\underline{x}}_{ij}(k+1|k) &= \Phi^*[I - G^*\Lambda]\hat{\underline{x}}_{ij}(k|k-1) + \Phi^*G^*\underline{s}_{ij}(k) \\ \underline{e}_{ij}(k) &= \underline{s}_{ij}(k) - \Lambda\hat{\underline{x}}_{ij}(k|k-1) \\ \hat{\underline{x}}_{ij}(1|0) &\triangleq \underline{0} \quad \forall i, j : \text{ zero initial conditions} \end{aligned} \quad (89)$$

where  $\Phi^*$  and  $G^*$  are the transition and gain matrices, respectively, for the identified Wiener filter.

The solution to (86) is obtained as

$$\begin{aligned} \hat{\underline{x}}_{ij}(k|k-1) &= \sum_{\ell=1}^{k-1} [\Phi^*(I - G^*\Lambda)]^{k-1-\ell} \Phi^*G^*\underline{s}_{ij}(\ell) \\ \underline{e}_{ij}(k) &= \underline{s}_{ij}(k) - \sum_{\ell=1}^{k-1} \Lambda[\Phi^*(I - G^*\Lambda)]^{k-1-\ell} \Phi^*G^*\underline{s}_{ij}(\ell) \end{aligned} \quad (90)$$

It is shown in Appendix B that the quantity  $\Lambda[\Phi^*(I - G^*\Lambda)]^{k-1-\ell} \Phi^*G^*$  has the canonical form

$$\Lambda[\Phi^*(I - G^*\Lambda)]^{k-1-\ell} \Phi^*G^* = \begin{bmatrix} f(k, \ell) & f'(k, \ell) \\ -f'(k, \ell) & f(k, \ell) \end{bmatrix} \quad (91)$$

To evaluate (86) requires the signals,  $\underline{s}_{00}(k)$  and  $\underline{s}_{01}(k)$ . For binary PSK or FSK (coherent), the signal vectors are

$$\begin{aligned}\underline{\Delta}(k; m=0) &= \begin{bmatrix} \Delta_I(k) \\ \Delta_Q(k) \end{bmatrix} \\ \underline{\Delta}(k; m=1) &= \begin{bmatrix} \Delta_I(k) \\ -\Delta_Q(k) \end{bmatrix}\end{aligned}\quad (92)$$

where

$$\begin{aligned}\Delta_I(k) &= A \cos(\Delta\phi) && : \text{PSK} \\ &= A \cos(\Delta\omega t_k) && : \text{FSK} \\ \Delta_Q(k) &= A \sin(\Delta\phi) && : \text{PSK} \\ &= A \sin(\Delta\omega t_k) && : \text{FSK}\end{aligned}\quad (93)$$

The quantities  $\Delta\phi$  and  $\Delta\omega$  are PSK phase deviation and FSK (radian) frequency deviation respectively. The quantity,  $t_k$ , is sampled time value, given by

$$t_k = \frac{k - \frac{1}{2}}{K} T \quad (94)$$

where  $k$  is sample number,  $K$  is number of samples per symbol, and  $T$  is symbol duration.

Then,

$$\begin{aligned}\underline{S}_{00}(k) &= \underline{\Delta}(k; m=0) - \hat{a}_{\underline{\Delta}}(k; n=0) \\ &= \begin{bmatrix} (1-\hat{a})\Delta_I(k) \\ (1-\hat{a})\Delta_Q(k) \end{bmatrix} \\ \underline{S}_{01}(k) &= \underline{\Delta}(k; m=0) - \hat{a}_{\underline{\Delta}}(k; n=1) \\ &= \begin{bmatrix} (1-\hat{a})\Delta_I(k) \\ (1+\hat{a})\Delta_Q(k) \end{bmatrix}\end{aligned}\quad (95)$$

It follows that

$$\begin{aligned}
\underline{e}_{00}(k) &= (1-\hat{a}) \begin{bmatrix} s_I(k) - \sum_{\ell=1}^{k-1} [f(k, \ell)s_I(\ell) + f'(k, \ell)s_Q(\ell)] \\ s_Q(k) - \sum_{\ell=1}^{k-1} [f(k, \ell)s_Q(\ell) - f'(k, \ell)s_I(\ell)] \end{bmatrix} \\
\underline{e}_{01}(k) &= \begin{bmatrix} (1-\hat{a})s_I(k) - \sum_{\ell=1}^{k-1} [(1-\hat{a})f(k, \ell)s_I(\ell) + (1+\hat{a})f'(k, \ell)s_Q(\ell)] \\ (1+\hat{a})s_Q(k) - \sum_{\ell=1}^{k-1} [(1+\hat{a})f(k, \ell)s_Q(\ell) - (1-\hat{a})f'(k, \ell)s_I(\ell)] \end{bmatrix}
\end{aligned}
\tag{96}$$

Next, the results of (96) are substituted into the expressions for  $\mu$  and  $\sigma^2$ , given in (86). These expressions are rewritten as

$$\begin{aligned}
\mu &= b \sum_{k=1}^K [\underline{e}_{01}^T(k) \underline{e}_{01}(k) - \underline{e}_{00}^T(k) \underline{e}_{00}(k)] \\
\sigma^2 &= 4(b^2 + (b')^2) \sum_{j=1}^K \sum_{k=1}^K v_{\xi\xi}(j-k) [\underline{e}_{00}(j) - \underline{e}_{01}(j)]^T \cdot \\
&\quad \cdot [\underline{e}_{00}(k) - \underline{e}_{01}(k)]
\end{aligned}
\tag{97}$$

Substituting (96) into (97) yields for the  $\mu$ -term,

$$\begin{aligned}
\mu &= b \sum_{k=1}^K \{ 4\hat{a} [s_Q(k) - \sum_{\ell=1}^{k-1} f(k, \ell)s_Q(\ell)]^2 + \\
&\quad + [\sum_{\ell=1}^{k-1} f'(k, \ell)s_I(\ell)] [4(1-\hat{a})s_Q(k) + (3\hat{a}^2 - 4\hat{a} + 1) \cdot \\
&\quad \cdot \sum_{\ell=1}^{k-1} f(k, \ell)s_Q(\ell)] - [\sum_{\ell=1}^{k-1} f'(k, \ell)s_Q(\ell)] [2\hat{a}(1-\hat{a})s_I(k) + \\
&\quad + (3\hat{a}^2 - 2\hat{a} - 1) \sum_{\ell=1}^{k-1} f(k, \ell)s_I(\ell) - 4\hat{a}^2 \sum_{\ell=1}^{k-1} f'(k, \ell)s_Q(\ell)] \}
\end{aligned}
\tag{98}$$

The result for  $\sigma^2$  is

$$\begin{aligned}
\sigma^2 = & 4(b^2 + (b')^2) \{ 4\hat{a}^2 \sum_{j=1}^K \sum_{k=1}^K u_{\xi\xi}(j-k) [(\sum_{\ell=1}^{j-1} f'(j, \ell) \Delta_Q(j)) \cdot \\
& \cdot (\sum_{\ell=1}^{k-1} f'(k, \ell) \Delta_Q(k)) + (\Delta_Q(j) - \sum_{\ell=1}^{j-1} f(j, \ell) \Delta_Q(\ell)) \cdot \\
& \cdot (\Delta_Q(k) - \sum_{\ell=1}^{k-1} f(k, \ell) \Delta_Q(\ell))] \} \quad (99)
\end{aligned}$$

It may be seen from (98) and (99) that in the argument  $\frac{\mu}{\sqrt{2}\sigma}$ , the  $\hat{a}$  factors will cancel only if  $f'(k, \ell) = 0$ , identically. This latter will occur only if the Wiener filter is structured in the form where the I and Q states are uncoupled. Note that the restriction is not that the I and Q terms of the colored noise process,  $y(k)$ , be uncoupled (spectrum symmetric w.r.t. signal carrier frequency), but only that the filter be structured for uncoupled I and Q processes. In case the  $y(k)$  process represented a one-sided interference spectrum, the uncoupled Wiener filter would not be optimum and some penalty would be exacted for the additional white noise admitted to the filter. However, in order to retain the Uniformly Most Powerful property, the possible SNR penalty must be accepted.

If it is assumed that the Wiener filter is always structured for uncoupled I-Q processes, then  $b' = 0$  and the dependence of the argument  $\frac{\mu}{\sqrt{2}\sigma}$  on  $b$  also disappears. Thus, the final argument becomes

$$\begin{aligned}
\frac{\mu}{\sqrt{2}\sigma} = & \frac{\sum_{k=1}^K [\Delta_Q(k) - \sum_{\ell=1}^{k-1} f(k, \ell) \Delta_Q(\ell)]^2}{\sqrt{2 \sum_{j=1}^K \sum_{k=1}^K u_{\xi\xi}(j-k) [\Delta_Q(j) - \sum_{\ell=1}^{j-1} f(j, \ell) \Delta_Q(\ell)] [\Delta_Q(k) - \sum_{\ell=1}^{k-1} f(k, \ell) \Delta_Q(\ell)]}} \quad (100)
\end{aligned}$$

Thus, under the conditions stated,  $P(e)$  is independent of  $\hat{a}$ . It should also be noted in passing that the argument  $\frac{\mu}{\sqrt{2}\sigma}$  also has no dependence on

the in-phase signal component,  $\Delta_I(k)$ . This is reassuring since  $\Delta_I(k)$  contains no information concerning the message symbol. It should be recalled that the only reason for allowing  $\Delta_I(k) \neq 0$  was to maintain an unmodulated



residual carrier component for anti-multipath (multiplicative noise) detection.

Retention of the UMP property is most desirable, since it alleviates what would otherwise be a most difficult requirement to satisfy, identification of the desired signal strength in the presence of possibly stronger interference. Use of the UMP property may, however, conflict with identification of the colored interfering process, depending on how such identification is implemented. ML identification, which is described in the following chapter, is achieved by processing the pseudo-innovations, or tracking error. With an improperly scaled signal waveform reference,  $\hat{a}_s(k;n)$ , the tracking error is perturbed and may cause error in the ML identification. However, if the ad hoc identification method, alluded to in Chapter IV, is employed, then UMP-induced identification error may not be as significant, since detection error rate is later shown to be quite tolerant of ad hoc identification error. An exact characterization of the identification error induced effects of using the UMP property requires further research than has been performed to date.

The UMP property was shown to obtain for a class of signal structures of the form of (92). PSK and FSK happen to belong to this class, as do PAM signals, also. The requirement to implement the tracking filter in uncoupled form is not critical since the only effect is to allow some additional white noise into the filter. The worst effect would be a 3 db degradation for a truly single-sideband interfering signal.

SECTION III  
MAXIMUM LIKELIHOOD IDENTIFICATION  
OF IN-PHASE/QUADRATURE VECTOR PROCESSES

1. THE I-Q CANONICAL MODEL

To examine the statistical relations for the In-phase and Quadrature low-pass processes, consider the bandpass formulation, thereof. Define a bandpass Gaussian process,  $y(t)$ , as

$$y(t) = y_i(t)\cos\omega_c t - y_q(t)\sin\omega_c t \quad (101)$$

which has power spectral density,  $S_{yy}(\omega)$ . The power spectral density is the Fourier transform of an autocorrelation function,  $V_{yy}(\tau)$ , and is therefore real, positive, and an even function of  $\omega$ . However, note that the density need not be locally symmetric with respect to the frequency,  $\omega_c$ .

Now,  $y_i(t)$  and  $y_q(t)$  are the low-pass Gaussian In-phase and Quadrature components of  $y(t)$ , respectively. Assuming that  $y(t)$  is zero-mean, then  $y_i(t)$  and  $y_q(t)$  are zero-mean and completely described by their autocorrelation and cross-correlation functions,  $V_{ii}(\tau)$ ,  $V_{qq}(\tau)$ , and  $V_{qi}(\tau)$ . For  $y(t)$  to be stationary it is necessary and sufficient for [14]

$$\begin{aligned} V_{ii}(\tau) &= V_{ii}(-\tau) = V_{qq}(\tau) = V_{qq}(-\tau) \\ V_{qi}(\tau) &= V_{iq}(-\tau) = -V_{qi}(-\tau) \end{aligned} \quad (102)$$

That is,  $V_{ii}(\tau)$  and  $V_{qq}(\tau)$  are even functions and  $V_{qi}(\tau)$  is an odd function. Note that it is not required for  $y_i(t)$  and  $y_q(t)$  to be orthogonal (or independent).

The power spectral densities for  $y_i(t)$  and  $y_q(t)$  are defined by the Fourier transforms

$$\begin{aligned} S_{ii}(\omega) &= F\{V_{ii}(\tau)\} \\ S_{qq}(\omega) &= F\{V_{qq}(\tau)\} \\ S_{qi}(\omega) &= F\{V_{qi}(\tau)\} \end{aligned} \quad (103)$$

Since  $V_{ii}(\tau)$  and  $V_{qq}(\tau)$  are real and even,  $S_{ii}(\omega)$  and  $S_{qq}(\omega)$  are real, even, and positive. Since  $V_{qi}(\tau)$  is real and odd,  $S_{qi}(\omega)$  is imaginary and odd.

Now,  $S_{ii}(\omega)$ ,  $S_{qq}(\omega)$ , and  $S_{qi}(\omega)$  may be determined directly from  $S_{yy}(\omega)$  by [15]

$$\begin{aligned} S_{ii}(\omega) &= S_{yy}(\omega_c + \omega) U(\omega_c + \omega) + S_{yy}(\omega_c - \omega) U(\omega_c - \omega) \\ S_{qi}(\omega) &= j[S_{yy}(\omega_c - \omega) U(\omega_c - \omega) - S_{yy}(\omega_c + \omega) U(\omega_c + \omega)] \end{aligned} \quad (104)$$

where  $U(\cdot)$  is the Unit-Step function defined by

$$\begin{aligned} U(x) &= 1 \quad ; \quad 0 \leq x \\ &= 0 \quad ; \quad x < 0 \end{aligned} \quad (105)$$

Figure 3 shows the various spectral relations from (104) for a hypothetical non-symmetric bandpass power spectral density. Note that if  $S_{yy}(\omega)$  were locally even symmetric with respect to the frequency,  $\omega_c$ , then  $S_{qi}(\omega)$  would be identically zero. Hence,  $V_{qi}(\tau)$  would be identically zero (limiting case of an odd function). Thus,  $y_i(t)$  and  $y_q(t)$  would be orthogonal, uncorrelated, and independent (since they are Gaussian).

If  $y_i(t)$  and  $y_q(t)$  were independent, they could be identified independently, using Single-Input-Single-Output (SISO) identification techniques. Unfortunately, in general, the Doppler spectra or additive colored interference spectra are not locally even symmetric. Thus, in general,  $y_i(t)$  and  $y_q(t)$  are correlated, and Multi-Input-Multi-Output (MIMO) identification must be used.

For the present problem, the I-Q Generator Model is the stationary version of a linear discrete-time invariant system. System parameters are assumed to be constant or so slowly time-varying that they may be taken as constant for the purposes of recursive identification. This means that the elements are constant over the interval of time corresponding to the memory of the identifying algorithms.

Thus, the I-Q model is defined by the equations

$$\underline{x}(k+1) = \underline{\phi} \underline{x}(k) + \Gamma \underline{w}(k) \quad (\text{continued})$$

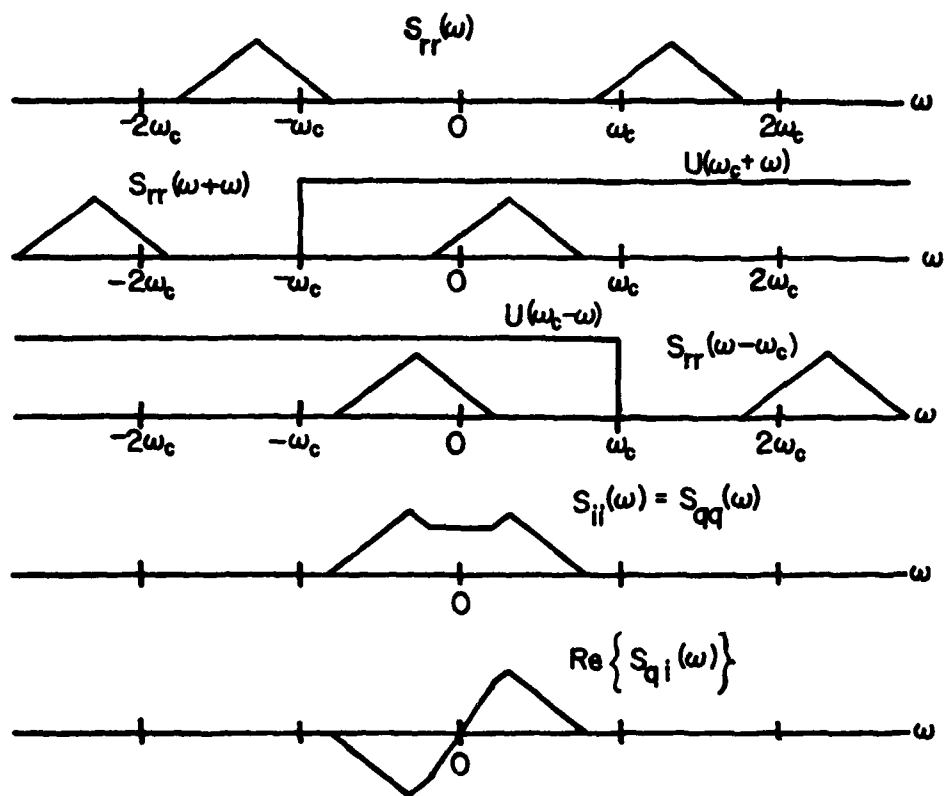


Figure 3. Spectral Relations

$$\begin{aligned}\underline{y}(k) &= \Lambda \underline{x}(k) \\ \underline{z}(k) &= \underline{y}(k) + \underline{n}(k)\end{aligned}\quad (106)$$

Now,  $\underline{y}(k)$ ,  $\underline{n}(k)$ ,  $\underline{z}(k)$ , and  $\underline{w}(k)$  are all 2-vectors. In terms of the I-Q formulation, they are defined by

$$\begin{aligned}\underline{y}(k) &= \begin{bmatrix} y_i(k) \\ y_q(k) \end{bmatrix} ; & \underline{n}(k) &= \begin{bmatrix} n_i(k) \\ n_q(k) \end{bmatrix} \\ \underline{z}(k) &= \begin{bmatrix} z_i(k) \\ z_q(k) \end{bmatrix} ; & \underline{w}(k) &= \begin{bmatrix} w_i(k) \\ w_q(k) \end{bmatrix}\end{aligned}\quad (107)$$

Both  $\underline{n}(k)$  and  $\underline{w}(k)$  are independent, zero-mean, white and Gaussian. It is assumed that  $y_i(k)$  and  $y_q(k)$  are each Markov-N. Thus, the state-vector,  $\underline{x}(k)$ , must have 2N state (system order), and the obvious definitions follow:

$$\begin{aligned}\underline{x}(k) &= \begin{bmatrix} \underline{x}_i(k) \\ \underline{x}_q(k) \end{bmatrix} ; & \Phi &= \begin{bmatrix} \Phi_{ii} & \Phi_{iq} \\ \Phi_{qi} & \Phi_{qq} \end{bmatrix} \\ \Gamma &= \begin{bmatrix} \Upsilon_{ii} & \Upsilon_{iq} \\ \Upsilon_{qi} & \Upsilon_{qq} \end{bmatrix} ; & \Lambda &= \begin{bmatrix} \Lambda_{ii}^T & \Lambda_{iq}^T \\ \Lambda_{qi}^T & \Lambda_{qq}^T \end{bmatrix}\end{aligned}\quad (108)$$

where the  $\underline{x}_i(k)$ ,  $\underline{x}_q(k)$ ,  $\Upsilon_{ii}$ ,  $\Upsilon_{iq}$ ,  $\Upsilon_{qi}$ ,  $\Upsilon_{qq}$ ,  $\Lambda_{ii}$ ,  $\Lambda_{iq}$ ,  $\Lambda_{qi}$ , and  $\Lambda_{qq}$  are all N-vectors. The  $\Phi_{ii}$ ,  $\Phi_{iq}$ ,  $\Phi_{qi}$ , and  $\Phi_{qq}$  are each NxN matrices.

The major emphasis of the modelling is to find the system parameters for the colored radio frequency interferences and/or the complex Doppler-spreading process so that the system produces a given output covariance function. This system must satisfy three system properties.

- (1) The stationarity of the I-Q process.
- (2) Markov-Gauss process.
- (3) Output statistics

The output covariance relations for the general models are

$$\begin{aligned} V_{zz}(k+j, k) &= E\{z(k+j)z(k)\} \\ &= \Lambda V_{xx}(k+j, k) \Lambda^T + V_{nn} \end{aligned} \quad (109)$$

where

$$V_{nn} = \sigma_n^2 I_{2 \times 2} \delta_{jk}$$

From the Markov process, the covariance of the state,  $V_{xx}(k+j, k)$  is given by

$$\begin{aligned} V_{xx}(k+1, k+1) &= \Phi V_{xx}(k, k) \Phi^T + \Gamma \Gamma^T \\ V_{xx}(k+j, k) &= \Phi^j V_{xx}(k, k) \end{aligned} \quad (110)$$

It may be assumed without loss of generality that  $w(k)$  has unit variance. It is assumed that the generator has reached steady-state and that  $x(k)$  is stationary. Under these conditions, equations (108) and (109) become

$$\begin{aligned} V_{zz}(k+j, k) &= \Lambda \Phi^j V_{xx} \Lambda^T + V_{nn} \\ V_{xx} &= \Phi V_{xx} \Phi^T + \Gamma \Gamma^T \end{aligned} \quad (111)$$

Now, the requirements of equation (102) are that for  $y_i(k)$  and  $y_q(k)$  to be low-pass I-Q components, it must be satisfied that

$$\begin{aligned} V_{zz}(k+j, k) &\triangleq V_{zz}(j) = \begin{bmatrix} V_{ii}(j) & V_{iq}(j) \\ V_{qi}(j) & V_{qq}(j) \end{bmatrix} \\ V_{ii}(j) &= V_{qq}(j) ; \text{ an even function} \\ V_{iq}(j) &= -V_{iq}(-j) = -V_{qi}(j) ; \text{ an odd function} \end{aligned} \quad (112)$$

The canonical modelling problem is to choose a structure  $\{\Gamma, \Phi, \Lambda\}$  for the data generator such that the number of non-zero elements is minimal. So far as realization of a specified output autocovariance matrix is concerned,  $\Gamma$  and  $\Lambda$  are redundant. That is, one or the other of  $\Gamma$  and  $\Lambda$  may be fixed and the remaining matrix varied to realize the autocovariance. In the present model,  $\Lambda$  is fixed and is therefore known, A Priori. By Theorems

1, 2, and 3 of [16], the generator structure is given by

$$\begin{aligned} \Phi &= \begin{bmatrix} \phi & \phi' \\ -\phi' & \phi \end{bmatrix}, & \Gamma &= \begin{bmatrix} \underline{y} & \underline{y}' \\ -\underline{y}' & \underline{y} \end{bmatrix} \\ \Lambda &= \begin{bmatrix} \underline{\lambda}^T & 0 \\ 0 & \underline{\lambda}^T \end{bmatrix} \end{aligned} \quad (113)$$

where  $\underline{y}$ ,  $\underline{y}'$ , and  $\underline{\lambda}$  are all N-vectors and  $\phi$  and  $\phi'$  are each NxN symmetric matrices.

This system structure was derived by continuous-time modelling since time is a parameter in (101). This system structure of (113) satisfies the continuous-time model for the stationary I-Q process. The relation between the continuous-time model and the discrete-time can be found in [16].

The system equations are given as follows.

$$\begin{aligned} \underline{x}(k+1) &= \begin{bmatrix} \phi & \phi' \\ -\phi' & \phi \end{bmatrix} \underline{x}(k) + \begin{bmatrix} \underline{y} & \underline{y}' \\ -\underline{y}' & \underline{y} \end{bmatrix} \underline{w}(k) \\ \underline{z}(k) &= \begin{bmatrix} \underline{\lambda}^T & 0 \\ 0 & \underline{\lambda}^T \end{bmatrix} \underline{x}(k) + \underline{n}(k) \end{aligned} \quad (114)$$

where

$$\begin{aligned} E\{\underline{w}(i)\underline{w}(j)\} &= I\delta_{ij} \\ E\{\underline{n}(i)\underline{n}(j)\} &= \sigma_n^2 I\delta_{ij} \\ E\{\underline{w}(i)\underline{n}(j)\} &= 0 \quad \text{for all } i, j \end{aligned}$$

and  $\phi$  and  $\phi'$  matrices are assumed to be

$$\begin{aligned} \phi &= \begin{bmatrix} \phi_1 & & 0 \\ & \phi_2 & \\ 0 & & \phi_N \end{bmatrix}, & \phi' &= \begin{bmatrix} \phi_1' & & 0 \\ & \phi_2' & \\ 0 & & \phi_N' \end{bmatrix} \\ \underline{\lambda}^T &= (1, 1, \dots, 1) \end{aligned} \quad (115)$$

Figure 4 shows the partially decoupled system where  $\begin{bmatrix} \cdot \\ \cdot \end{bmatrix}$  denotes the juxtaposition matrix.

The steady-state Kalman gain,  $G$ , and the innovation variance corresponding to this system have the following structures, as shown in Appendix B.

$$G = \begin{bmatrix} \underline{g} & \underline{g}' \\ -\underline{g}' & \underline{g} \end{bmatrix} ; \quad V_{vv} = \begin{bmatrix} v & v' \\ -v' & v \end{bmatrix} \quad (116)$$

where  $\underline{g}$  and  $\underline{g}'$  are each  $N$ -vectors. When the output spectrum is symmetric, then the off-diagonal blocks of (112) and (115) are zeros.

## 2. DERIVATION OF THE MAXIMUM LIKELIHOOD ALGORITHM

Maximum Likelihood Estimation was introduced into statistics by R. A. Fisher in 1906. It is probably the most widely used method for estimation in statistics. The vector of unknown parameters  $\{\phi, \Gamma, V_{nn}\}$  of the system is denoted by  $\underline{\beta}$ . The maximum likelihood estimate of  $\underline{\beta}$ , given a sequence of observations,  $z(1), z(2), \dots, z(K)$  is given by

$$\hat{\underline{\beta}} = \max_{\underline{\beta}} p(\underline{Z}(K) | \underline{\beta}) \quad (117)$$

where  $\underline{Z}(K) = \{z(1), z(2), \dots, z(K)\}$   
and

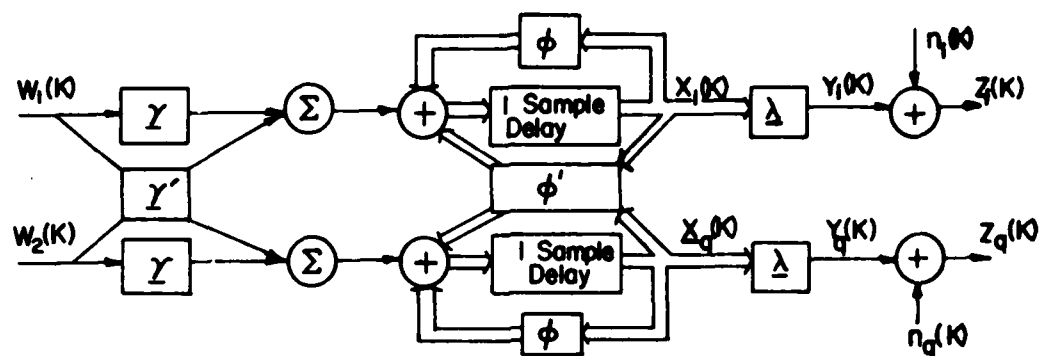
$$p(\underline{Z}(K) | \underline{\beta}) = \text{conditional probability density function of } \underline{Z}(K) \text{ given } \underline{\beta}. \quad (118)$$

The method of maximum likelihood consists of finding that value  $\hat{\underline{\beta}}$  of parameters which is "most likely" to have produced the data.

An expression for  $p(\underline{Z}(K) | \underline{\beta})$  is derived as

$$\begin{aligned} p(\underline{Z}(K) | \underline{\beta}) &= p(z(1), z(2), \dots, z(K) | \underline{\beta}) \\ &= p(z(K) | z(K-1), \underline{\beta}) p(z(K-1) | \underline{\beta}) \\ &= p(z(K) | z(K-1), \underline{\beta}) p(z(K-1) | z(K-2), \underline{\beta}) p(z(K-2) | \underline{\beta}) \\ &= \prod_{k=1}^K p(z(k) | z(k-1), \underline{\beta}) \end{aligned} \quad (119)$$





PARTIALLY DECOUPLED SYSTEM

Figure 4. Partially Decoupled System

$p(z(k)|\underline{Z}(k-1), \underline{\beta})$  is Gaussian since  $w(k)$  and  $n(k)$  are Gaussian and the generator is linear. Therefore, the density function,  $p(z(k)|\underline{Z}(k-1), \underline{\beta})$ , is completely characterized by the conditional mean and variance.

$$E\{z(k)|\underline{Z}(k-1), \underline{\beta}\} = z(k|k-1, \underline{\beta})$$

$$\begin{aligned} E\{[z(k) - z(k|k-1, \underline{\beta})][z(k) - z(k|k-1, \underline{\beta})]^T | \underline{Z}(k-1), \underline{\beta}\} \\ = E\{v(k, \underline{\beta})v^T(k, \underline{\beta}) | \underline{Z}(k-1), \underline{\beta}\} = V_{vv}(k, \underline{\beta}) \end{aligned} \quad (120)$$

where  $v(k, \underline{\beta}) = z(k) - z(k|k-1, \underline{\beta})$ .  $v(k, \underline{\beta})$  is the Innovation process and  $V_{vv}(k, \underline{\beta})$  denotes its variance.

The negative log-cost function,  $J(\underline{\beta})$ , can now be written as

$$\begin{aligned} J(\underline{\beta}) &= -\log p(\underline{Z}(K) | \underline{\beta}) \\ &= \frac{1}{2} \sum_{k=1}^K \{ \underline{v}^T(k, \underline{\beta}) V_{vv}^{-1}(k, \underline{\beta}) \underline{v}(k, \underline{\beta}) + \log |V_{vv}^{-1}(k, \underline{\beta})| \} \end{aligned} \quad (121)$$

The problem of determining the ML estimate has now become one of finding a way of calculating the conditional mean,  $z(k|k-1, \underline{\beta})$ , and the error variance,  $V_{vv}(k, \underline{\beta})$ . The quantities can be obtained from a Kalman filter state estimate given  $\underline{\beta}$ . Note that the ML estimation process is identical to the MAP detection strategy so that this ML estimation is imbedded in the detection algorithm. The Kalman filter algorithm is the following

$$\hat{X}(k|k-1) = \Phi \hat{X}(k-1|k-1) \quad (122)$$

$$v(k, \underline{\beta}) = z(k) - \Lambda \hat{X}(k|k-1) \quad (123)$$

$$\hat{X}(k|k) = \hat{X}(k|k-1) + G(k)v(k, \underline{\beta}) \quad (124)$$

and

$$V_{xx}(k|k-1) = \Phi V_{xx}(k-1|k-1) \Phi^T + \Gamma \Gamma^T \quad (125)$$

$$V_{vv}(k, \underline{\beta}) = \Lambda V_{xx}(k|k-1) \Lambda^T + V_{nn} \quad (126)$$

$$G(k) = V_{xx}(k|k-1) \Lambda^T V_{vv}^{-1}(k, \underline{\beta}) \quad (127)$$

$$V_{xx}(k|k) = (I - G(k)\Lambda) V_{xx}(k|k-1) \quad (128)$$

In the steady state, equations (125) - (128) are also in steady state and a real-time computation is not necessary. Therefore, the ML estimation is to find  $v(k, \underline{\beta})$  which minimizes the cost function,  $J(\underline{\beta})$ , with respect to  $\underline{\beta}$  since the logarithm is a monotonic function. This is a very difficult non-linear problem because of the constraints in the Kalman filter equations. In the steady-state, the filter gain,  $G(k, \underline{\beta})$  and covariance,  $V_{vv}(k, \underline{\beta})$  have reached constant values  $G$  and  $V$ . The vector  $\underline{\beta}$  of unknown parameters is now defined to include  $G$  and  $V_{vv}$  instead of  $V_{nn}$  and  $\Gamma$  since the latter are subsumed in the former. Then

$$J(\underline{\beta}) = \frac{1}{2} \sum_{k=1}^k \{ \underline{v}^T(k, \underline{\beta}) V_{vv}^{-1} \underline{v}(k, \underline{\beta}) + \log |V_{vv}| \} \quad (129)$$

where

$$\underline{\beta} = \text{unknown parameters in } \{\Phi, G\}$$

Once  $\underline{\beta}$  is estimated, then  $\Gamma$  and  $V_{nn}$  may be obtained from (125) - (128) if desired. When the numbers of unknown parameters in  $\underline{\beta}$  and in  $V_{nn}$  and  $\Gamma \Gamma^T$  are identical, it may be possible to use  $\underline{\beta}$  to solve for unique estimates of the unknowns in  $V_{nn}$  and  $\Gamma \Gamma^T$ . Otherwise it is not.

The cost function can be minimized with respect to  $V_{vv}$  to give

$$V_{vv} = \frac{1}{K} \sum_{k=1}^K v(k, \hat{\underline{\beta}}) v^T(k, \hat{\underline{\beta}}) \quad (130)$$

where  $\hat{\underline{\beta}}$  is the ML estimate of unknowns of  $\phi, G$ . Substituting this value in cost function (129) we have

$$J(\hat{\underline{\beta}}) = \frac{K}{2} \log |V_{vv}| + \text{constant} \quad (131)$$

This function can be minimized using the gradient methods, referred to as the Newton-Raphson method. The separation between estimating  $\underline{\beta}$  and  $V_{vv}$  is not as complete as in the SISO [17].

The cost function has multiple maxima, saddle point, discontinuities, and singular Hessian in parameter space, in particular, a large number of unknown parameters. The application of the gradient method for this difficult non-linear programming problem causes extremely slow convergence, divergence, or convergence to a wrong stationary point. Thus, good initialization is important to ensure convergence to the absolute maximum. This is analogous to the "acquisition" problem for any non-linear tracking estimator.

The basic iteration in gradient-type non-linear programming methods is

$$\underline{\beta}_{i+1} = \underline{\beta}_i - \Delta \underline{\beta}_i = \underline{\beta}_i - p_i R_i \underline{g}_i \quad (132)$$

where  $\Delta \underline{\beta}_i$  is the step size and  $\underline{\beta}_i$  is the unknown parameter vector at the  $i$ th iteration  $\underline{g}_i$  is a vector of gradients of the cost function  $J(\underline{\beta})$ , i.e.,

$$\underline{g}_i = \left. \frac{\partial J(\underline{\beta})}{\partial \underline{\beta}} \right|_{\underline{\beta} = \underline{\beta}_i} \quad (133)$$

$R_i$  is an approximation to the inverse of Hessian matrix:

$$R_i = \left[ \left. \frac{\partial^2 J(\underline{\beta})}{\partial \underline{\beta}^2} \right|_{\underline{\beta} = \underline{\beta}_i} \right]^{-1} \quad (134)$$

and  $p_i$  is a scalar step size parameter chosen to ensure that  $J(\underline{\beta}_{i+1}) < J(\underline{\beta}_i)$ . The main differences between many non-linear programming schemes is in selection of  $R_i$ , and in some cases  $p_i$  and  $q_i$  [18].

The first gradient of the cost function,  $J(\underline{\beta})$  is

$$\frac{\partial J(\underline{\beta})}{\partial \underline{\beta}} = \sum_{k=1}^K \underline{v}^T(k, \underline{\beta}) V_{vv}^{-1} \frac{\partial \underline{v}(k, \underline{\beta})}{\partial \underline{\beta}} \quad (135)$$

Generally, the computation of the Hessian matrix is not desirable since it is very expensive to compute the extra terms and may not pay off in terms of the improved convergence rate. Instead one chooses  $R_i$  as the inverse of the Fisher information matrix  $M_i$  where

$$M_i = E \left\{ \left. \frac{\partial^2 J(\underline{\beta})}{\partial \underline{\beta}^2} \right| \underline{\beta} = \underline{\beta}_i \right\} = E \left\{ \left. \left[ \frac{\partial J(\underline{\beta})}{\partial \underline{\beta}} \right] \left[ \frac{\partial J(\underline{\beta})}{\partial \underline{\beta}} \right]^T \right| \underline{\beta} = \underline{\beta}_i \right\} \quad (136)$$

The expectation is taken over the whole sample space.  $M_i$  is a nonnegative definite symmetric matrix. This technique is called by modified Newton-Raphson, quasilinearization.  $M_i$  is generally estimated from the samples as

$$\hat{M}_i(n, m) = \sum_{k=1}^K \left[ \frac{\partial \underline{v}(k, \underline{\beta})}{\partial \beta(n)} \right]^T V_{vv}^{-1} \frac{\partial \underline{v}(k, \underline{\beta})}{\partial \beta(m)} \quad (137)$$

where  $\beta(n)$  is the  $n$ th component of the  $\underline{\beta}$  vector. A more exact expression for  $q_i$  and  $M_i$  can be found in [18, 19] but in general the extra calculations are not worth the improvement in convergence rate. Note that the first derivative  $J(\underline{\beta})$  with respect to  $\underline{\beta}$  is needed to compute the approximate inverse of the Hessian matrix. But the Fisher information method has a difficulty when  $\hat{M}_i$  is singular. To avoid this difficulty, the step size  $\Delta \beta_i$  is decomposed by

$$\Delta \beta_i = \sum_{j=1}^m \frac{p_j}{\lambda_j} (\underline{v}_j^T \underline{g}_j) \underline{v}_j \quad (138)$$

where  $\lambda_j$  is an eigenvalue of  $\hat{M}_i$  corresponding to the eigenvector  $u_j$ . It can be seen that the step size in direction  $u_j$  may be very large for small  $\lambda_j$ . This means that, when  $\hat{M}_i$  is nearly singular, the step size takes large steps in those parameter directions about which the least information is available.

The rank deficient method is to use a pseudo-inverse of  $M$  for  $R$  as

$$R = \sum_{j=1}^{m-k} \frac{1}{\lambda_j} u_j u_j^T \quad (139)$$

where  $\lambda_j$  are the eigenvalues of  $M$  and  $u_j$  are the corresponding eigenvectors such that  $\lambda_1 > \lambda_2 > \dots > \lambda_{m-k} > b > \lambda_{m-k+1} > \dots > \lambda_m$  and  $b$  is a suitably chosen threshold value.

Numerically, better accuracy is obtained by modifying (132) as

$$\underline{\beta}_{i+1} = \underline{\beta}_i - \rho \sum_{j=1}^{m-k} \frac{u_j^T g_i}{\lambda_j} u_j \quad (140)$$

It is difficult to find a proper value for  $\rho$  and eigenvalue threshold  $b$ . Mehra [19] has suggested a modified rank deficient method but there are no general rules to determine a proper  $b$  value, in particular, for a large number of unknown parameters. Experimentally, when the initial values are far from true values,  $b$  may be large enough to prevent the estimator from diverging.

Now, useful computational steps for the gradient are obtained through the "state sensitivity" for parameter  $\underline{\beta}$ .

Consider the following steady-state Kalman filter equations:

$$\hat{X}(k|k-1) = \phi \hat{X}(k-1|k-1) \quad (141)$$

$$v(k) = z(k) - \Lambda \hat{X}(k|k-1) \quad (142)$$

$$\hat{X}(k|k) = \hat{X}(k|k-1) + G v(k) \quad (143)$$

The gradient of  $v(k)$  with respect to  $\phi_j$  ( $j = 1, 2, \dots, N$ ) can be obtained sequentially from (141) - (143) as

$$\frac{\partial \hat{X}(k|k-1)}{\partial \phi_j} = \phi \frac{\partial \hat{X}(k-1|k-1)}{\partial \phi_j} + \frac{\partial \phi}{\partial \phi_j} \hat{X}(k-1|k-1) \quad (144)$$

$$\frac{\partial v(k)}{\partial \phi_j} = -\Lambda \frac{\partial \hat{X}(k|k-1)}{\partial \phi_j} \quad (145)$$

$$\frac{\partial \hat{X}(k|k)}{\partial \phi_j} = (I - G\Lambda) \frac{\partial \hat{X}(k|k-1)}{\partial \phi_j} \quad (146)$$

where  $\phi_j$  is an unknown parameter of  $\phi$  matrix. So is the gradient of  $v(k)$  with respect to  $g_j$  ( $j = 1, 2, \dots, N$ ) given by

$$\frac{\partial \hat{X}(k|k-1)}{\partial g_j} = \phi \frac{\partial \hat{X}(k|k-1)}{\partial g_j} \quad (147)$$

$$\frac{\partial v(k)}{\partial g_j} = -\Lambda \frac{\partial \hat{X}(k|k-1)}{\partial g_j} \quad (148)$$

$$\frac{\partial \hat{X}(k|k)}{\partial g_j} = (I - G\Lambda) \frac{\partial \hat{X}(k|k-1)}{\partial g_j} + \frac{\partial G}{\partial g_j} v(k) \quad (149)$$

where  $g_j$  is an unknown parameter of  $G$  matrix. Equations (147) - (149) should be processed simultaneously and sequentially to solve the gradient of  $v(k)$  with respect to  $\underline{\beta}$ . Note that the number of unknown parameters are  $2N$  which is a minimum.

For stationary I-Q process, the gradient of  $J(\underline{\beta})$  with respect to  $\underline{\beta}$  is simplified as

$$\begin{aligned} \frac{\partial J(\underline{\beta})}{\partial \underline{\beta}} &= \sum_{k=1}^K \underline{v}^T(k) V_{vv}^{-1} \frac{\partial \underline{v}(k)}{\partial \underline{\beta}} \\ &= \sum_{k=1}^K [v_1(k)u - v_2(k)u'] \frac{\partial v_1(k)}{\partial \underline{\beta}} + [v_1(k)u' + v_2(k)u] \frac{\partial v_2(k)}{\partial \underline{\beta}} \end{aligned} \quad (150)$$

where

$$v(k) = \begin{bmatrix} v_1(k) \\ v_2(k) \end{bmatrix} \quad \text{and} \quad V_{vv}^{-1} = \begin{bmatrix} v & v' \\ -v' & v \end{bmatrix}$$

The Fisher information matrix is

$$\begin{aligned} M(n, m) &= \sum_{k=1}^K \left[ \frac{\partial v(k)}{\partial \beta(n)} \right]^T V_{vv}^{-1} \frac{\partial v(k)}{\partial \beta(m)} \\ &= \sum_{k=1}^K \left[ \frac{\partial v_1(k)}{\partial \beta(n)} v - \frac{\partial v_2(k)}{\partial \beta(n)} v' \right] \frac{\partial v_1(k)}{\partial \beta(m)} \\ &\quad + \left[ \frac{\partial v_1(k)}{\partial \beta(n)} v' + \frac{\partial v_2(k)}{\partial \beta(n)} v \right] \frac{\partial v_2(k)}{\partial \beta(m)} \end{aligned} \quad (151)$$

When the system is decoupled, then (150) and (151) may be reduced as

$$\frac{\partial J(\beta)}{\partial \beta} = v \sum_{k=1}^K \left[ v_1(k) \frac{\partial v_1(k)}{\partial \beta} + v_2(k) \frac{\partial v_2(k)}{\partial \beta} \right]$$

and

$$M(n, m) = v \sum_{k=1}^K \left[ \frac{\partial v_1(k)}{\partial \beta(n)} \frac{\partial v_1(k)}{\partial \beta(m)} + \frac{\partial v_2(k)}{\partial \beta(n)} \frac{\partial v_2(k)}{\partial \beta(m)} \right] \quad (152)$$

or

$$\frac{\partial J(\beta)}{\partial \beta} = v \sum_{k=1}^K v_1(k) \frac{\partial v_1(k)}{\partial \beta}$$

and

$$M(n, m) = v \sum_{k=1}^K \frac{\partial v_1(k)}{\partial \beta(n)} \frac{\partial v_1(k)}{\partial \beta(m)} \quad (153)$$

We may have some insight about the decoupled system and verify the innovation variance structure. Fortunately, in the estimate of  $v$  it is not necessary to compute (140) in the case of the decoupled system or (2x2) system since it is cancelled in (140). Otherwise, the innovations variance should be estimated first with a good initialization value and used in (140).

The computational steps for the ML estimation are as follows:

- (1) Assume inition conditions,  $\beta_0$ ,  $p_0$ , and  $\hat{X}(0|0)$
- (2) Compute  $v(k) = z(k) - \Lambda \hat{X}(k|k-1)$  for  $k = N+1, \dots, N+M$
- (3) Compute cost function associated with a priori parameter estimate

$$J(\beta_i) = \frac{1}{2} \left[ \sum_{k=1}^K v^T(k) V_{vv}^{-1} v(k) + \log |V_{vv}| \right]$$

- (4) Evaluate the sensitivity function sequentially and simultaneously after M measurement and store these

$$\frac{\partial v(k)}{\partial \beta} = -\Lambda \frac{\partial \hat{X}(k|k-1)}{\partial \beta}$$

where

$$\frac{\partial \hat{X}(k|k-1)}{\partial \beta} = F \frac{\partial \hat{X}(k-1|k-2)}{\partial \beta} + \frac{\partial F}{\partial \beta} \hat{X}(k|k-1) + \frac{\partial D}{\partial \beta} z(k-1) \quad (154)$$

$$F = \Phi[I - G\Lambda]$$

$$D = \Phi G$$

- (5) Compute the gradient of  $J(\beta)$

$$\frac{\partial J(\beta)}{\partial \beta} = \sum_{k=N+1}^{N+M} v(k) V_{vv}^{-1} \frac{\partial v(k)}{\partial \beta} \quad (155)$$

- (6) Compute the information matrix

$$M(i, j) = \sum_{k=N+1}^{N+M} \frac{\partial v(k)}{\partial \beta} V_{vv}^{-1} \left[ \frac{\partial v(k)}{\partial \beta} \right]^T \quad (156)$$

- (7) Compute eigenvalues  $\lambda_j$  and eigenvector  $u_j$  of  $M$  ( $\lambda_1 > \lambda_2 > \dots > \lambda_{2N}$ )

- (8) Determine the threshold value for eigenvalue  $\lambda_m$  ( $\lambda_1 > \dots > \lambda_m >$

$\lambda_{m+1} \dots > \lambda_{2N}$ )

- (9) Compute Rank deficient method

$$\beta_{i+1} = \beta_i - p_i \sum_{j=1}^m \frac{u_j^T g_i}{\lambda_j} u_j \quad (157)$$

- (10) Adjust the scalar  $p_i$  to satisfy  $J(\beta_{i+1}) < J(\beta_i)$

- (11) Initialize  $\hat{X}(k|k)$  and  $\beta_{i+1}$  to go to step (2)



In step (7), many of the computational difficulties with the rank deficient method are involved with the large spread in the eigenvalues of  $M$ . To avoid this inaccurate choice of  $\lambda_m$  in step (8), Mehra [19] has suggested that with a proper choice of  $\lambda_m$ , steps (9) - (10) are done and the cost function value is computed. This same procedure is repeated until  $m = 2N$  and a  $\underline{g}$  is obtained producing a minimum cost function value. This is called the sweep rank deficient method. Experimentally, when the number of unknown parameters is small, then Mehra's method improves the convergence rate. But, with a large number of unknowns, this method does not work because of the large spread of eigenvalues. Instead, fixing a threshold value for  $\lambda_m$  is better even though the convergence rate is slow.

If the new cost is larger than the previous cost, the step size is cut in half, setting  $p_i$  in half in step (10). This same procedure is repeated a given number of times. The reason for this step size cutting is the non-quadratic nature of the cost function. Also, the constraint boundaries for system stability are adapted to restrict the  $\phi$  matrix.

The values of  $\hat{X}(k|k)$  and  $\underline{g}_{i+1}$  are stored to be initialized for the next  $M$  measurements.

To escape from the computation loop, the gradient of  $J(\underline{g})$  is used instead of testing the whiteness of the innovation process, which is frequently used by many, since, in practice, the whiteness test may be ill-conditioned.

### 3. ESTIMATION PERFORMANCE OF THE M-L IDENTIFICATION ALGORITHMS

In this example, the actual system is given by

$$\begin{aligned}\underline{X}(k+1) &= \underline{\phi X}(k) + \underline{\Gamma w}(k) \\ \underline{z}(k) &= \underline{\Lambda X}(k) + \underline{n}(k)\end{aligned}\tag{158}$$

where the numerical values are

$$\Phi = \begin{bmatrix} .97 & .1 \\ -.1 & .97 \end{bmatrix} ; \quad \Gamma = \begin{bmatrix} 1.5 & 0.5 \\ -.5 & 1.5 \end{bmatrix}$$

$$\Lambda = \begin{bmatrix} 1 & 0 \\ 0 & 1 \end{bmatrix}$$

$$V_{nn} = E\{n(i)n(j)\} = 1.58 \begin{bmatrix} 1 & 0 \\ 0 & 1 \end{bmatrix} \quad E\{w(i)w(j)\} = I\delta_{ij} \quad (159)$$

This system is a coupled (2x2) system. The true Kalman gain,  $G$ , for (159) is given

$$G = \begin{bmatrix} .613064 & , & 0 \\ 0 & , & .613064 \end{bmatrix}$$

and the true innovation variance,  $V_{vv}$ , is given

$$V_{vv} = \begin{bmatrix} 6.45171 & , & 0 \\ 0 & , & 6.45171 \end{bmatrix}$$

For the (2x2) coupled system, the Kalman gain and the innovation variance are decoupled.

Given initial values as

$$\Phi_0^* = \begin{bmatrix} .99 & .15 \\ -.15 & .99 \end{bmatrix} \quad G_0^* = \begin{bmatrix} .55 & 0 \\ 0 & .55 \end{bmatrix}$$

the number of samples,  $K$ , is varied 100, 500 and 800.

The following Figures show the convergences for these three cases. As we can see in Figures 5 - 6 , the convergence of the Kalman gain is more sensitive to the initial guesses than the transition matrix. It will be shown later in a (6x6) decoupled case that accurate initialization is required for the Kalman gain to ensure convergence. In Figure 6, the greater  $K$  becomes, the smaller deviation the innovation variance has. The calculated  $v'$  for  $K = 800$  is closer to zero than  $K = 100$ . The cases of  $K = 500$  and  $K = 800$  produce little difference in convergence.

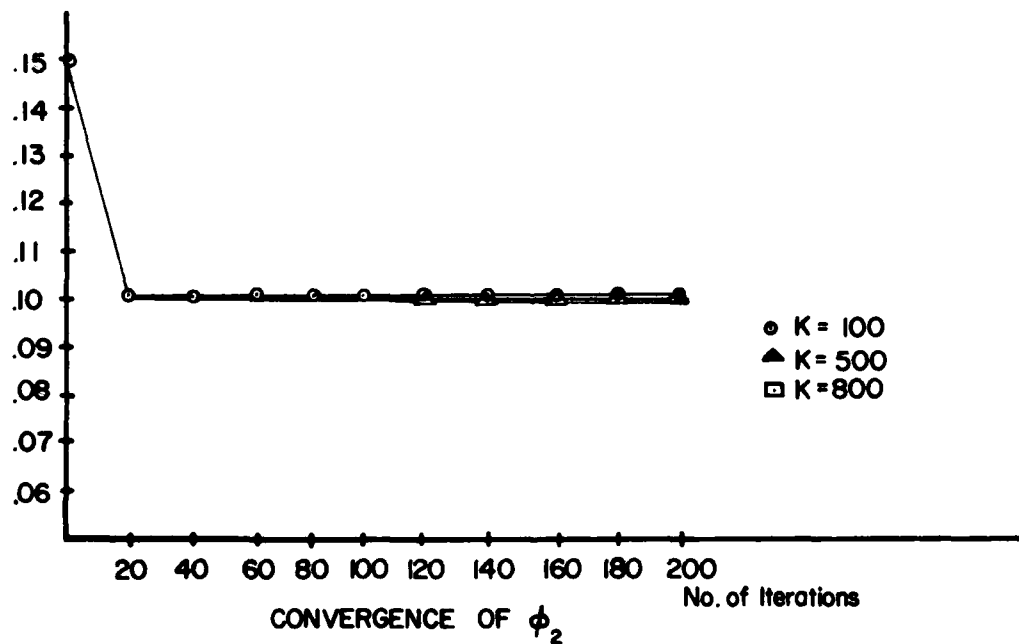
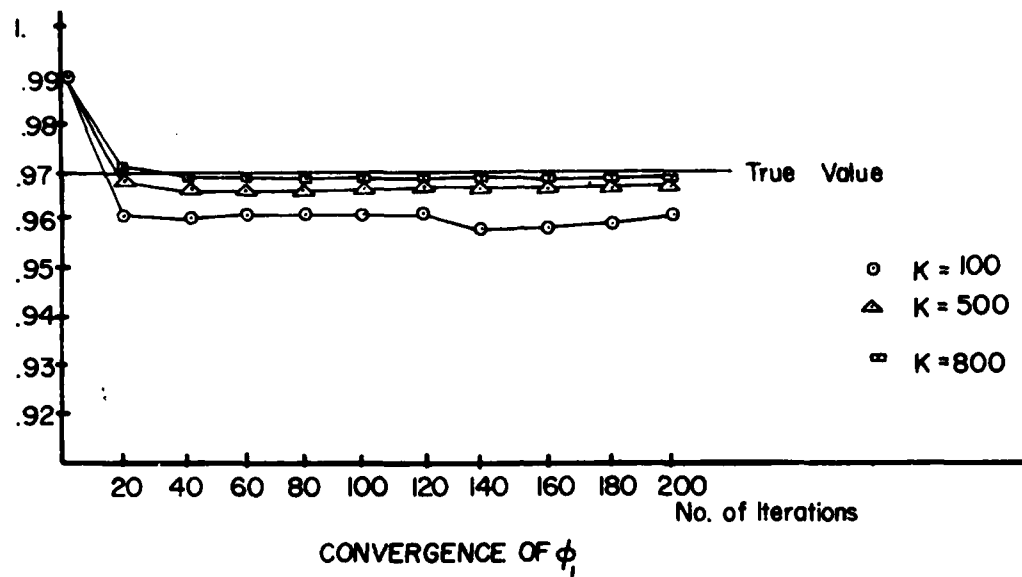


Figure 5. Identification Convergence for Transition Matrix

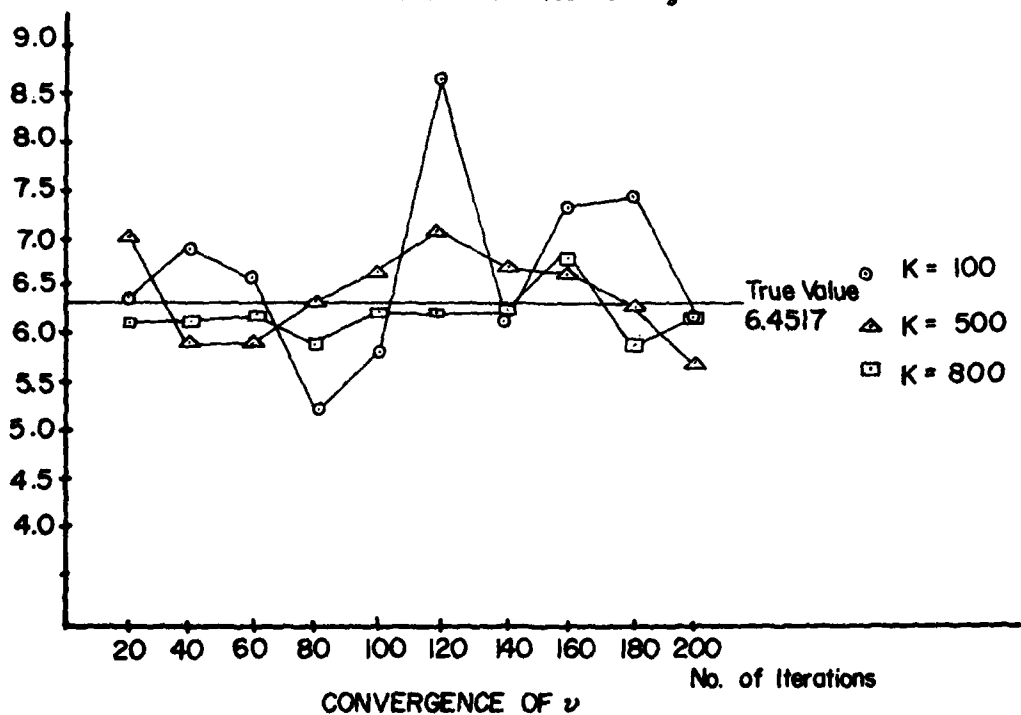
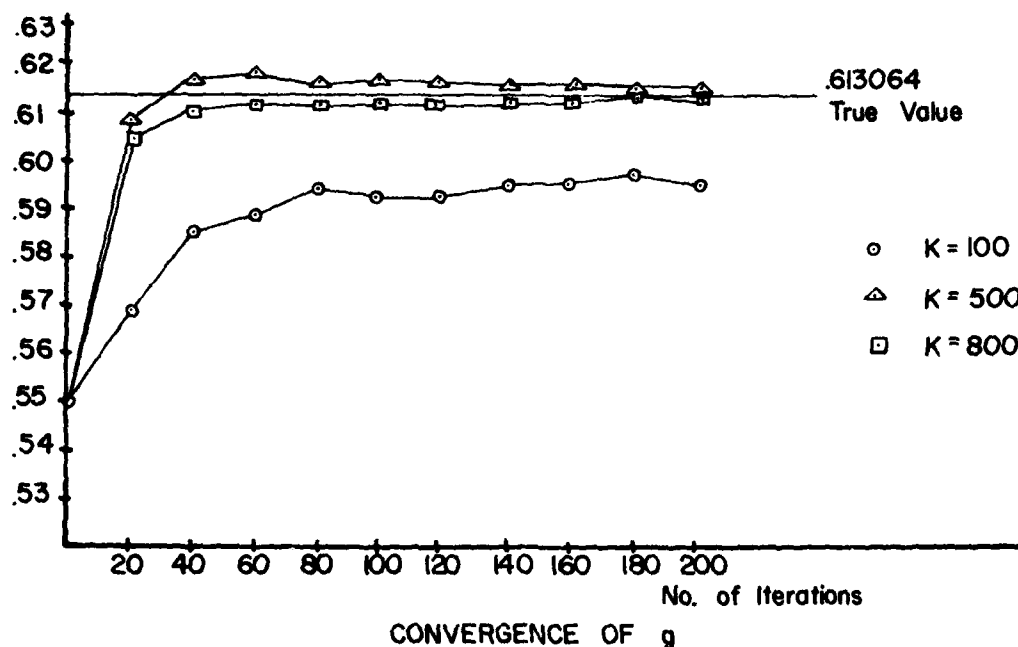


Figure 6. Identification Convergence for Gain and Innovations Variance

Next, a (6x6) decoupled case is considered for  $K = 100$  and  $K = 400$ . As previously mentioned, the decoupled system can be considered as a SISO system in terms of identification.

Consider the (3x3) SISO system as

$$\underline{x}_i(k+1) = \begin{bmatrix} \phi_1 & 0 & 0 \\ 0 & \phi_2 & 0 \\ 0 & 0 & \phi_3 \end{bmatrix} \underline{x}_i(k) + \begin{bmatrix} \gamma_1 \\ \gamma_2 \\ \gamma_3 \end{bmatrix} \underline{w}_i(k)$$

$$\underline{z}(k) = (1,1,1)\underline{x}_i(k) + \underline{n}_i(k) \quad (160)$$

where

$$\phi_1 = .927374$$

$$\phi_2 = .881911$$

$$\phi_3 = .777768$$

$$\gamma_1 = 1.11439$$

$$\gamma_2 = -1.40932$$

$$\gamma_3 = .303111$$

and

$$\sigma_v = .499801$$

The true Kalman filter is calculated as

$$g_1 = 1.27345$$

$$g_2 = -1.22638$$

$$g_3 = .147568$$

$$\text{NSPB} = 10$$

$$\text{TB} = 1 \text{ E-04}$$

$$\text{BW} = 2745$$

$$\text{ENOPB} = 10 \text{ DB}$$

$$\text{SFRDB} = 0 \text{ DB}$$

Its signal-to-noise ratio is 2.0016. Initial values are given by

$$\phi_1^* = .94$$

$$\phi_2^* = .9$$

$$\phi_3^* = .75$$

$$g_1^* = 1.15$$

$$g_2^* = -1.3$$

$$g_3^* = .05$$

The following tables are the convergence rates for this case.

TABLE 2

CONVERGENCE OF  $\phi$

Number Iteration	$\phi_1 = .927374$		$\phi_2 = .881911$		$\phi_3 = .777768$	
	K = 100	K = 400	K = 100	K = 400	K = 100	K = 400
20	.931523	.935041	.895041	.897619	.760655	.767604
40	.924770	.926946	.888993	.886991	.763505	.768910
60	.924573	.927804	.887979	.888393	.764136	.769145
80	.922456	.927717	.885366	.887378	.764860	.769262
100	.921746	.928777	.883289	.888936	.765356	.769461

TABLE 3  
CONVERGENCE OF G AND  $V_{vv}$

Number Iteration	$g_1 = 1.27345$	$g_2 = -1.22638$	$g_3 = .147569$	$v = .310170$
	K = 100 K = 400	K = 100 K = 400	K = 100 K = 400	K = 100 K = 400
20	1.24253 1.25424	-1.20901 -1.19561	.120113 .132448	.350336 .298245
40	1.25845 1.25510	-1.19354 -1.19486	.132420 .131805	.320628 .315488
60	1.26415 1.25776	-1.18818 -1.19220	.136563 .134330	.339504 .309749
80	1.26660 1.25737	-1.18578 -1.19261	.138356 .133823	.264868 .352092
100	1.26826 1.25984	-1.18420 -1.19015	.139419 .136201	.342379 .299879

Again, is observed the sensitivity of the Kalman gain initial value. Experimentally, for a good Kalman gain initial value, the transition initial value is not overly critical. When the Kalman gain is large, this dominates the sample space in calculating  $\frac{\partial J(\underline{\beta})}{\partial \underline{\beta}}$  and M. When the Kalman gain

is too small, it is difficult for the estimates to converge to the absolute minimum value. Without good initial values, it is better to set a large eigenvalue ( $10^3 \sim 10^4$  in (3x3) case) for the threshold and use the rank deficient method instead of the sweep rank deficient method.

## SECTION IV

### RESULTS

#### 1. SIMULATION VERSUS CLOSED-FORM ERROR-RATE RESULTS FOR PSK AND FSK

The development of the Monte Carlo simulation for PSK and FSK in colored multiplicative or colored additive noises was performed in Phase I of the present contract and was reported in [1]. However, minimal simulation results were reported therein. Those six figures are repeated here for completeness and because of their relation to the present work.

Figure 7 shows the comparison of Monte Carlo results with closed-form results for PSK in white noise only. This curve verified that the Monte Carlo simulation routine was operating properly.

Figure 8 shows the variation of Monte Carlo error rate for PSK in 275 Hz. colored noise as a function of modulation index. This curve showed that the transmitted signal must have a residual unmodulated carrier component to enable the IDEI detector in colored multiplicative noise.

Figures 9 and 10 show Monte Carlo results for PSK and FSK, respectively, in heavy multiplicative noise. The cases were set as though the diffuse multipath reflection were equal in strength to the direct path (MPR = 0 dB). For these cases any additive colored interference was essentially removed (SJR = 53 dB). These results were analyzed in [1] and [12]. The expected 3-dB difference in white-noise only  $E/N_0$  performance [20] is due to the different values of correlation coefficient,  $\rho$ , in (53).

Figures 11 and 12 show a comparison of Monte Carlo and closed-form results for PSK and FSK, respectively, in colored plus white additive interference. Here the Monte Carlo results are plotted against the closed-form solid curves. In the FSK case the standard detector was noncoherent in the simulation, while the solid curve is for a standard coherent detector. These results were analyzed in [1] and [12].

Figure 13 is the first set of results not previously documented. Here, PSK is subjected to strong narrow-band additive colored interference plus white interference. The ratio of colored interference to desired signal is 23 dB (SJR = -23 dB). The error rate is plotted versus signal energy per symbol to white noise spectral density ( $E/N_0$ ). The ratio of interference bandwidth to symbol rate is

$$\frac{BW}{BR} = \frac{275}{2500} = 0.11$$



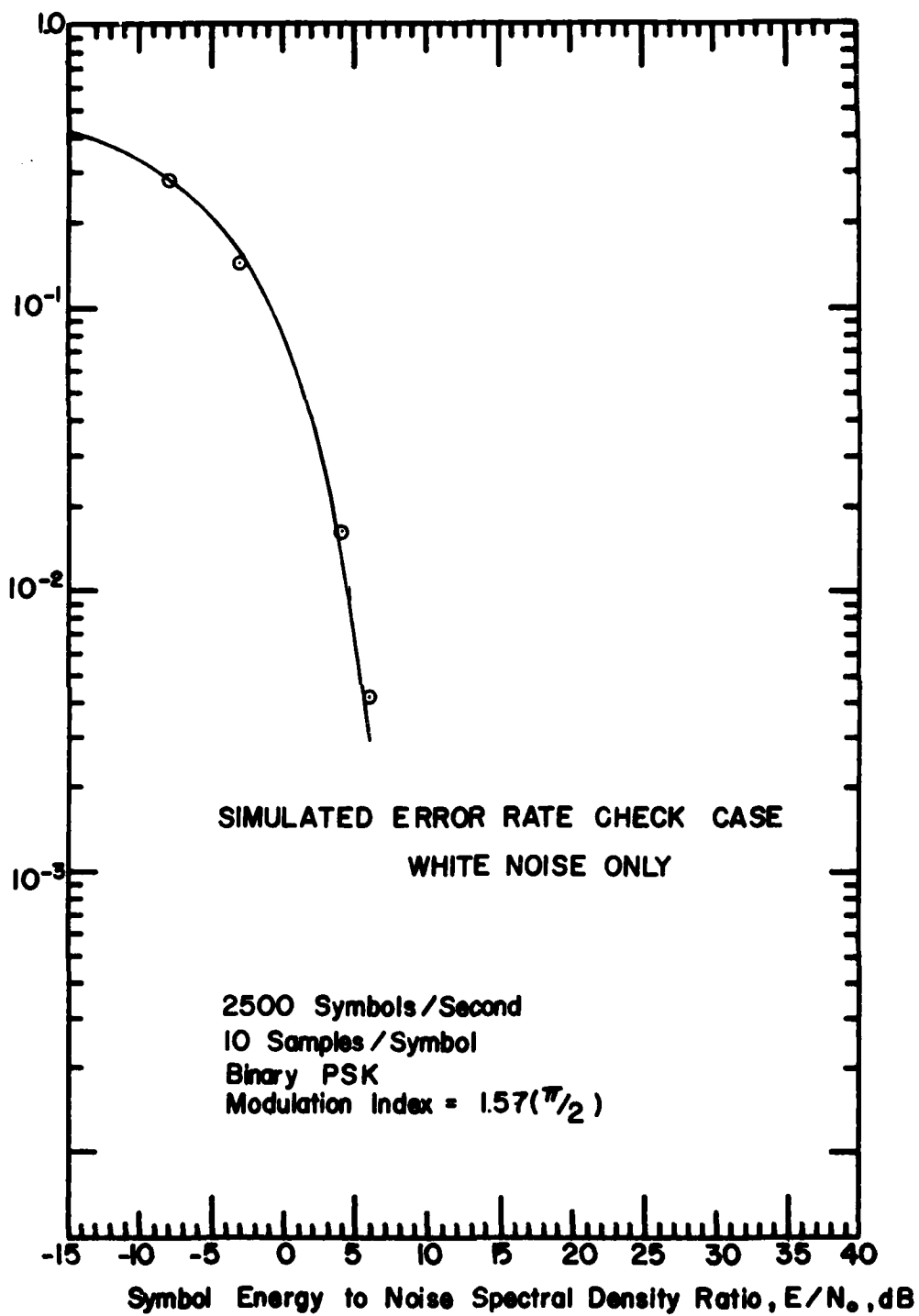


Figure 7. Simulated Error Rate Check Case

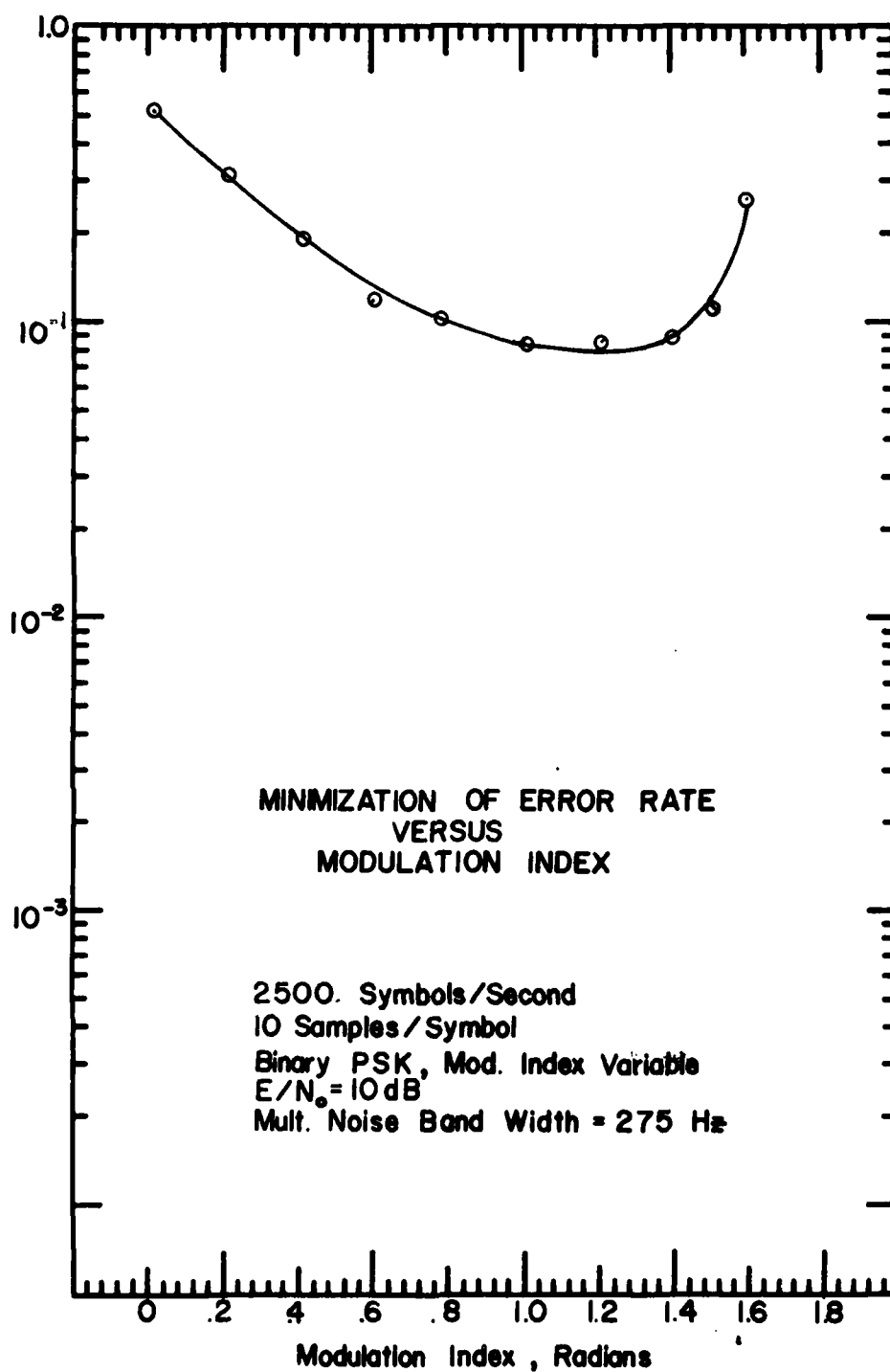


Figure 8. Minimization of Error Rate Versus Modulation Index

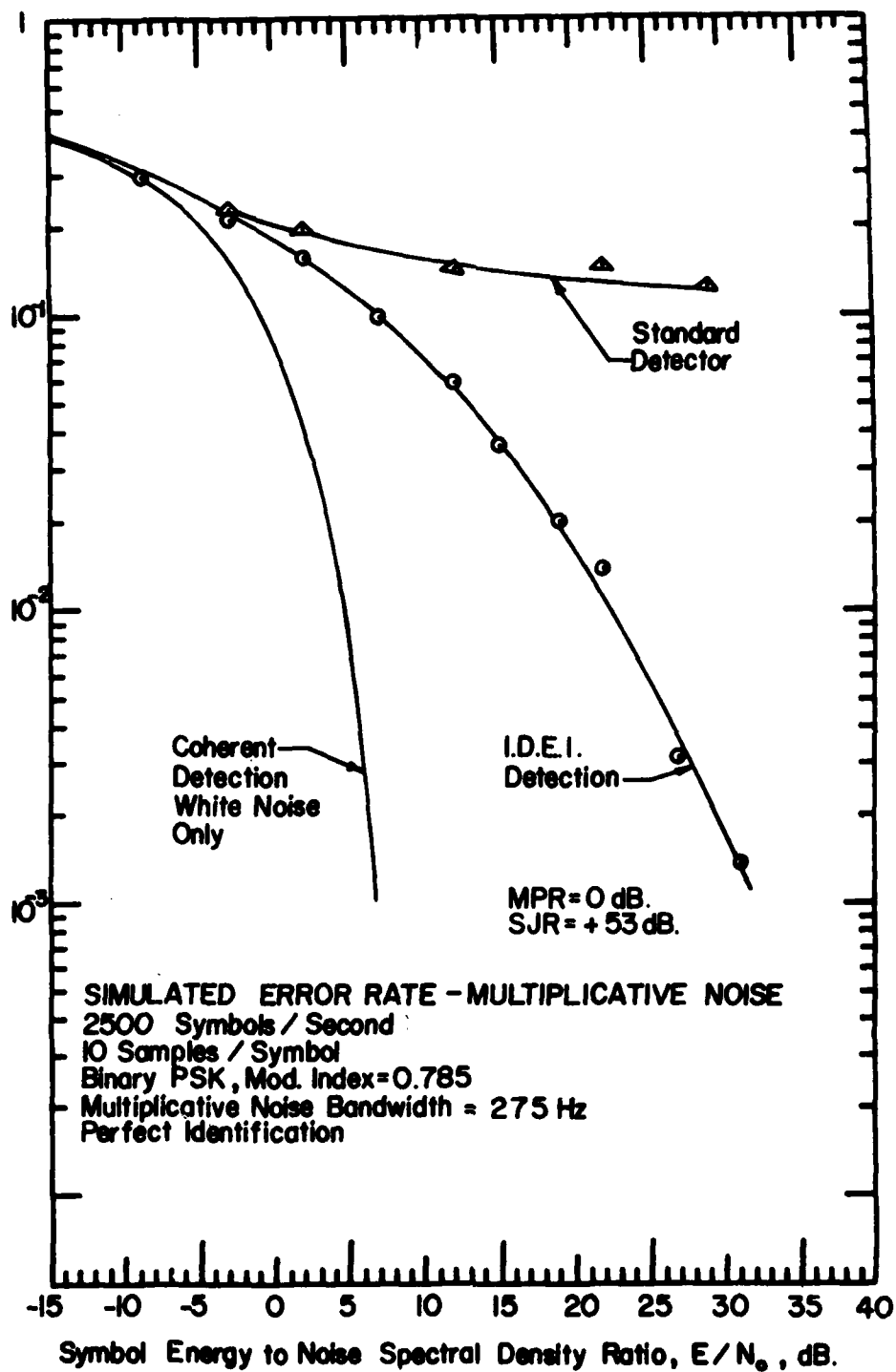


Figure 9. Simulated PSK Error Rate, Multiplicative Noise

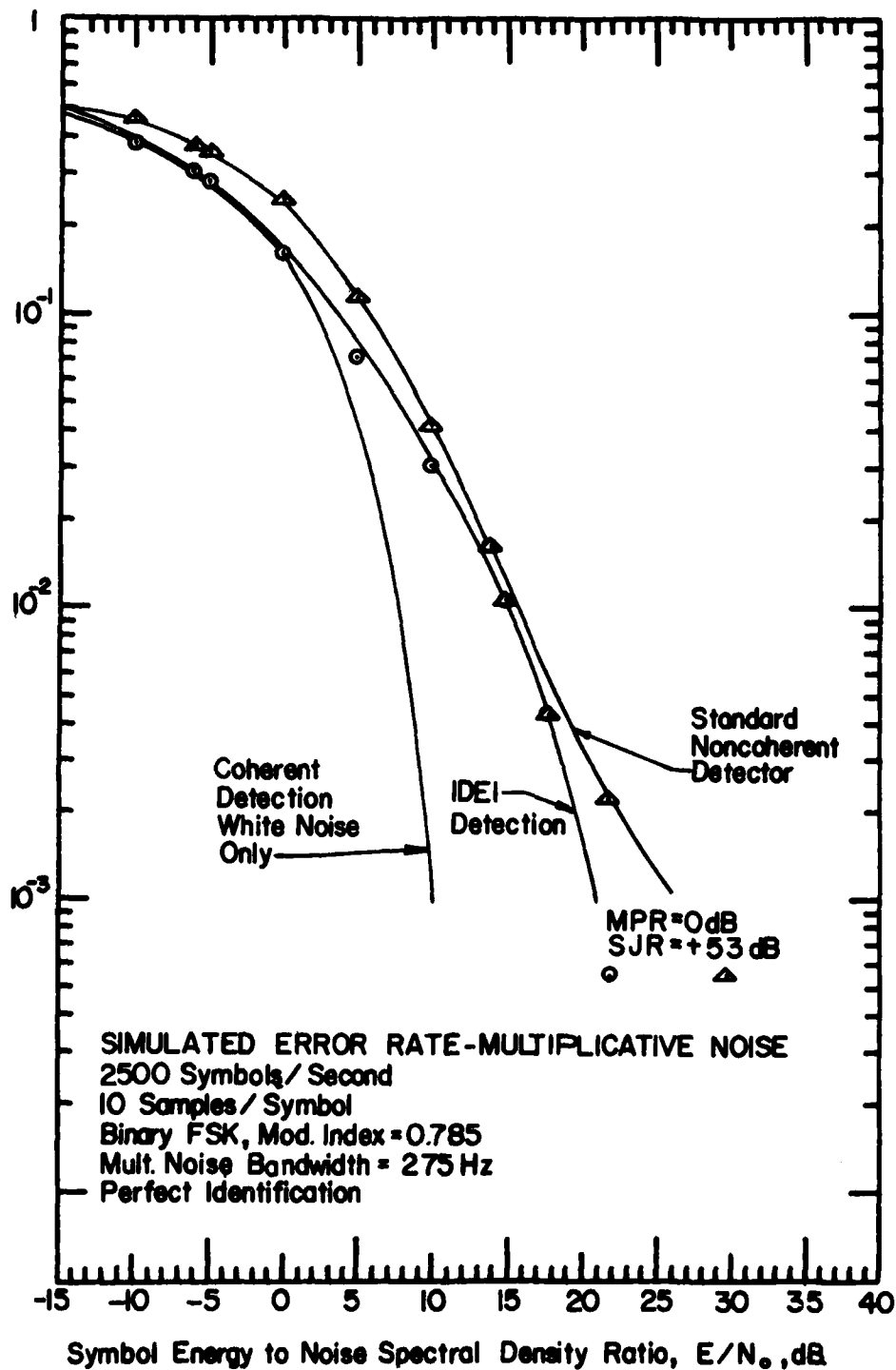


Figure 10. Simulated FSK Error Rate - Multiplicative Noise

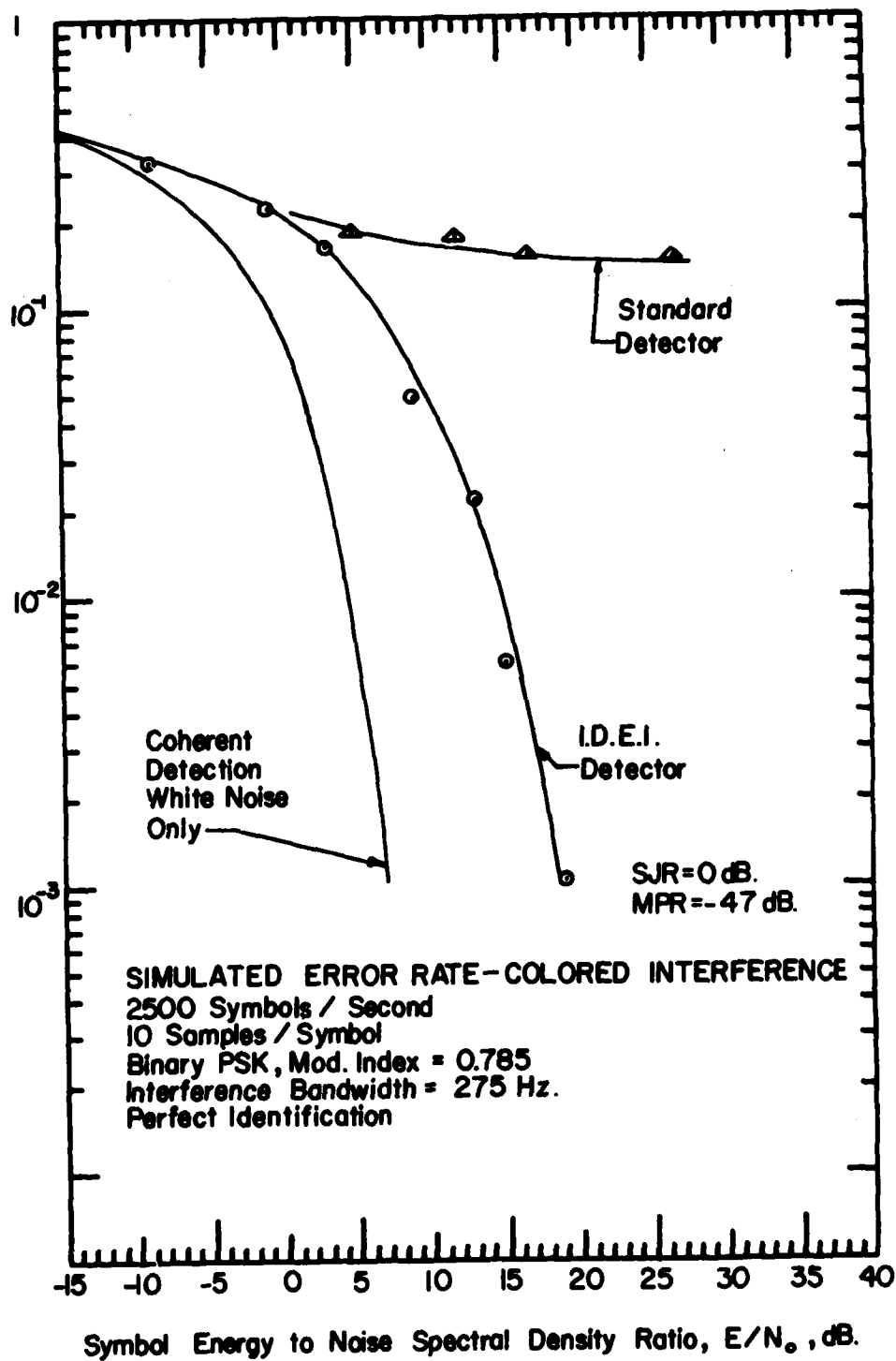


Figure 11. Simulated PSK Error Rate - Colored Additive Interference

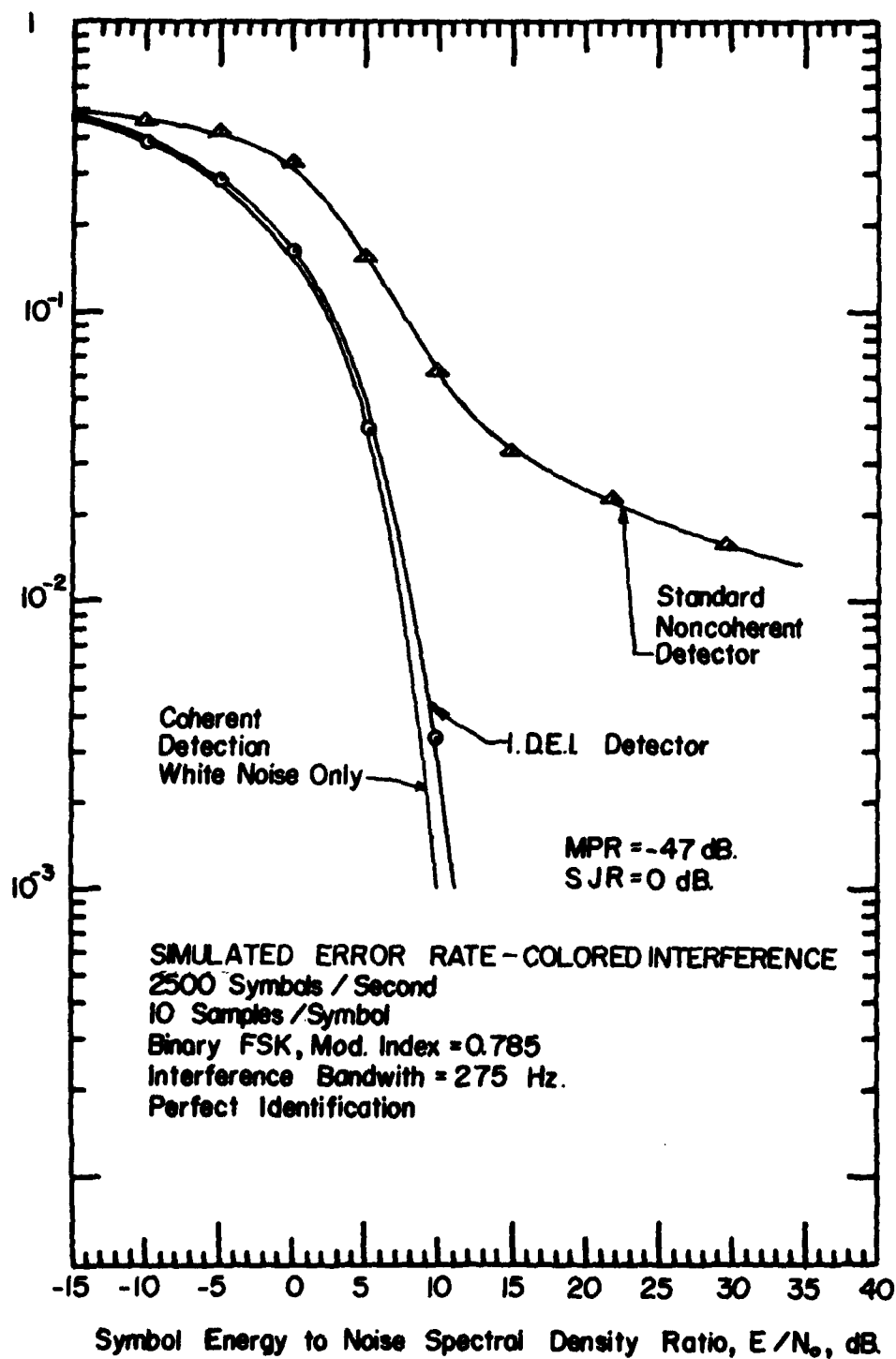


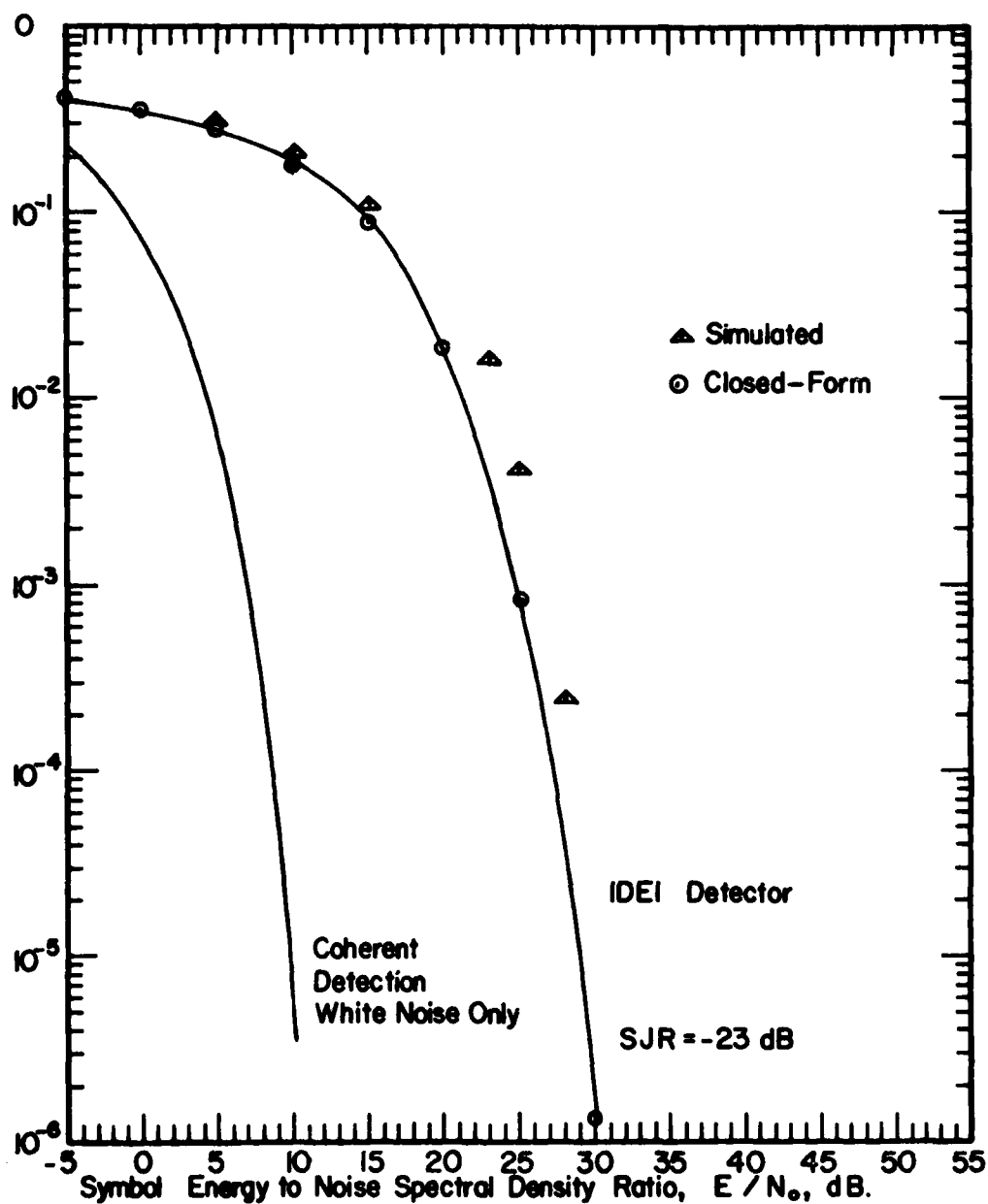
Figure 12. Simulated FSK Error Rate - Colored Additive Interference

The simulated results are plotted next to the closed-form solid curve. Note that the discrepancy between simulated and closed-form results here amounts to 1-2 dB of signal to white noise ratio, or a factor of 5-6 in error rate. The explanation is that when the ratio of colored interference to desired signal becomes quite large ( $SJR = -23$  dB), the detection errors are no longer independent and isolated. Rather, detection errors occur in "bursts" of 5 to 7. This is a consequence of improper decision-directed re-initialization of the tracking filters after a single detection error. In Figure 13, the standard detector error rate was 0.5 and was not plotted.

In Figure 14, the Monte Carlo and closed-form results are compared for the IDEI detector for FSK in heavy additive colored plus white interference. Again, the agreement between closed-form and simulation is good. However, the poor performance of FSK in Figure 14 relative to PSK in Figure 13 is surprising. This is the difference alluded to in Section II.2., on page 18. Figure 15 shows a similar FSK run for  $SJR = -20$  dB with the standard FSK detector closed-form and simulation results also plotted. It is apparent that the FSK results are valid. However, the difference between PSK and FSK results is not explainable on the basis of signal and noise spectra, as noted in section II.2.

Figures 16, 17, and 18 show the qualitative relationships between the PSK and FSK signal spectra and the colored noise spectra. In Figure 16 is shown the PSK spectrum (low-pass) for a 2500 symbol per second signal. Superimposed are narrow-band and full-band colored noise spectra for  $SJR = -5$  dB. The noise bandwidths are 275 Hz and 2744 Hz, respectively, which yield bandwidth to symbol rate ratios of  $BW/BR = 0.109$  and  $BW/BR = 1.09$ , respectively. As detailed in [1], the colored noise is generated from a filter having three real poles and one real zero (in the s-plane). Any desired noise bandwidth is obtained by simply scaling the poles and zeros by the same factor. The colored interferences used in Figures 9-15 had the spectral shape of the narrow-band noise shown in Figures 16 and 17. It is shown in Figure 16 that this type of colored interference decays in frequency as  $1/f^4$ , whereas the PSK spectrum decays as  $1/f^2$ .

In Figure 17 is shown the FSK signal spectrum corresponding to the model of equation (33). This spectrum also decays as  $1/f^2$ .

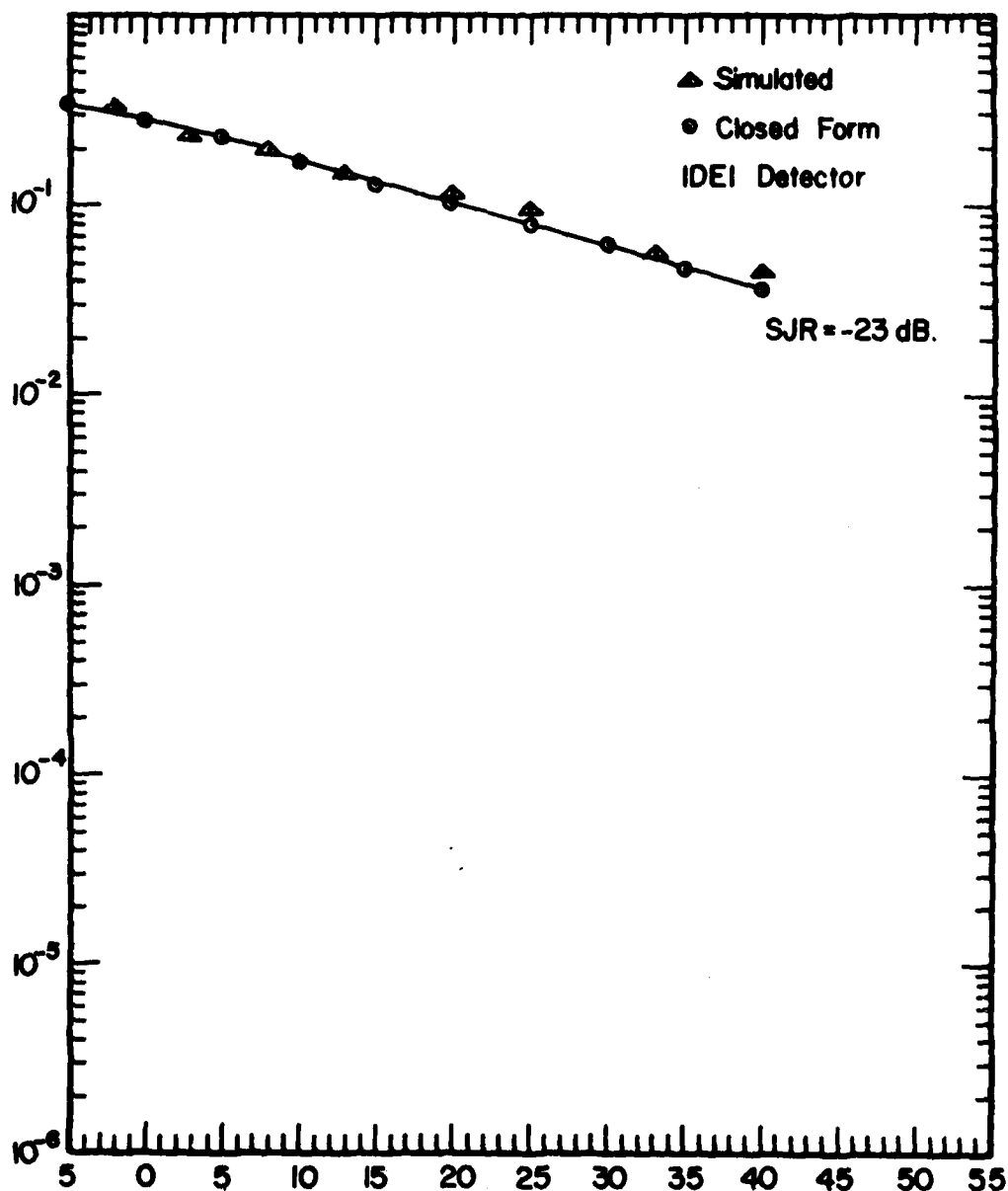


SYMBOL ERROR RATE-NARROW-BAND INTERFERENCE  
 2500 Symbols / Second  
 10 Samples / Symbol  
 Binary PSK, Mod. Index = 0.785  
 Interference Bandwidth = 275 Hz.  
 Perfect Identification

Aggle Form No. 2  
 P & P Graphics

Figure 13. Simulated and Closed-Form PSK  
 Error Rate - Narrow-band Interference





Symbol Energy to Noise Spectral Density Ratio,  $E/N_0$ , dB.

2500 Symbols / Sec.

10 Samples / Symbol

Binary FSK, Mod. Index = 0.785

Interference Bandwidth = 275 Hz.

Perfect Identification

Aggie Form No. 2

**SYMBOL ERROR RATE-NARROW-BAND INTERFERENCE**

Figure 14. Simulated and Closed-Form FSK  
Error Rate - Narrow-band Interference

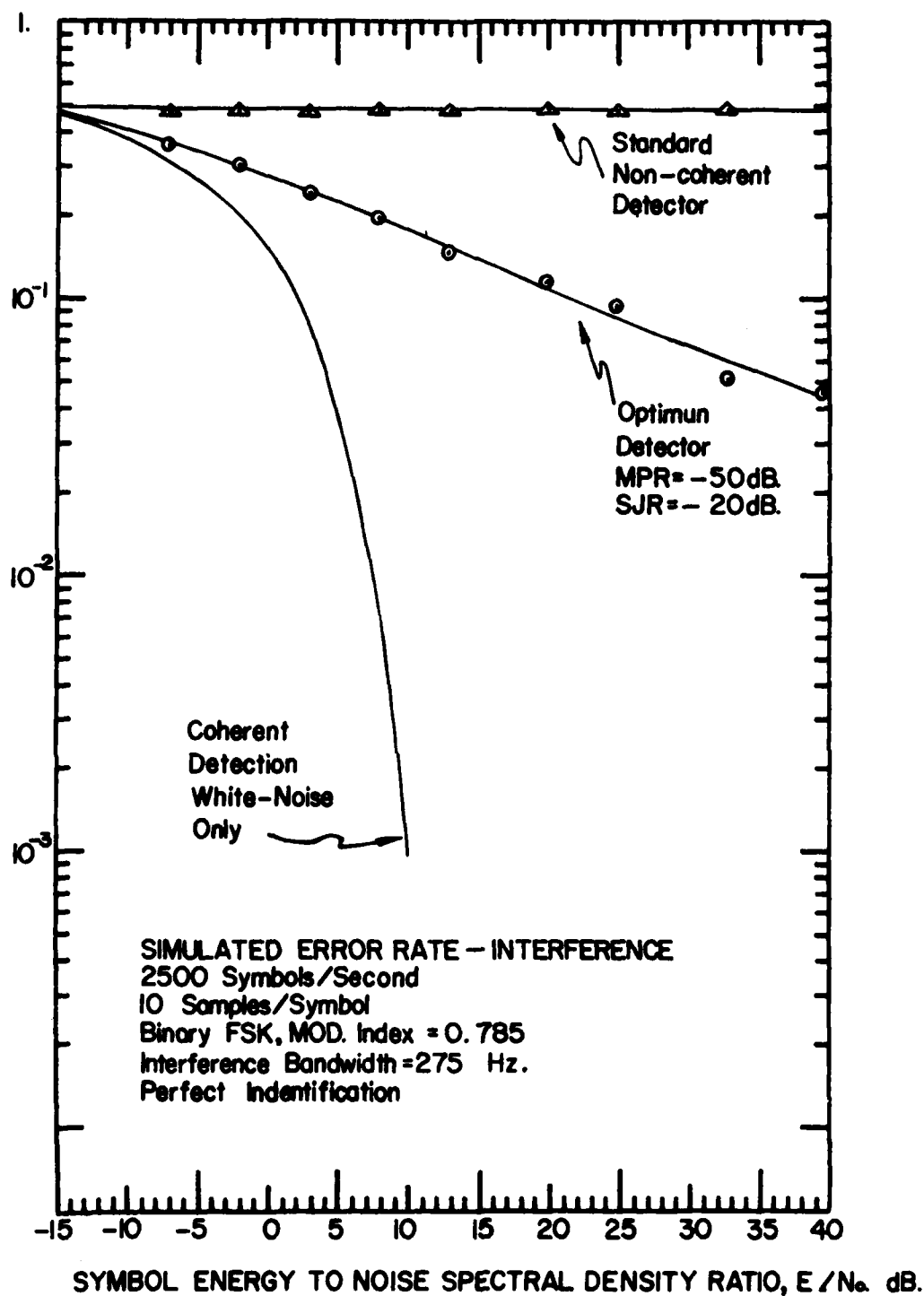
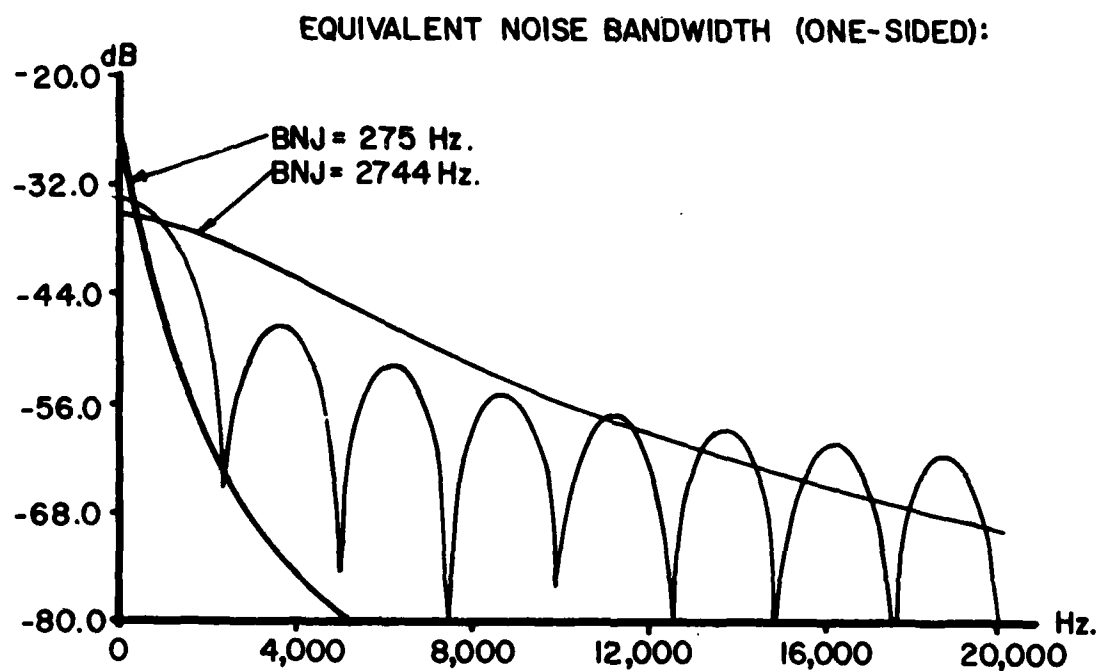


Figure 15. IDEI and Standard Detector Error Rates for FSK in Colored Interference



Phase Shift Keyed Signal Spectrum, Mod. Index = 0.785  
 Symbol Rate = 2500 / Sec.  
 Signal to RFI Ratio: SJR = -5 dB  
 RFI Filter: 3 pole, 1-zero

Figure 16. Spectra of PSK and Full-band  
 Colored Interference of the First Kind

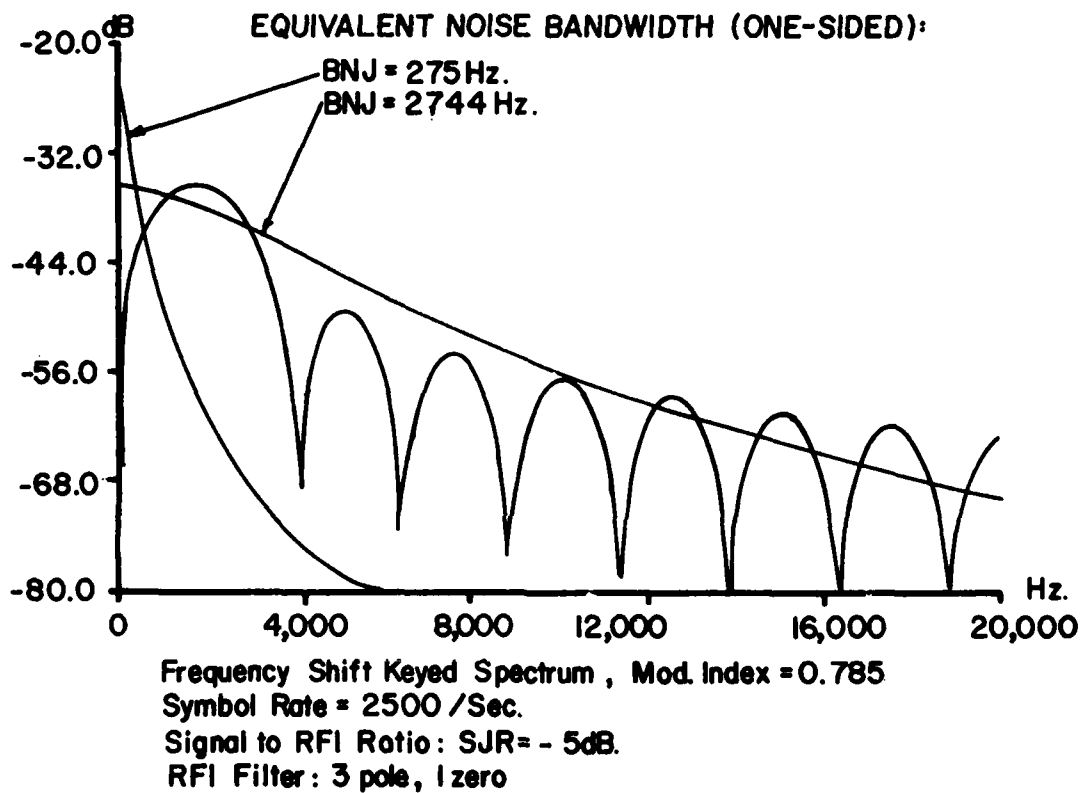


Figure 17. Spectra of FSK and Full-band Colored Interference of the First Kind

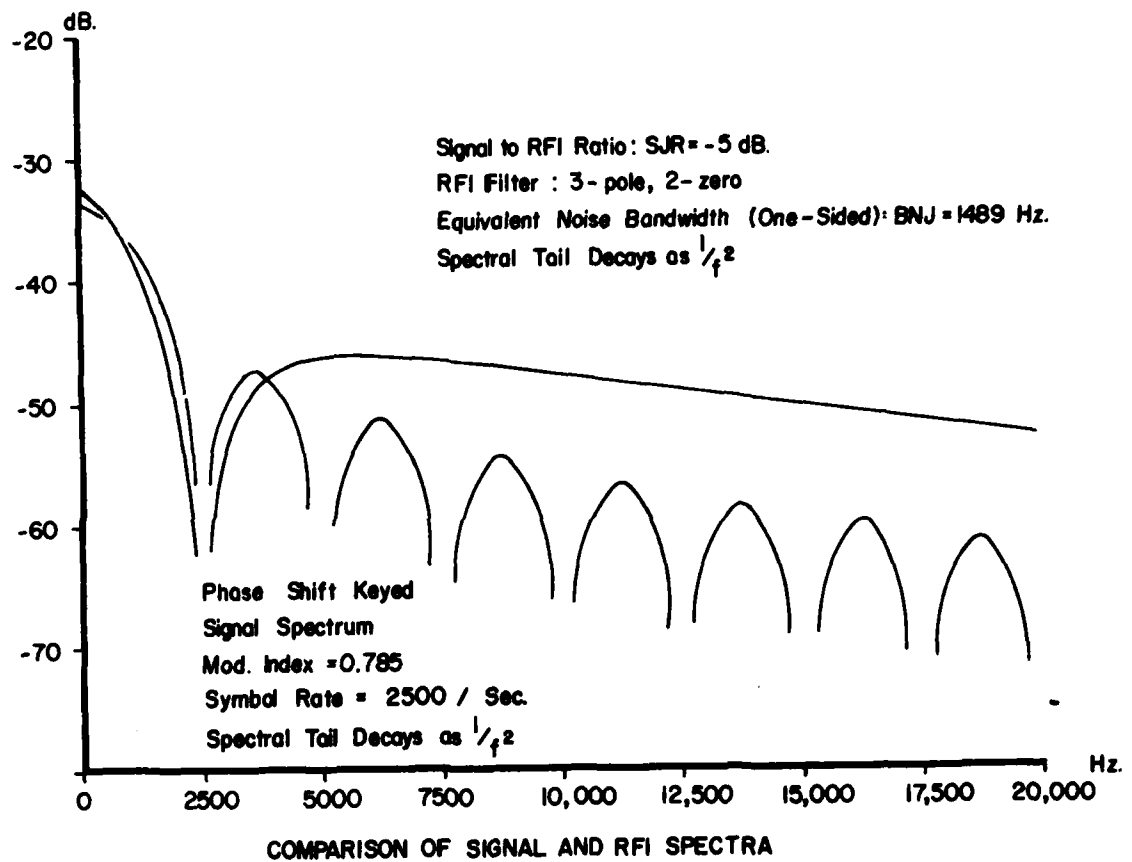


Figure 18. Spectra of PSK and Full-band Colored Interference of the Second Kind

In Figure 18 is shown a second type of available colored interference spectrum. This spectrum is synthesized by using 3 real poles and 2 imaginary zeroes (in the s-plane). The resulting null in the interference spectrum was placed coincident with the first null in the PSK signal spectrum. The interference spectrum decays at the same rate as the PSK spectrum, i.e., as  $1/f^2$ . It was hypothesized that such an interference spectrum would be a "worst case" for a PSK signal.

Figure 19 shows IDEI results for PSK and FSK in fullband interference of the first kind, which decays as  $1/f^4$ . Here the colored interference was as in Figure 16 with a strength 20 dB greater than that of the desired signal. Again the comparison of Monte Carlo and closed-form results is good, under the observation that the IDEI errors are occurring in bursts.

## 2. IDEI CLOSED-FORM PERFORMANCE FOR PSK IN COLORED INTERFERENCE WITH PERFECT IDENTIFICATION

At this point in the investigation, it was decided to devote the remaining time and resources to an in-depth examination for one signal type and one interference type. The signal chosen was PSK. The concentration on additive colored interference rather than multiplicative interference was implied by two factors. First, behavior of the IDEI detector for multiplicative noise has been rather thoroughly investigated previously, as reported in [3]. Also, the initial results presented in Figures 9 and 10 for PSK and FSK were not qualitatively different than those in [3] for a hybrid PSK-FSK 4-ary modulation. Second, the results for additive colored noise are of great interest in the context of radio jamming.

Figure 20 shows the first closed-form results for IDEI error-rate for PSK in additive colored plus white noise. Here, error rate is plotted versus a normalized colored interference bandwidth. The abscissa is the ratio of colored interference (equivalent) noise bandwidth to symbol rate,

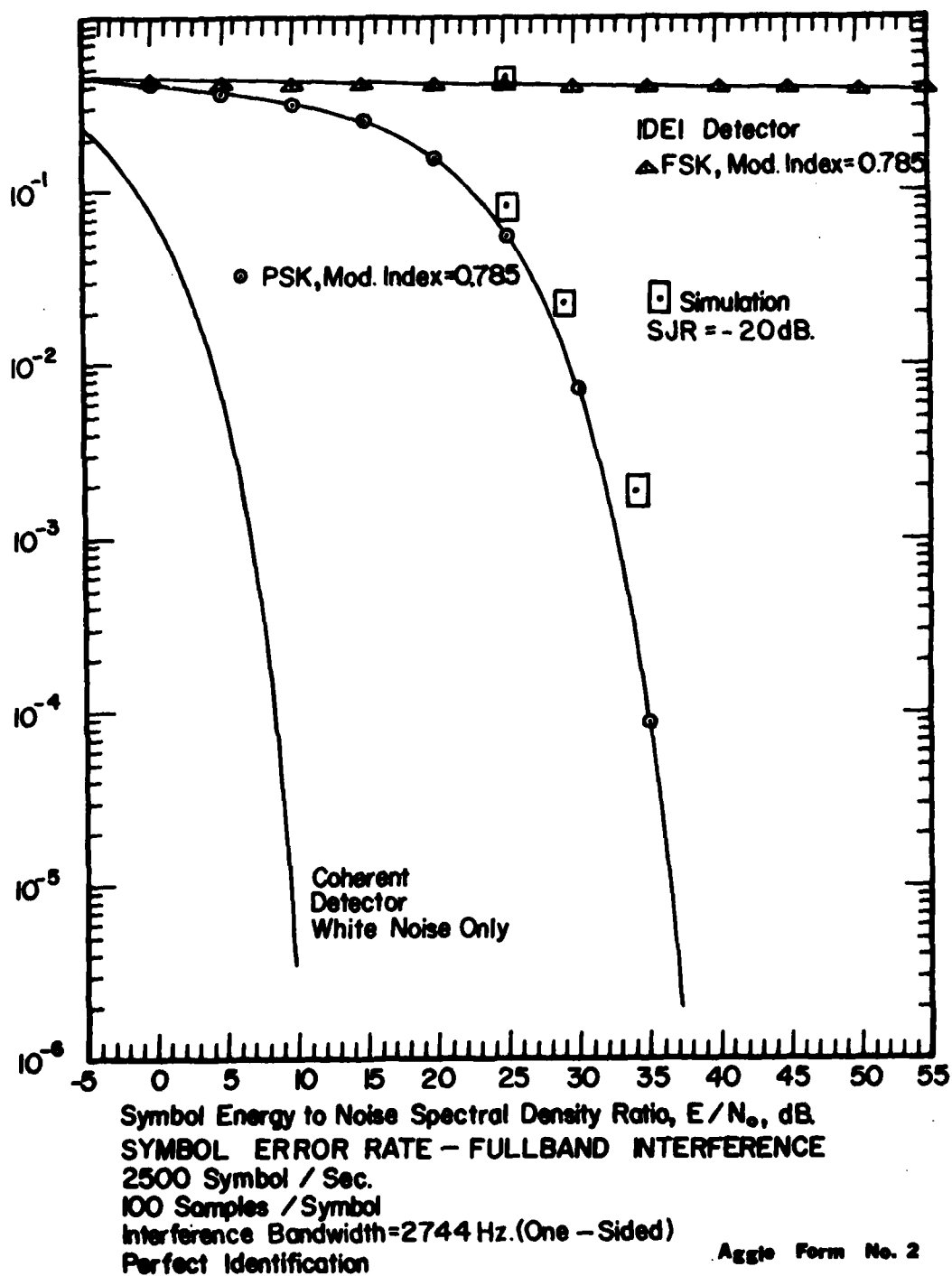
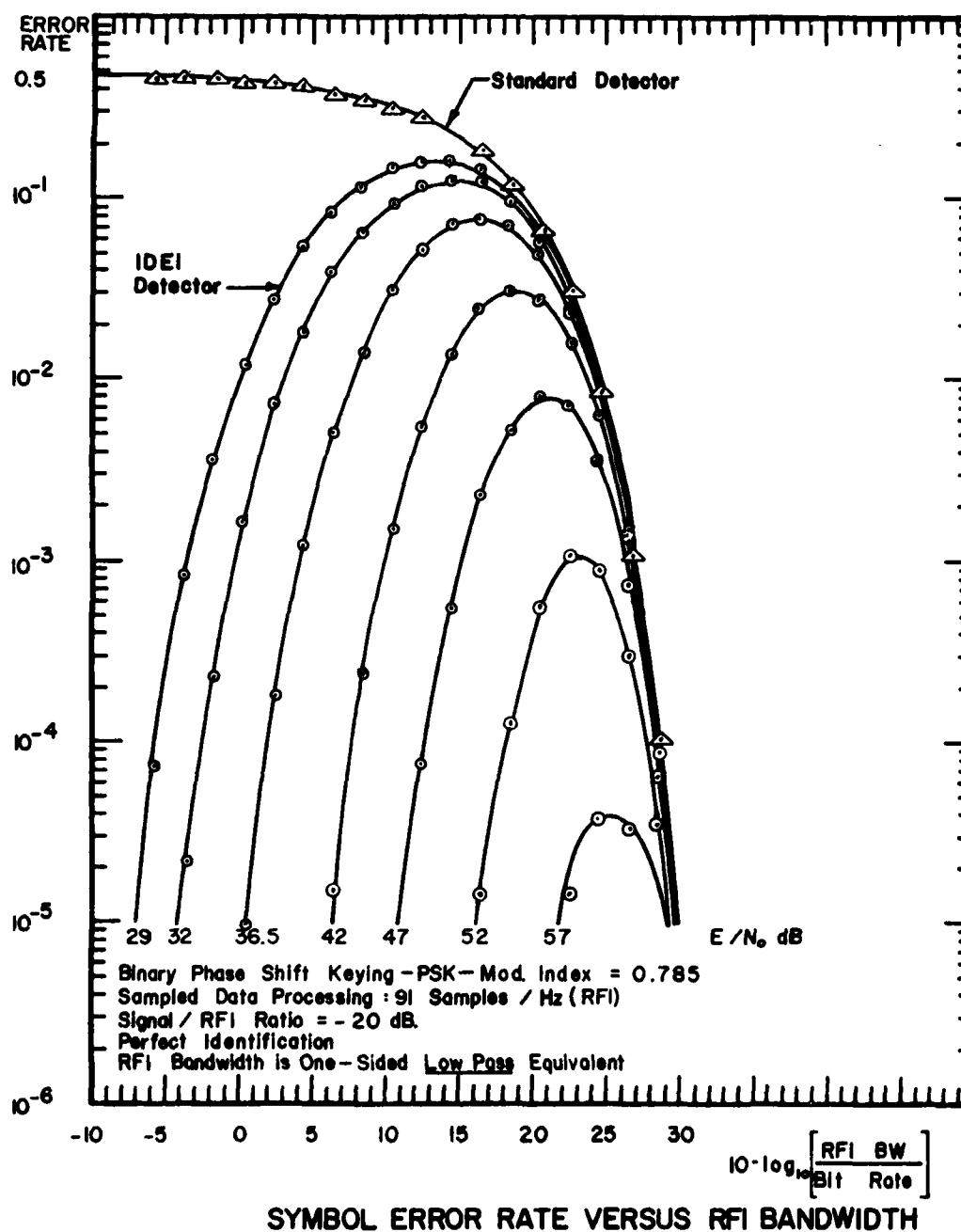


Figure 19. PSK and FSK Error Rates for the IDEI Detector in Full-band Colored Interference of the First Kind



Aggie Form No. 2  
 P & P Graphics

Figure 20. IDEI and Standard Error Rates Versus Normalized Interference Bandwidth, With  $E/N_0$  as Parameter



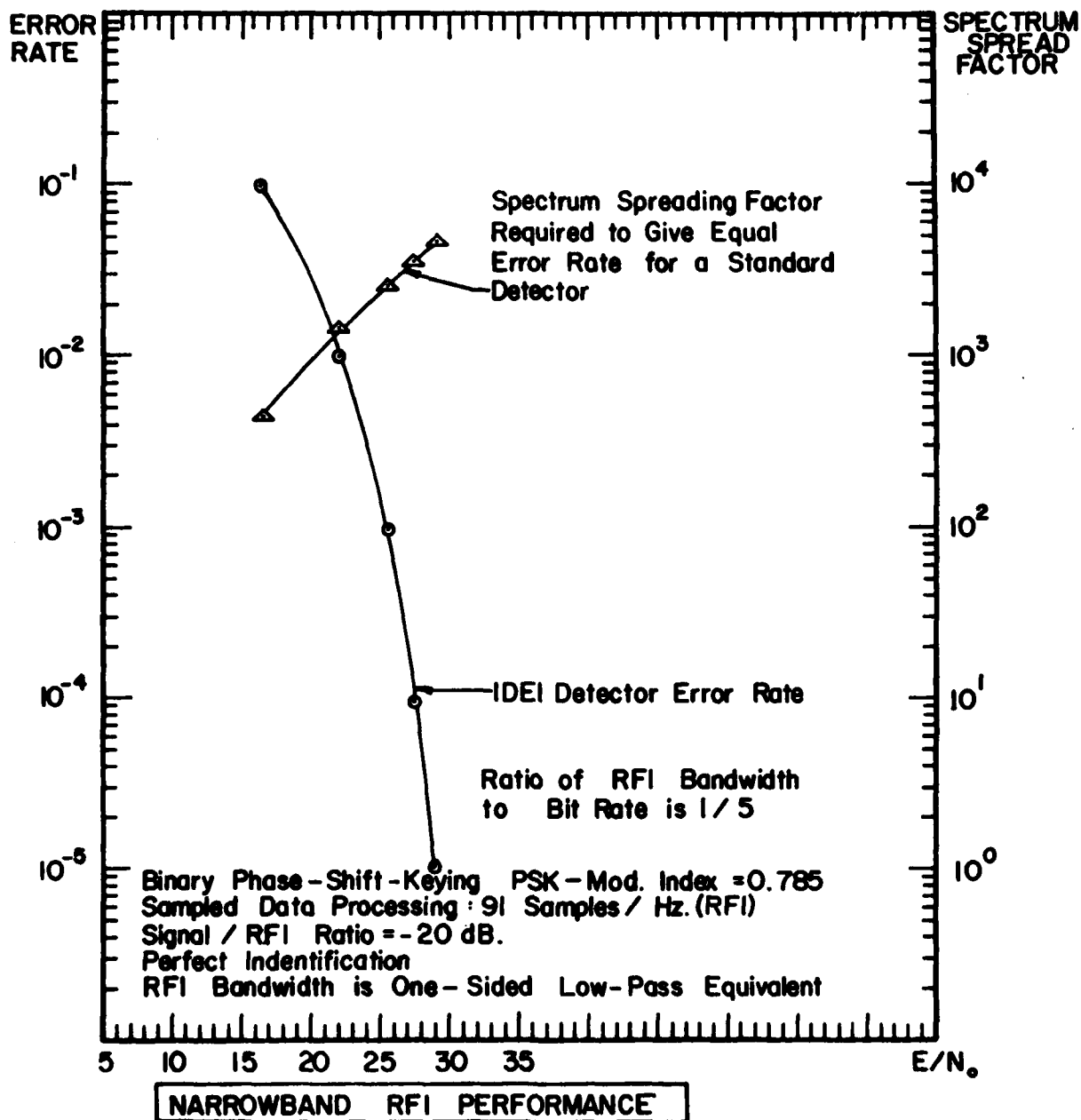
in decibels ( $10 \log_{10}(\cdot)$ ). A family of IDEI curves is plotted with  $E/N_0$  as parameter. The ratio of colored interference to desired signal power is 20 dB (SJR = -20 dB). The performance for the standard PSK detector is also plotted for comparison.

Figure 20 shows three general results of considerable interest. First, there is a worst case colored interference bandwidth which maximizes the error rate for each value of  $E/N_0$ . Second, the worst case maximum error rate decreases and the worst case bandwidth increases with increasing  $E/N_0$ . Third, for a given value of  $E/N_0$ , the IDEI detector error rate converges to that of the standard detector as the colored interference bandwidth increases.

An obvious inference to be drawn from Figure 20 is that the IDEI detector provides the most "gain" over a standard detector when the colored interference is narrow-band compared to the desired signal. A second inference is that under mini-max, or worst case, conditions, the IDEI detector still provides some gain over a standard detector. Two subsidiary figures, derived from Figure 20, illustrate these points.

In Figure 21 is plotted the IDEI error-rate performance versus  $E/N_0$  for PSK subject to 20 dB colored interference having normalized bandwidth,  $BW/BR = 1/5$ . For each IDEI error-rate point plotted in 21 it may be determined from 20 what value of  $BW/BR$  is required for the standard detector to yield an equal error rate. Thus, the required spectrum-spreading factor is determined and plotted in Figure 21. For  $BW/BR = 1/5$ , it is seen that the IDEI detector yields the same performance as would be obtained from a standard detector using spectrum-spreading by a factor of  $10^3 - 10^4$  for error rates of  $10^{-1} - 10^{-5}$ .

In Figure 22, the worst-case IDEI error-rates are plotted versus  $E/N_0$ . Each IDEI error-rate point corresponds to a unique value of  $BW/BR$ . The corresponding standard detector error-rate points are also plotted. It is seen that even under worst case conditions the IDEI detector has a 10 dB advantage over the standard detector in terms of white noise  $E/N_0$  ratio. For information purposes, the worst case bandwidth for the colored interference is plotted versus  $E/N_0$ . This plot shows that the worst case interference bandwidth for the IDEI detector is always considerably greater than the desired signal bandwidth. The converse is true for the standard detector, for which the worst case interference is narrow-band. These

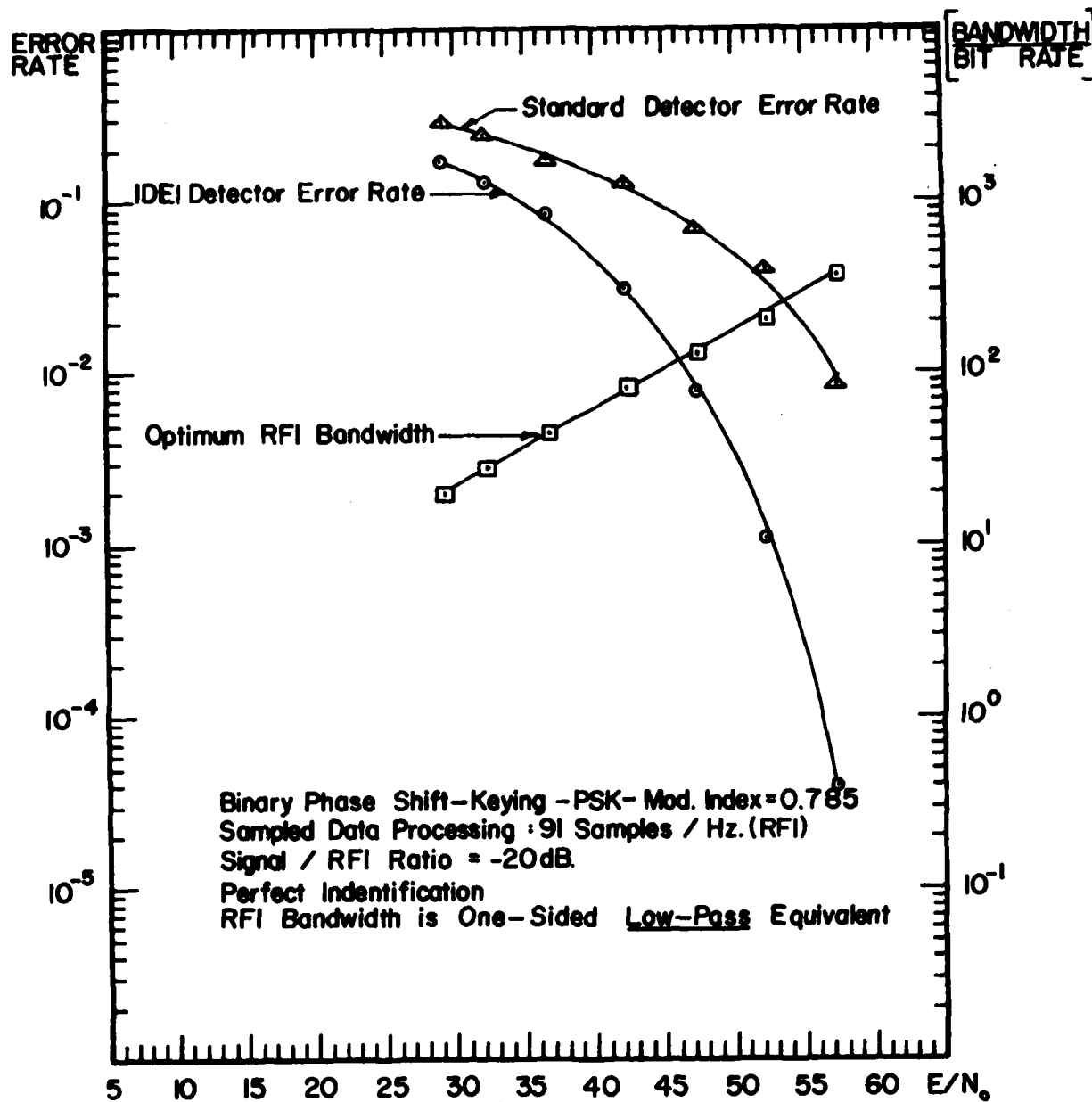


**IDEI SYMBOL ERROR RATE AND REQUIRED SPECTRUM SPREAD FACTOR FOR AN EQUIVALENT STANDARD DETECTOR**

**Aggie Form No. 2**

**P&P Graphics**

**Figure 21. Spread-Spectrum Equivalence of IDEI Detection for Narrow-band Interference**



**WIDE BAND RFI PERFORMANCE**

SYMBOL ERROR RATE - WORST CASE RFI  
 AND OPTIMUM RFI BANDWIDTH

Aggie Form No. 2  
 P & P Graphics

Figure 22. Worst Case IDEI Performance and  
 Optimum Interference Bandwidth

observations are based on the assumption that the interference source does not possess the sophistication to generate a spectrum which duplicates the signal spectrum.

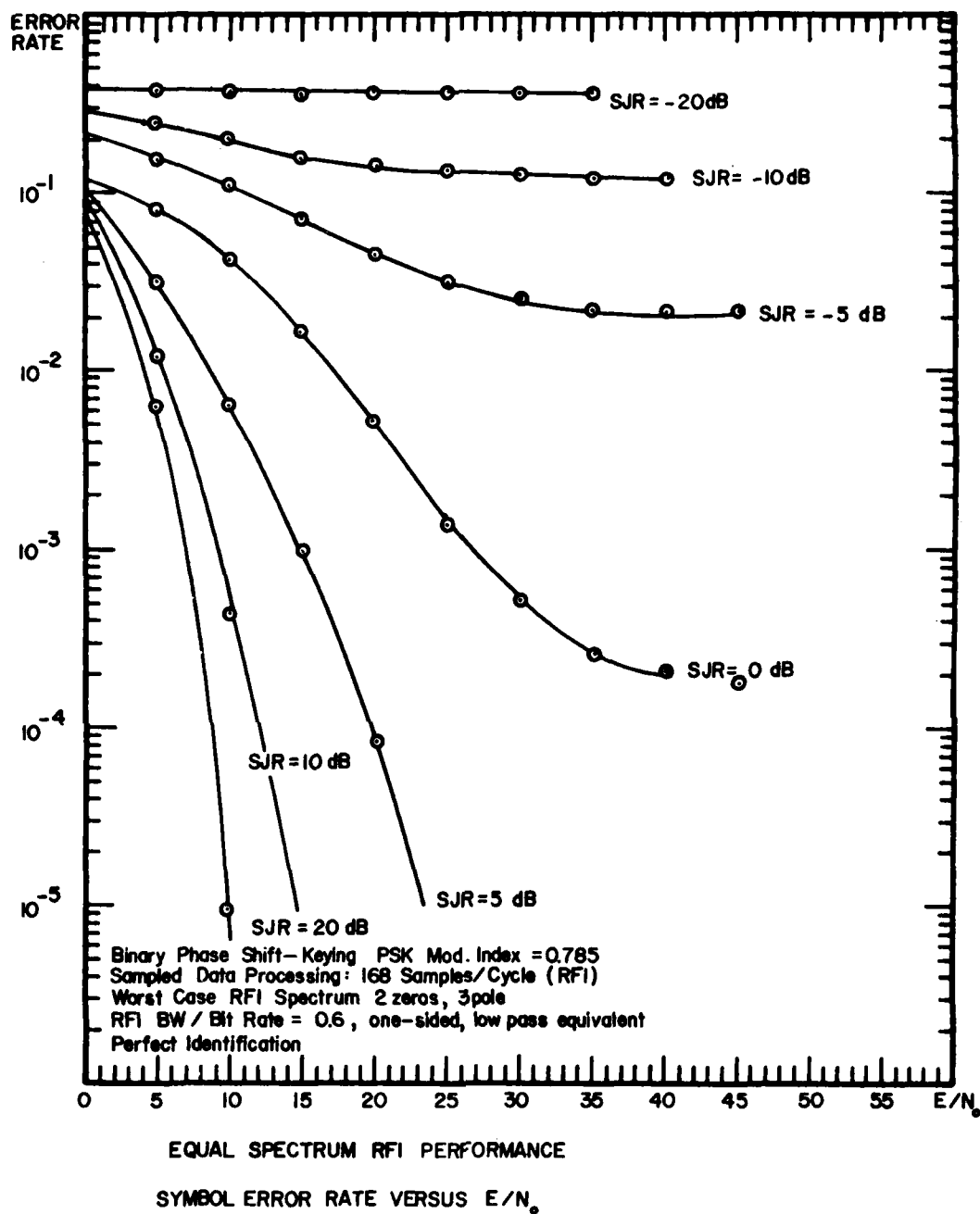
Figure 23 shows the results of the first attempt to evaluate the performance for colored additive noise of the second kind, whose spectral shape was shown in Figure 18. It is known that the observed saturation of the error-rate versus  $E/N_0$  occurs when there is an unmodelled disturbance present which has not been included in derivation of the detection algorithm. It was hypothesized that the unmodelled disturbance was aliasing, due to the considerable high frequency content of the colored interference. Thus, the case for  $SJR = -5$  dB was rerun with sampling rate increased by a factor of 10. The results are shown in Figure 24, confirming aliasing as the unmodelled disturbance.

In Figure 25, IDEI results are plotted for PSK subject to both types of full-band colored interference with  $SJR = -20$  dB. The better performance resulted for the full band interference spectrum with  $BW/BR = 1.09$  which decayed as  $1/f^4$ . The worse performance resulted for the interference spectrum which decayed as  $1/f^2$ . It is not known whether or not the slight indication of saturation for  $45 \text{ dB} < E/N_0$  is due to aliasing.

Figure 26 shows the results of the first attempt to evaluate the IDEI error-rate as a function of the ratio of colored interference to desired signal power ( $SJR$ ). Families of curves were plotted with normalized interference bandwidth ( $BW/BR$ ) as parameter. For each value of  $BW/BR$  a different value of  $E/N_0$  was used. This was because certain combinations of  $BW/BR$ ,  $E/N_0$ , and  $SJR$  caused the solutions on the 16-bit minicomputer to become numerically unstable.

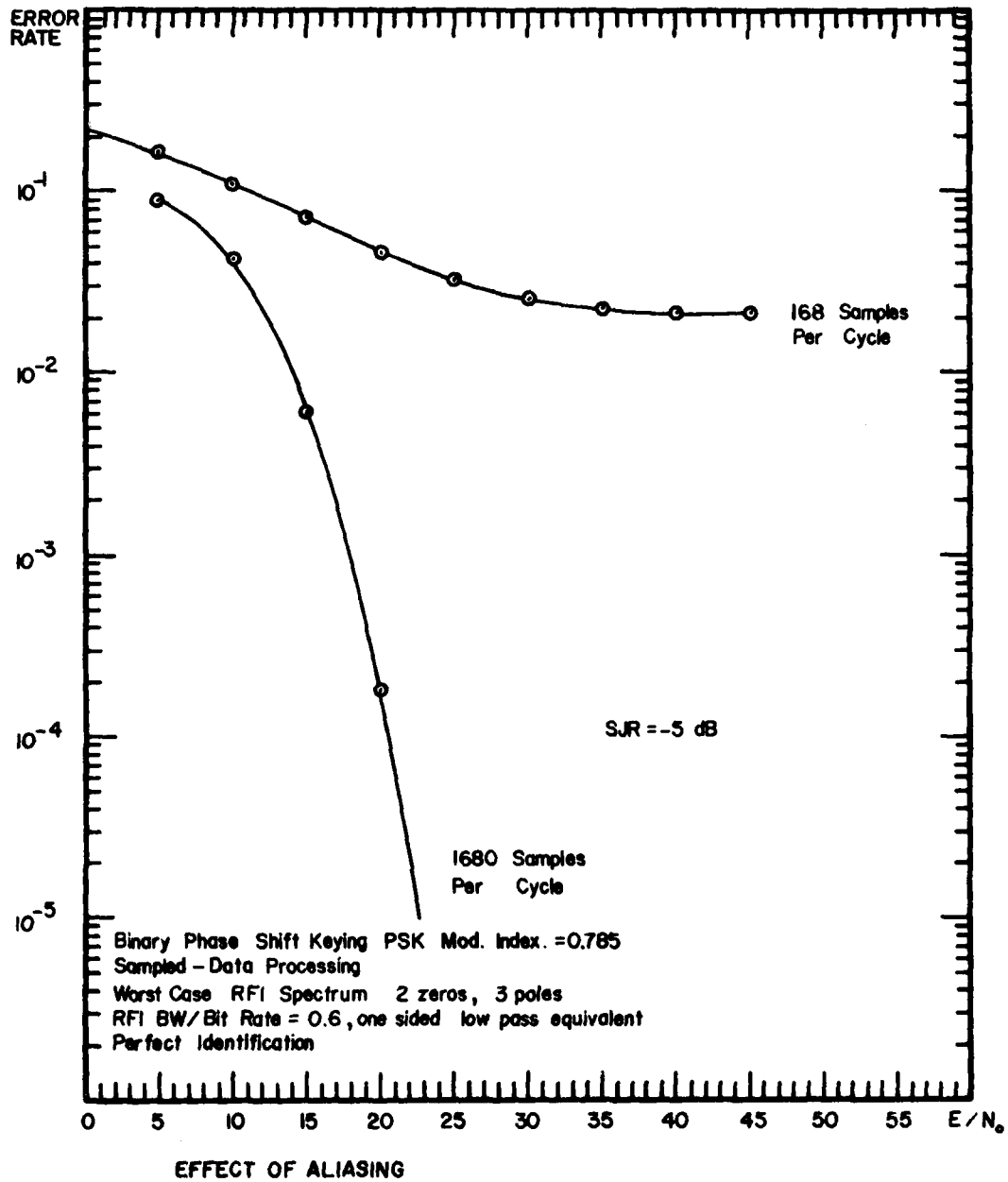
It was found that when cases were run where the ratio of interference power to white noise power (in the interference bandwidth),  $J/N$ , was greater than 60 dB, the numerical computer solution became unstable on the 16-bit PDP 11/40. This did not occur on the 60-bit CDC-6600. However, it was decided to limit the runs to conditions for which  $J/N < 60$  dB. The ratio,  $J/N$ , is related to the other parameters as

$$\frac{J}{N} = \frac{(E/N_0)}{(BW/BR) \cdot SJR \cdot L(\Delta\phi)} \quad (161)$$



Aggie Form No. 2  
 P & P Graphics

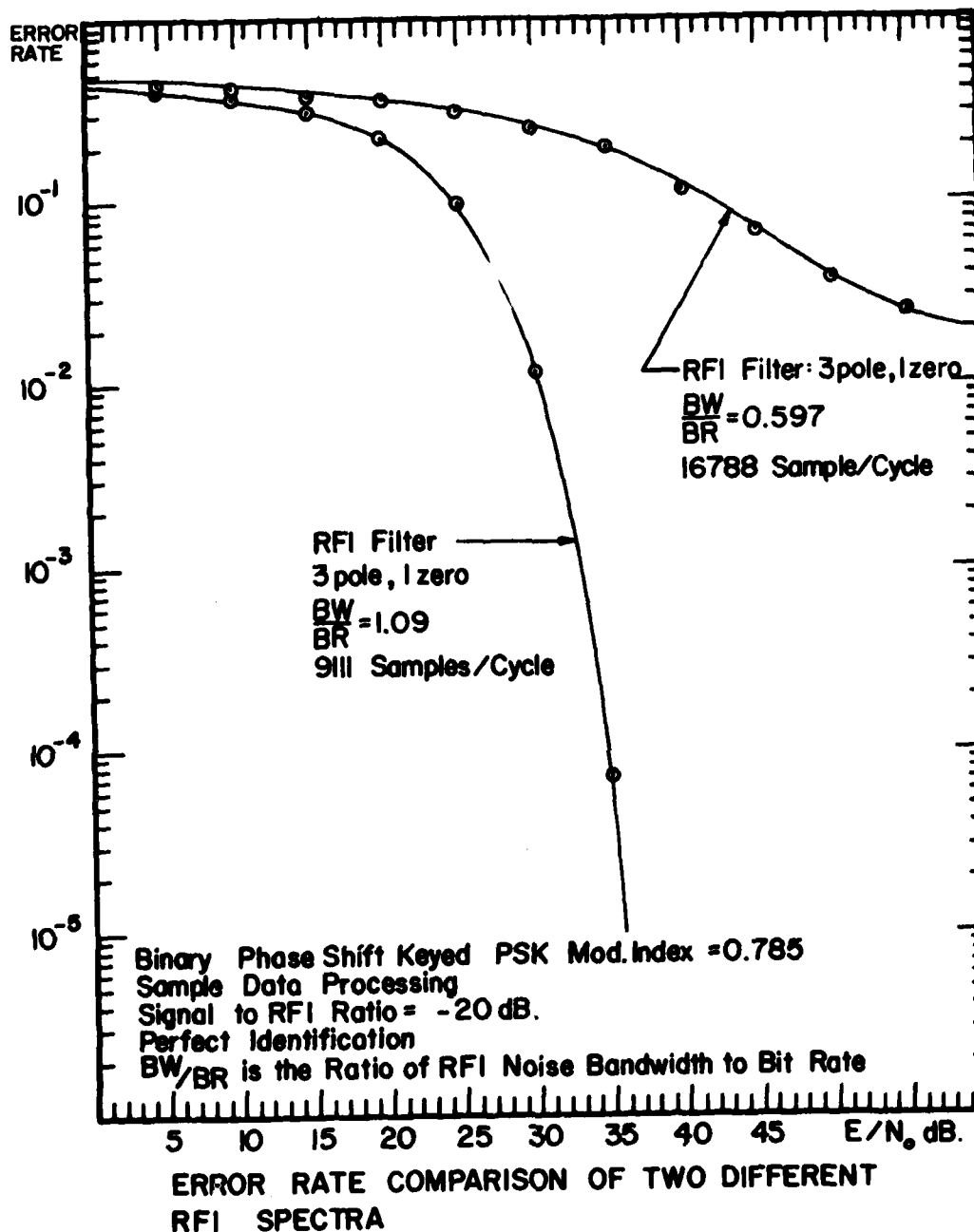
Figure 23. IDEI Performance for Colored Interference  
 of the Second Kind - Aliased Results



SYMBOL ERROR RATE VERSUS  $E/N_0$   
 RFI SPECTRUM SIMILAR TO SIGNAL SPECTRUM

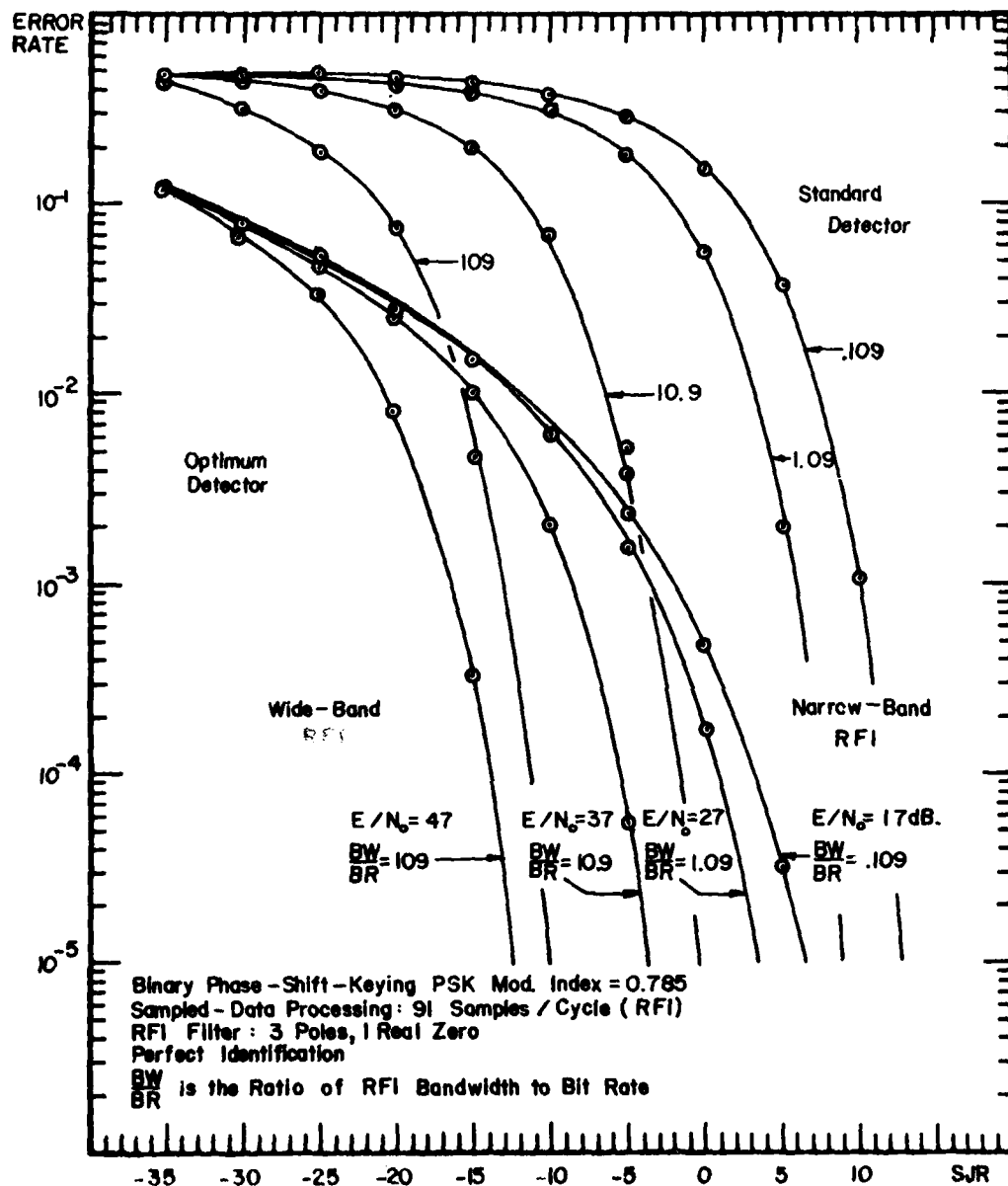
Aggie Form No. 2  
 P&P Graphics

Figure 24. Confirmation of Aliasing for Colored  
 Interference of the Second Kind



Aggie Form No. 2  
P&P Graphics

Figure 25. Comparison of Results for Both Kinds  
of Additive Colored Interference



SYMBOL ERROR RATE VERSUS SIGNAL TO RFI POWER RATIO WITH NORMALIZED RFI BANDWIDTH AS PARAMETER

Aggie Form No. 2  
 P&P Graphics

Figure 26. IDEI and Standard Detector Performance Versus Ratio of Signal to Colored Interference Power



In (161),  $L(\Delta\phi)$  is the modulation loss defined in (56).

In Figure 26, the values of  $E/N_0$  used were those required to set  $J/N = 60$  dB when  $SJR = -35$  dB. Under these conditions, it appears that the error rate performances of both the standard and optimum detectors increase as the colored interference bandwidth becomes greater. However, this apparent performance increase is illusory and does not occur if  $E/N_0$  is held constant as per Figure 20.

Figures 27 through 30, inclusive, show a series of four families of error-rate curves for standard and IDEI detectors. Each figure contains results for four values of normalized interference bandwidth,  $BW/BR = 0.109, 1.09, 10.9, \text{ and } 109.$ , respectively. From figure to figure,  $E/N_0$  is varied in 10 dB steps, from 17 in Figure 27 to 47 in Figure 30.

Note that in Figures 27 through 30, the standard detector performance is the same. This is because the standard detector error rate is dominated by the colored interfering process, rather than the white noise. The IDEI error-rate performance is seen to vary from figure to figure, depending on  $E/N_0$ . The general trend displayed is that the high-frequency tracking performance of the IDEI detector becomes better as  $E/N_0$  increases. In all cases the IDEI detector performs better than the standard. However, for a particular value of colored interference bandwidth, the margin of performance of the IDEI over the standard detector is a function of  $E/N_0$ .

Another method for comparing the performances of the IDEI and standard detector is to hold constant the ratio of colored interference power to white noise power in the bandwidth,  $1/T = BR$ , of a filter matched to the desired signal. The ratio,  $JT/N_0$ , is related to the other parameters as

$$\frac{JT}{N_0} = \frac{(E/N_0)}{L(\Delta\phi) \cdot SJR} \quad (162)$$

Figure 31 shows the results for four values of normalized bandwidth for the quantity  $JT/N_0$  held constant at a value of 70 dB. This shows rather clearly the SJR performance of the IDEI detector vis-a-vis the standard detector as a function of colored interference bandwidth.

AD-A082 327

TEXAS A AND M UNIV COLLEGE STATION DEPT OF ELECTRICAL--ETC F/6 17/4  
LOW COST ANTI-JAM DIGITAL DATA-LINKS TECHNIQUES INVESTIGATIONS.--ETC(U)  
MAY 79 J H PAINTER, C J YOON F33615-75-C-1011

UNCLASSIFIED

AFAL -TR-77-104-VOL-2

NL

2002

AD-A082 327



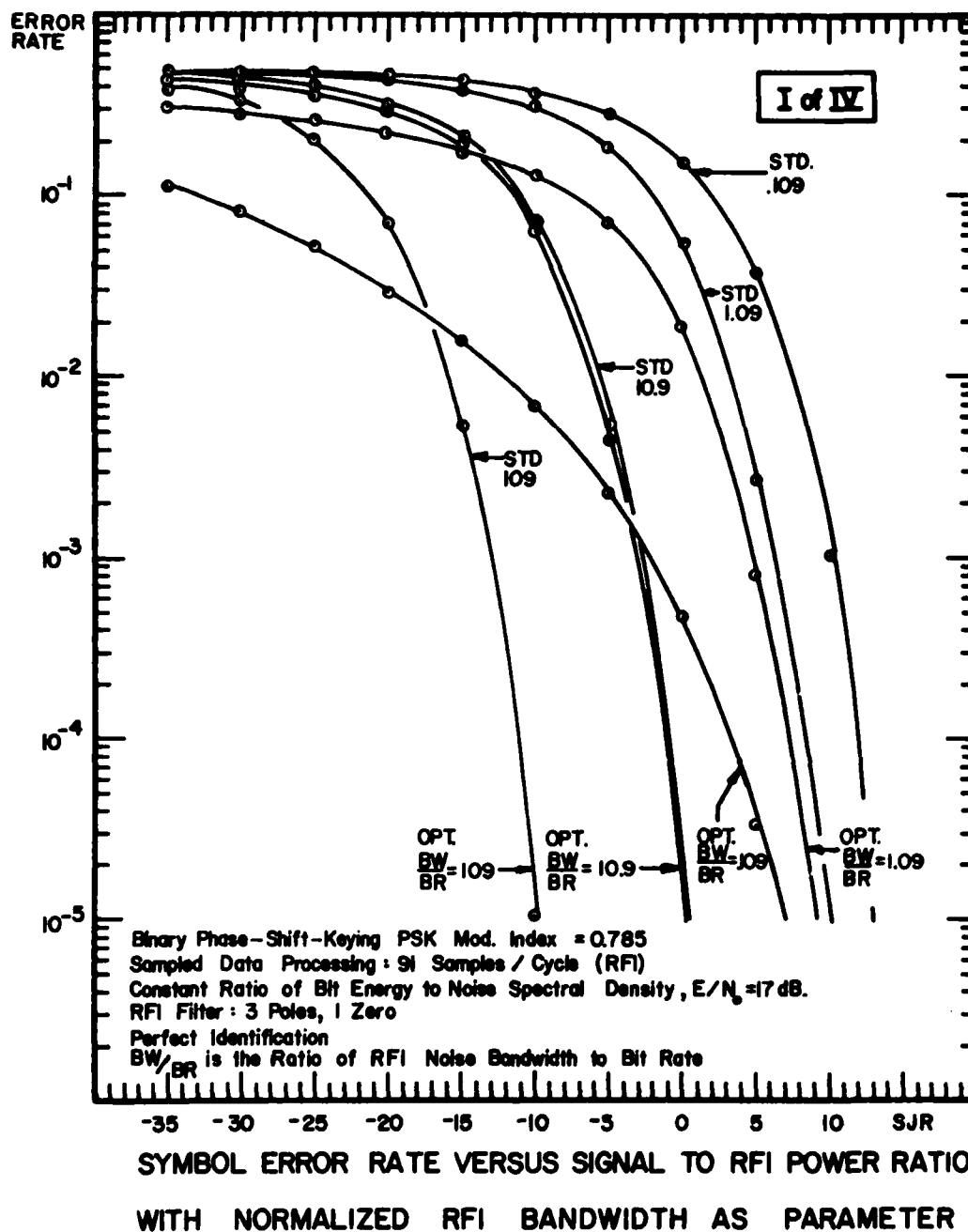

END

DATE

FILED

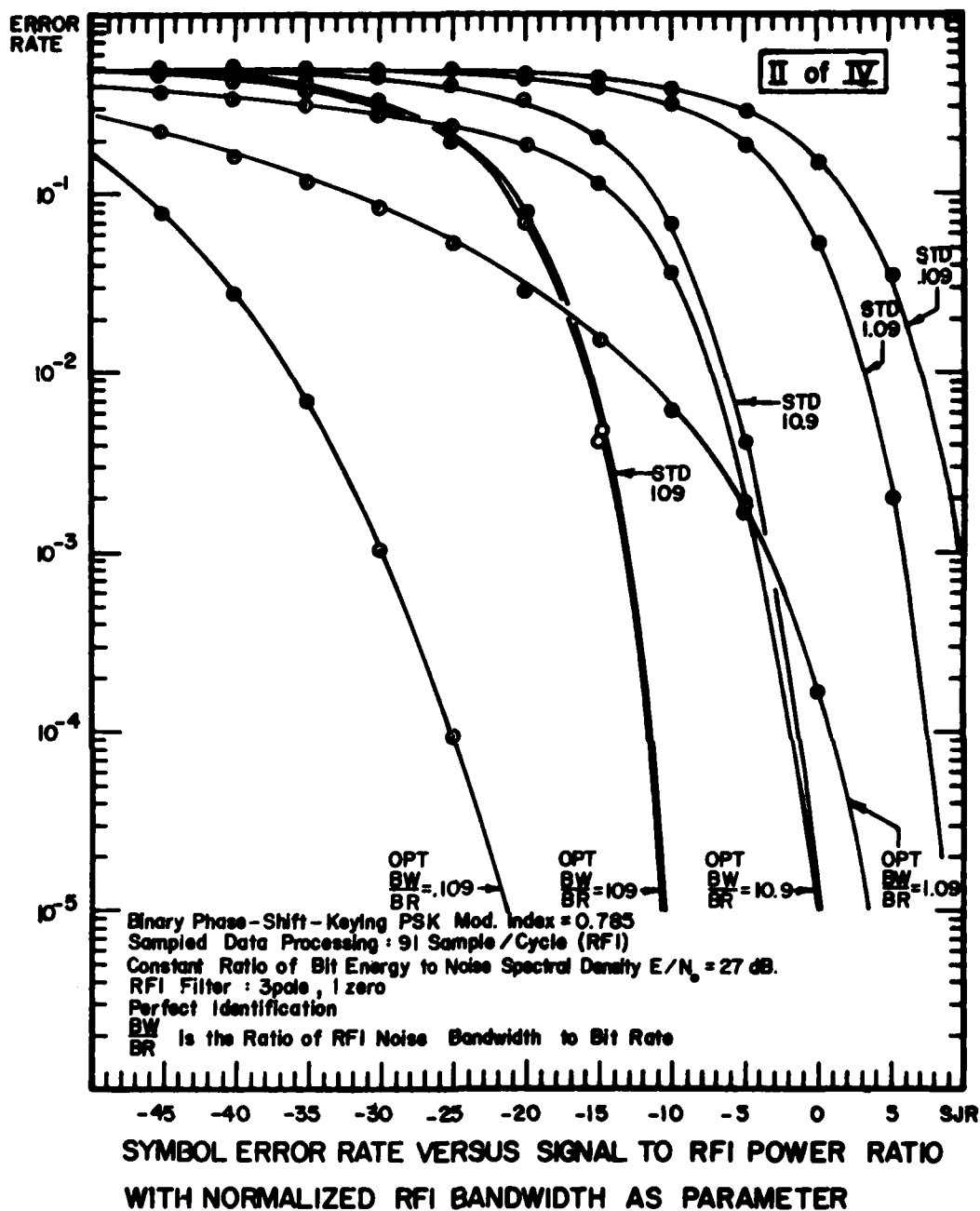
4-80

DTIC



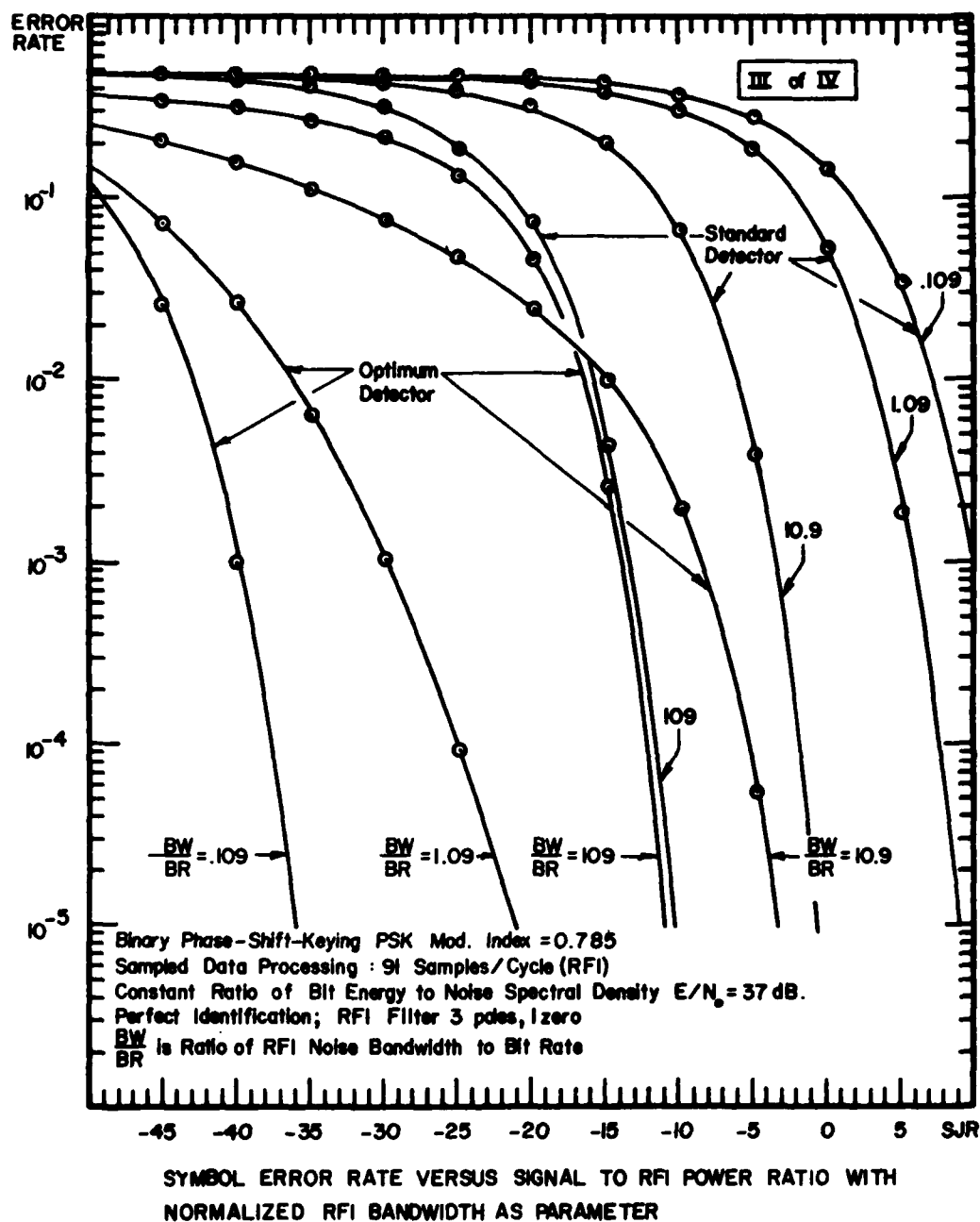
Aggie Form No. 2  
P&P Graphics

Figure 27. IDEI and Standard Detector Performance  
Versus SJR for  $E/N_0 = 17$  dB



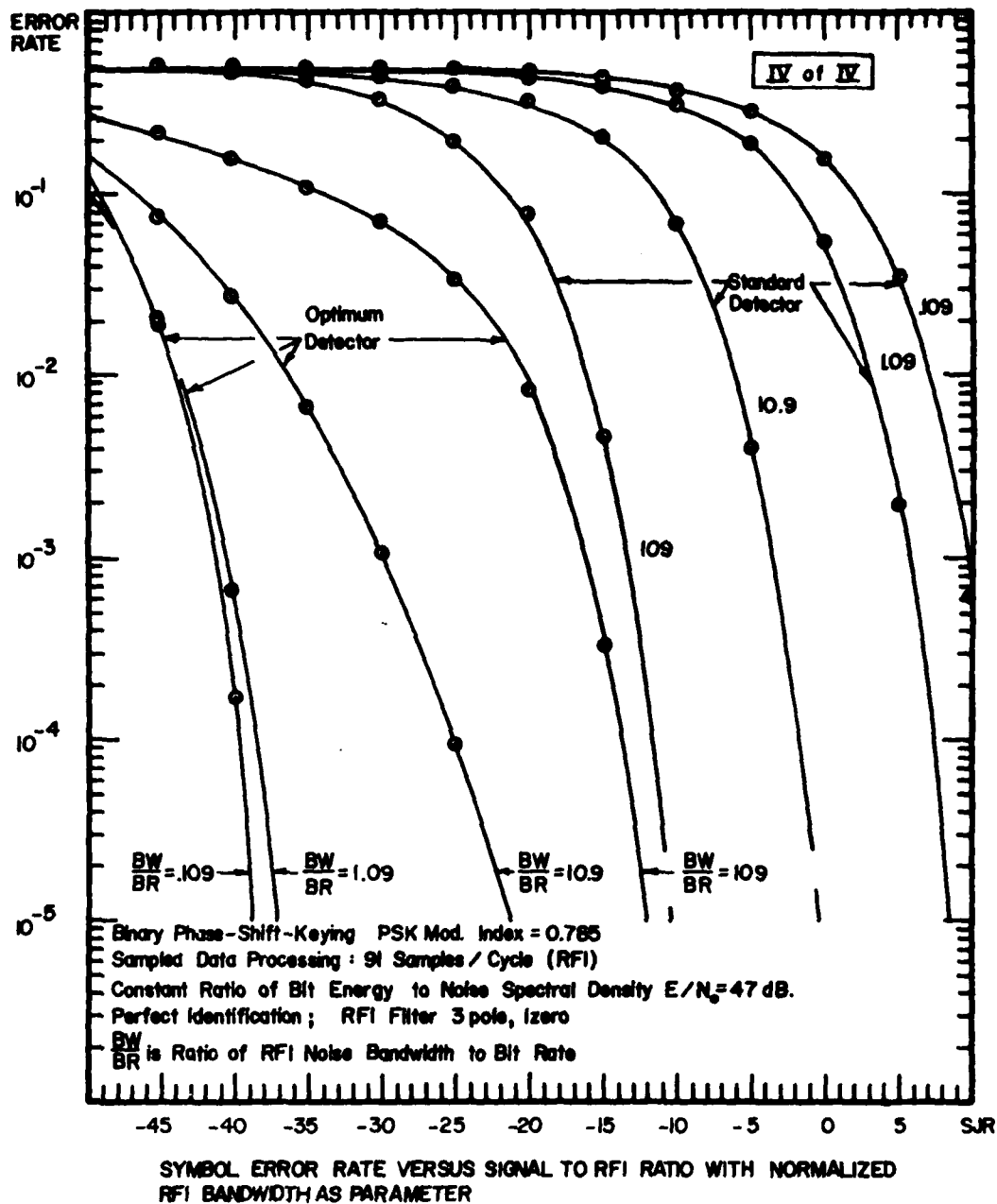
Aggie Form No. 2  
 P & P Graphics

Figure 28. IDEI and Standard Detector Performance  
 Versus SJR for  $E/N_0 = 27$  dB



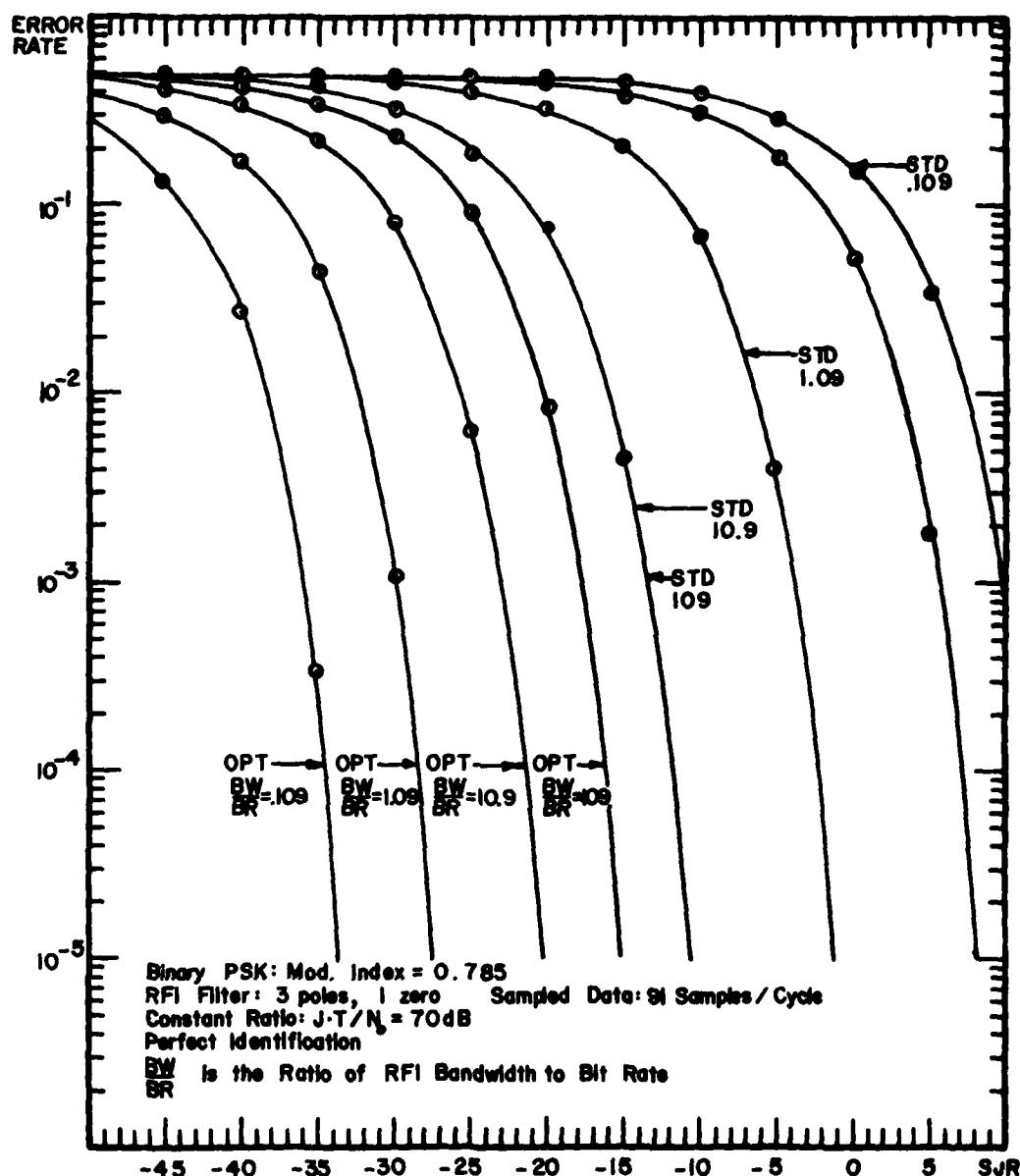
Aggie Form No. 2  
 P&P Graphics

Figure 29. IDEI and Standard Detector Performance  
 Versus SJR for  $E/N_0 = 37$  dB



Aggie Form No. 2  
P&P Graphics

Figure 30. IDEI and Standard Detector Performance  
Versus SJR for  $E/N_0 = 47$  dB



SYMBOL ERROR RATE VERSUS SIGNAL TO RFI RATIO FOR OPTIMUM AND STANDARD DETECTORS WITH NORMALIZED RFI BANDWIDTH AS PARAMETER AND A CONSTANT RATIO OF RFI POWER TO WHITE NOISE POWER IN A BANDWIDTH,  $1/T$  (SYMBOL RATE BANDWIDTH)

Aggie Form No. 2

P&P Graphics

Figure 31. IDEI and Standard Detector Performance Versus SJR with  $JT/N_0 = 70 \text{ dB}$

Comparing (161) and (162) it is evident that

$$\frac{J}{N} = \frac{JT/N_0}{BW/BR} \quad (163)$$

Now, it was conjectured that the error-rate performance of the IDEI detector is controlled by the ability of the filter to track the colored interference in white noise. Hence, the error-rate should be a function of  $J/N$ . Since (163) shows that  $J/N$  is a ratio of  $JT/N_0$  and  $BW/BR$ , the same error-rate should be obtained so long as the ratio is maintained constant. To demonstrate this empirically, the cases shown in Table (4) were computed.

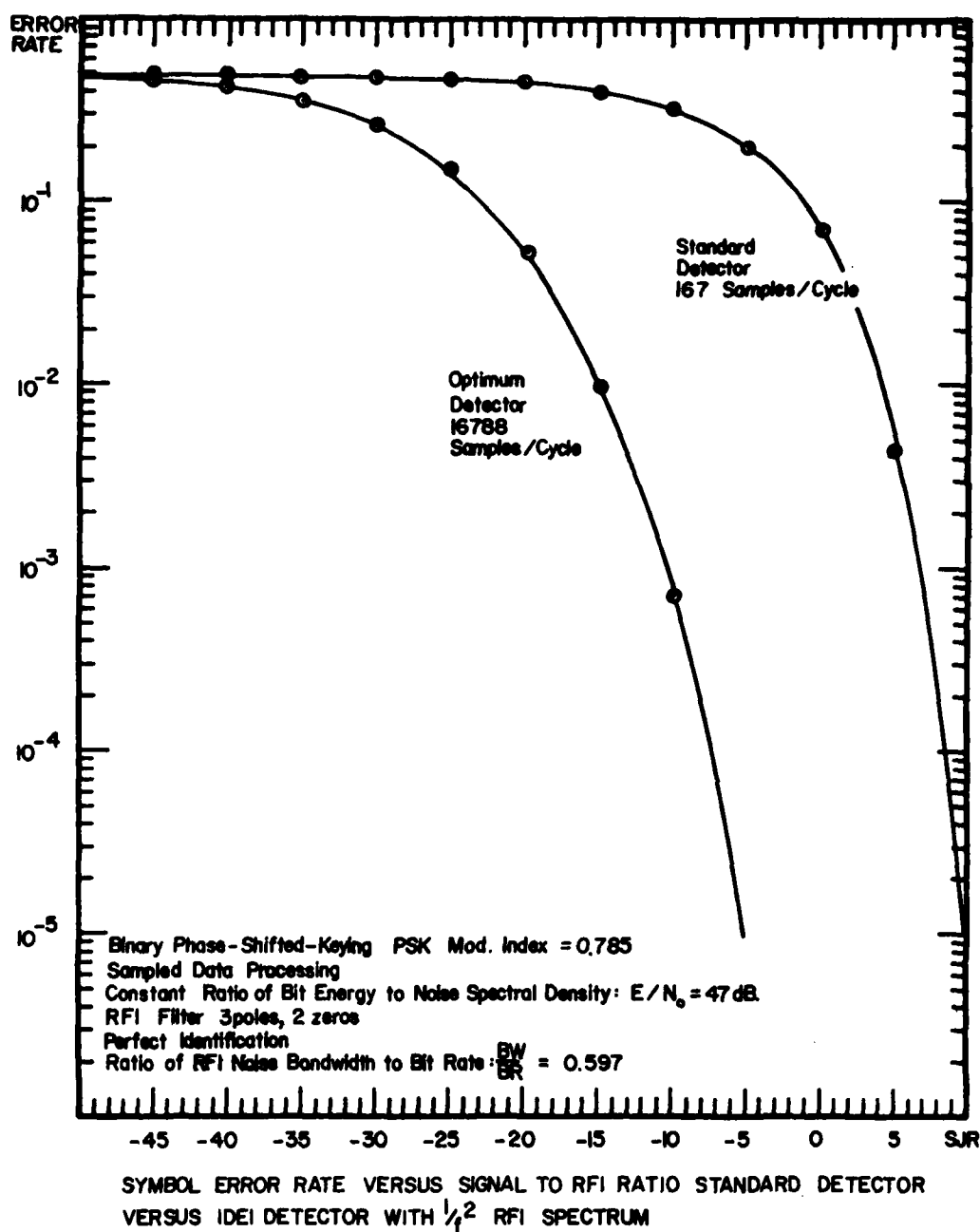
TABLE 4  
P(e) INVARIANCE

SJR dB	-16	-16	-16	-16
E/N <sub>0</sub> dB	42	37	32	27
T	$1.27 \times 10^{-3}$	$4 \times 10^{-4}$	$1.27 \times 10^{-4}$	$4 \times 10^{-5}$
BW/BR	3.46	1.09	0.346	0.109
JT/N <sub>0</sub> dB	55	50	45	40
P(e)	$2.34 \times 10^{-7}$	$2.50 \times 10^{-7}$	$2.60 \times 10^{-7}$	$2.56 \times 10^{-7}$

It is seen from Table 4 that over a wide range of normalized bandwidth, it is  $J/N$  which controls the error-rate,  $P(e)$ . Some computational advantage may be gained from this result by realizing that results for greater values of  $BW/BR$ , which normally require more samples per computation, may be obtained by fixing  $BW/BR$  and reducing  $JT/N_0$ .

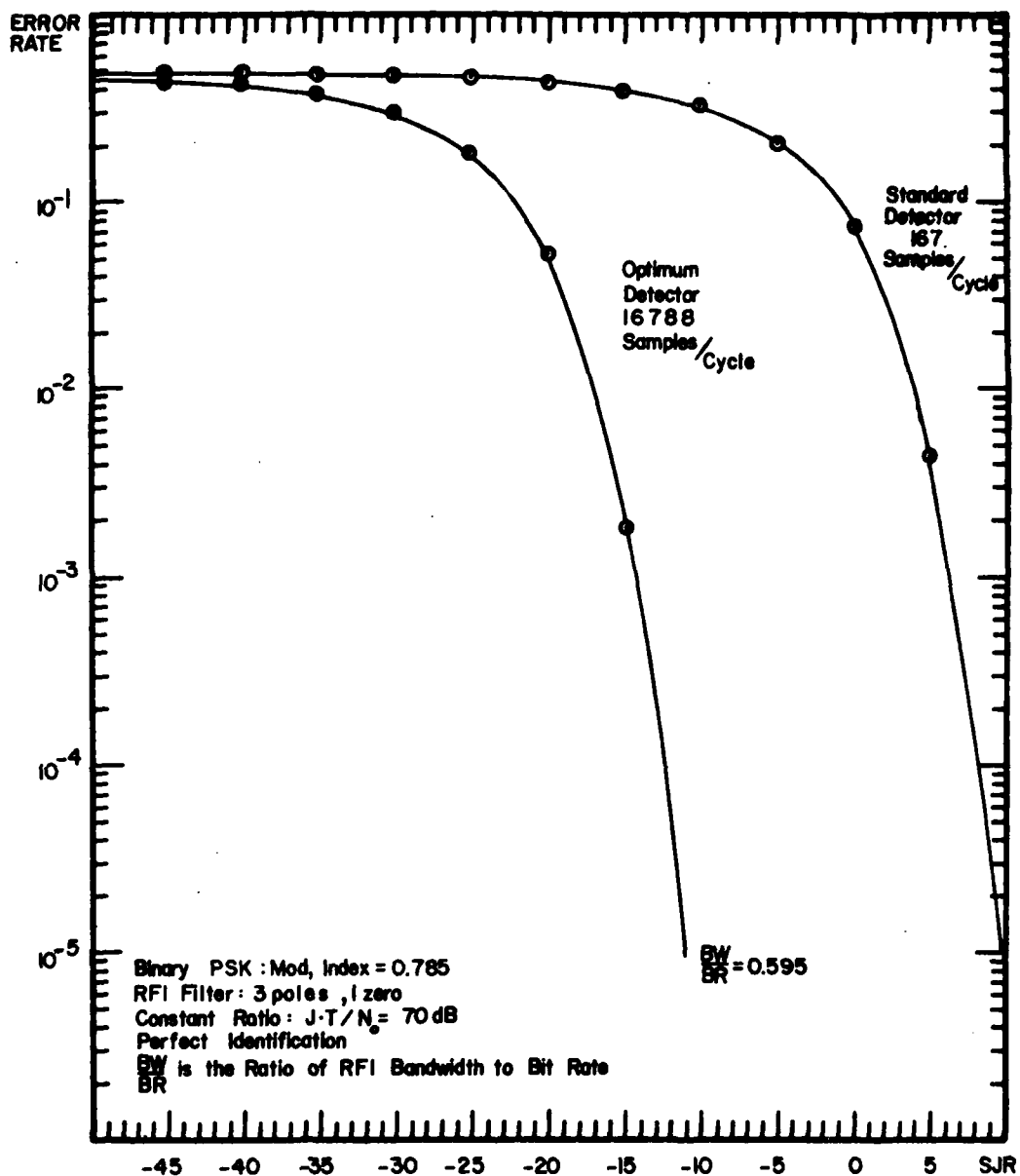
Two final sets of error-rate results for perfect identification were obtained for colored interference of the second kind which decays as  $1/f^2$ . In Figures 32 and 33 are plotted the error-rate results versus SJR for the IDEI and standard detectors. In Figure 32,  $E/N_0$  is held constant at 47 dB. In Figure 33,  $JT/N_0$  is held constant at 70 dB. Both curves show that the IDEI detector has a 15-20 dB advantage over the standard detector, depending on the basis of comparison, for this "worst-case" colored interference.





Aggie Form No. 2  
 P & P Graphics

Figure 32. IDEI and Standard Detector Performance for  
 Interference of the Second Kind with  $E/N_0 = 47$  dB



SYMBOL ERROR RATE VERSUS SIGNAL TO RFI RATIO FOR OPTIMUM AND STANDARD DETECTOR WITH "WORST CASE" RFI AND A CONSTANT RATIO OF RFI ENERGY PER SYMBOL PERIOD (T) TO WHITE NOISE SPECTRAL DENSITY

Aggie Form No. 2  
 P&P Graphics

Figure 33. IDEI and Standard Detector Performance for Interference of the Second Kind with  $JT/N_0 = 70 \text{ dB}$

### 3. ERROR-RATE SENSITIVITY OF IDEI DETECTOR TO IDENTIFICATION ERROR

The next step in the evaluation of the IDEI detector was to determine the loss in error-rate performance when identification of the required colored interference statistics was less than perfect. It was desired to perform some sort of controlled sensitivity study, varying only one statistical parameter at a time, rather than immediately trying the ML identification algorithms.

It was determined in Section III that the necessary statistical quantities to be identified are the state transition matrix,  $\phi$ , and Kalman (Wiener) gain matrix,  $G$ . Now,  $\phi$  is the transition matrix of the interference generating model. Given the order of the interference model,  $\phi$  determines the structure of the colored interference process and its equivalent noise bandwidth,  $BW$ . Thus, a controlled method for varying  $\phi^*$ , the identified matrix, is to obtain it from a frequency-scaled version of the "true" interference spectrum which produced  $\phi$ . In terms of the  $S$ -plane poles and zeroes of the continuous-time generator of the colored process, frequency-scaling simply means multiplying all poles and zeroes by the same constant,  $K$ , where

$$BW^* = K BW \quad (164)$$

and  $BW^*$  is the bandwidth of the identified process. This is the method used herein to set up  $\phi^*$  for the Wiener filter.

Given that  $\phi^*$  is related to the frequency-scaled interference spectrum, as above, the only other unknown statistic for the colored interference is its amplitude scale. Let  $J$  be defined as the mean-squared value (variance) of the true colored interference process and  $J^*$  as the identified value of  $J$ . Given  $J^*$ ,  $\phi^*$ , and the true white noise level ( $E/N_0$ ), the identified Kalman gain,  $G^*$ , may be easily calculated from the Kalman filter equations. This is the method used herein to set up  $G^*$  for the Wiener filter. Symbolically,

$$\begin{aligned} \{BW^*, BW\} &\rightarrow \phi^* \\ \{J^*, J, \phi^*, E/N_0\} &\rightarrow G^* \end{aligned} \quad (165)$$

Note that this controlled method for calculating  $\phi^*$  and  $G^*$  is not equivalent to the M-L method of Section III. There, the computation algorithm have no knowledge of white-noise level ( $E/N_0$ ).

The procedure for evaluating the sensitivity of the error-rate to errors in  $\phi^*$  and  $G^*$  is as follows. In one case,  $BW^* = BW$  and  $\phi^* = \phi$ . The closed-form error-rate is then computed for various specifications of  $J^*/J$ , using the resulting  $G^*$ , derived as above. In the other case,  $J^* = J$ . The closed-form error-rate is computed for various specifications of  $BW^*/BW$ , using the resulting  $\phi^*$  and  $G^*$ , derived as above.

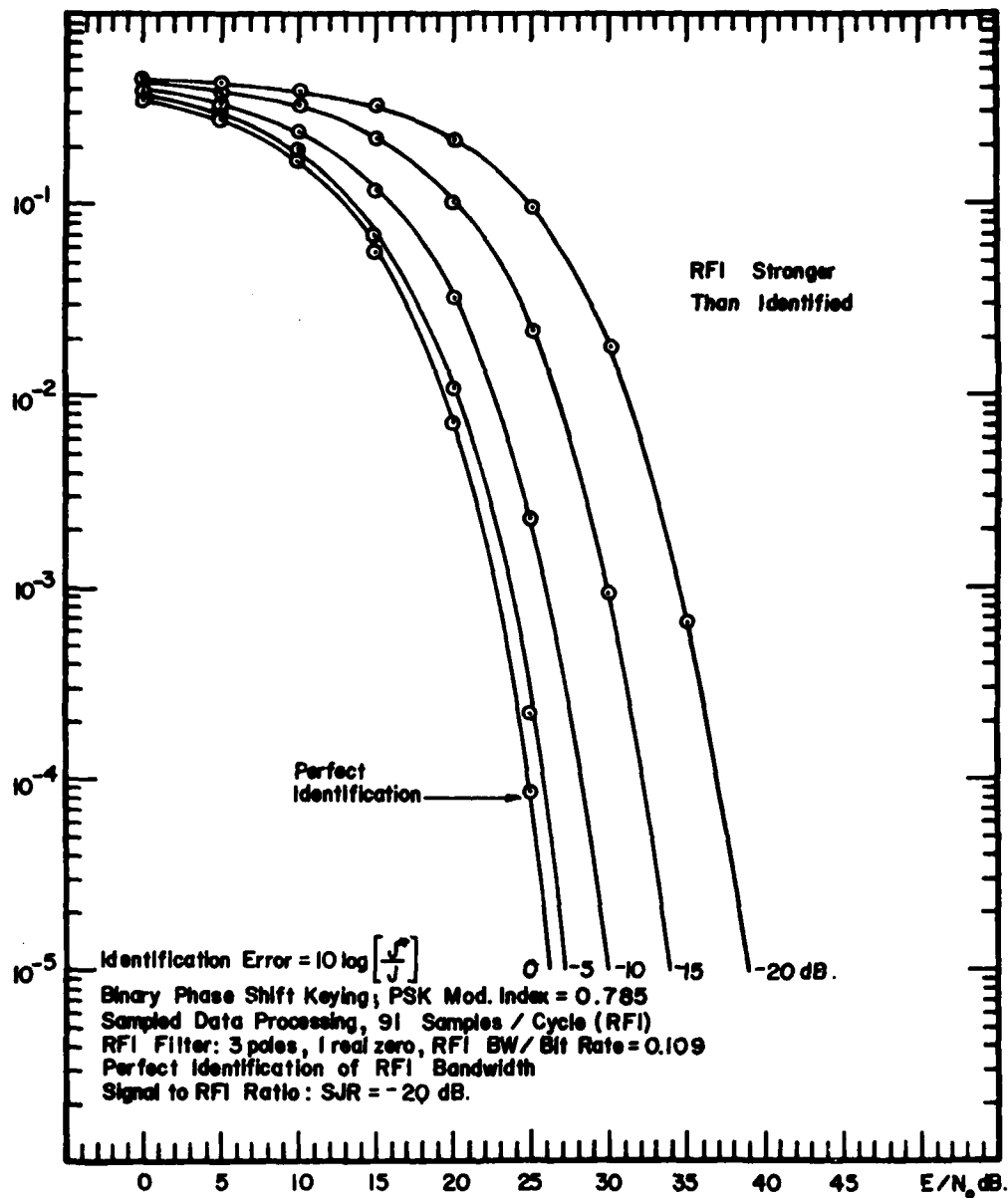
Figures 34 and 35 show the results for a case where the IDEI detector is implemented with the true  $\phi^* = \phi$ , but  $G^*$  is in error according to a scaling error in the strength (variance) of the colored noise process specified by  $J^*/J$ . The error rates are presented for  $SJR = -20$  dB and  $BW/BR = 0.109$  which is the narrow-band interference of the first kind. The results are plotted versus  $E/N_0$ . These two figures show that the first 5 dB of error in colored interference strength cost only about 1 dB in terms of  $E/N_0$  performance. Beyond 5 dB, identification error is much more costly if the colored interference strength is underestimated, rather than over-estimated.

Figure 36 shows a detailed examination of the behavior of the various elements which make up the argument of the error rate,  $P(e)$ . In terms of the expression for  $P(e)$ , given in (11),  $\mu$  is the mean, as calculated from (7) and  $\sigma$  is the standard deviation, as calculated from (8). The quantity,  $v$ , is the actual tracking error variance, which is  $V_{\xi\xi}(0)$ , as calculated from (9). It is seen that neither  $\mu$  nor  $\sigma$  reach extreme values for perfect identification, when  $J^* = J$ . However, the ratio,  $\mu/\sigma$ , does maximize for  $J^* = J$ . Also, the interference tracking error variance,  $v$ , does minimize for  $J^* = J$ .

It is possible to define a "Detection Loss" factor as the ratio of the maximum value of  $\mu/\sigma$  to its value as obtained for any particular value for  $J^*/J$ . This factor is plotted in Figure 37. Here the penalty for under-estimating the strength of the colored noise process is clearly shown.

Figures 38 and 39 show cases similar to those of 34 and 35 where now the plot is versus  $SJR$  with  $JT/N_0$  held constant at 60 dB. The same conclusions reached previously are also supported by these figures. Figure 40 gives the accompanying plot of detection loss.

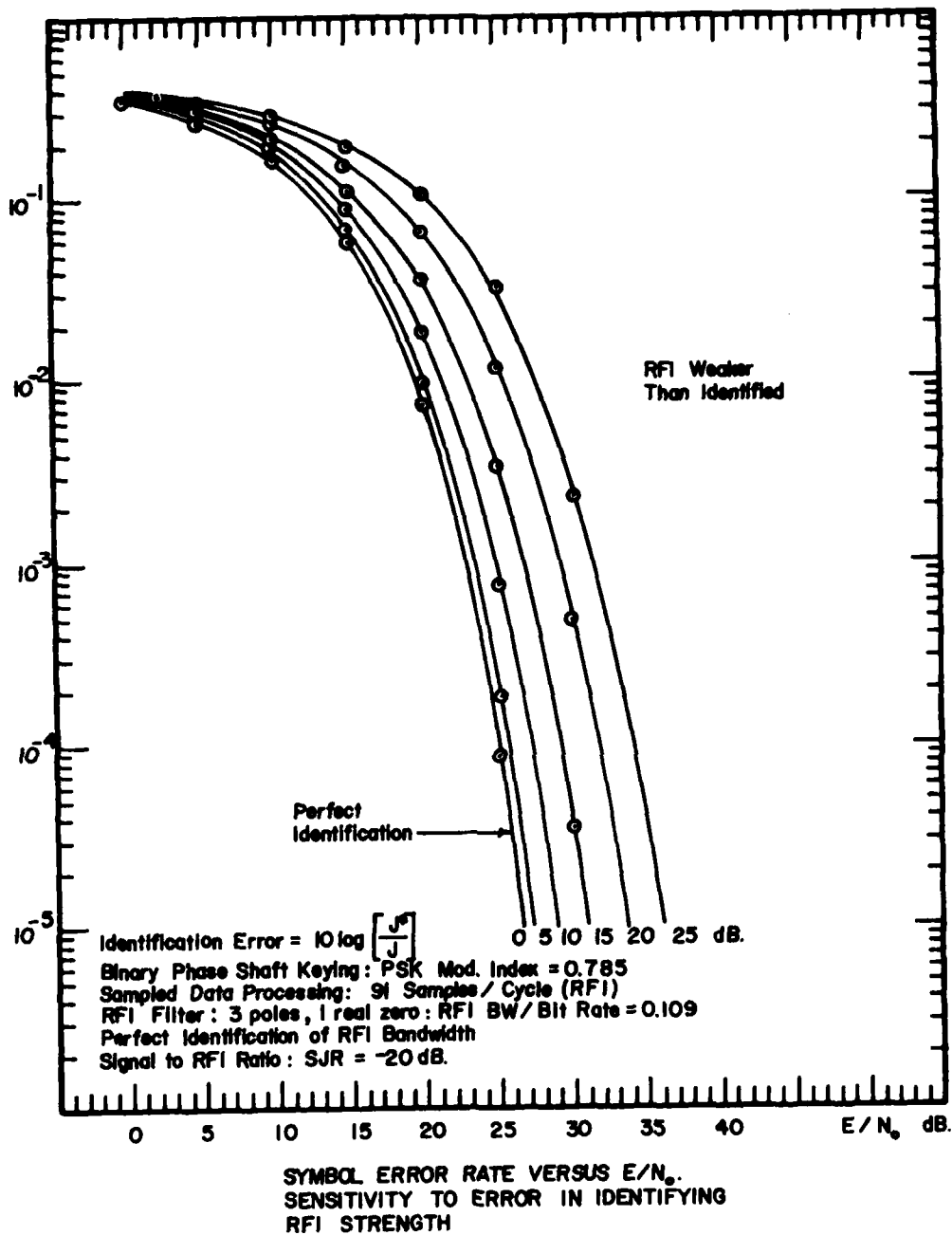
Figure 41 and 42 are for the same case as 34 and 35 where now the detector is implemented for  $J^* = J$  but  $\phi^*$  (and  $G^*$ ) are in error according



SYMBOL ERROR RATE VERSUS  $E/N_0$   
 SENSITIVITY TO ERROR IN IDENTIFYING RFI STRENGTH

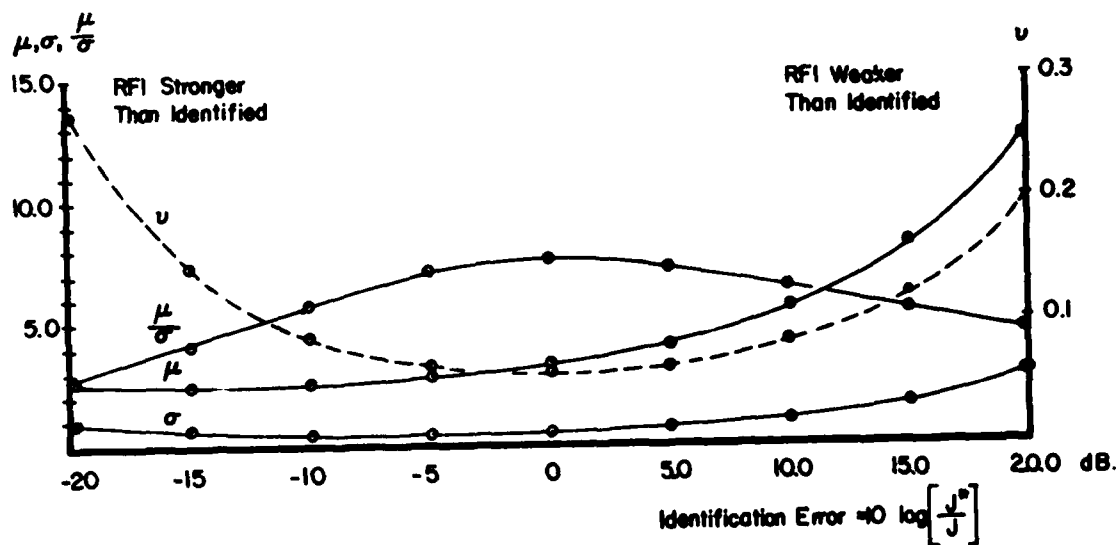
Aggie Form No. 2  
 P&P Graphics

Figure 34. IDEI Error Rate Versus  $E/N_0$  for  
 RFI Strength Underestimated



Aggie Form No. 2  
 P & P Graphics

Figure 35. IDEI Error Rate Versus  $E/N_0$  for  
 RFI Strength Overestimated

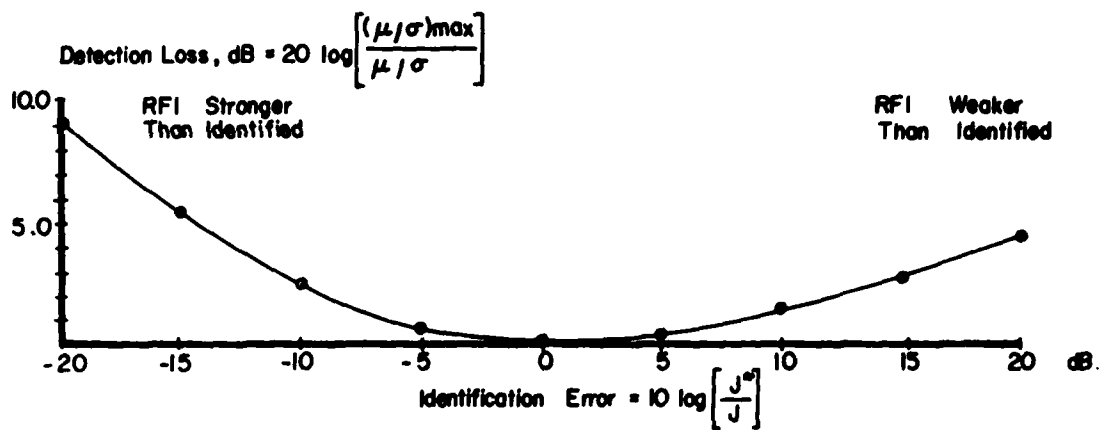


Binary Phase Shift Keying : PSK Mod. Index = 0.785  
 Sampled Data Processing : 91 Sample / Cycle (RFI)  
 Signal to RFI Ratio : SJR = -20 dB. :  $E/N_0$  25 dB.  
 Ratio of RFI Noise Bandwidth to Bit Rate :  $BW/BR = 0.109$   
 RFI Bandwidth is one-sided, Low-Pass, Equivalent  
 Perfect Identification of RFI Bandwidth:  $BW^*/BW = 1.0$

$\mu$  : Mean ,  $\sigma$  : Std. Dev. ,  $\nu$  : Tracking Error Variance

VARIATION OF DETECTION STATISTICS VERSUS RFI STRENGTH IDENTIFICATION ERROR

Figure 36. Variation of Detection Statistics Versus  
 RFI Strength Identification Error,  $E/N_0 = 25$  dB

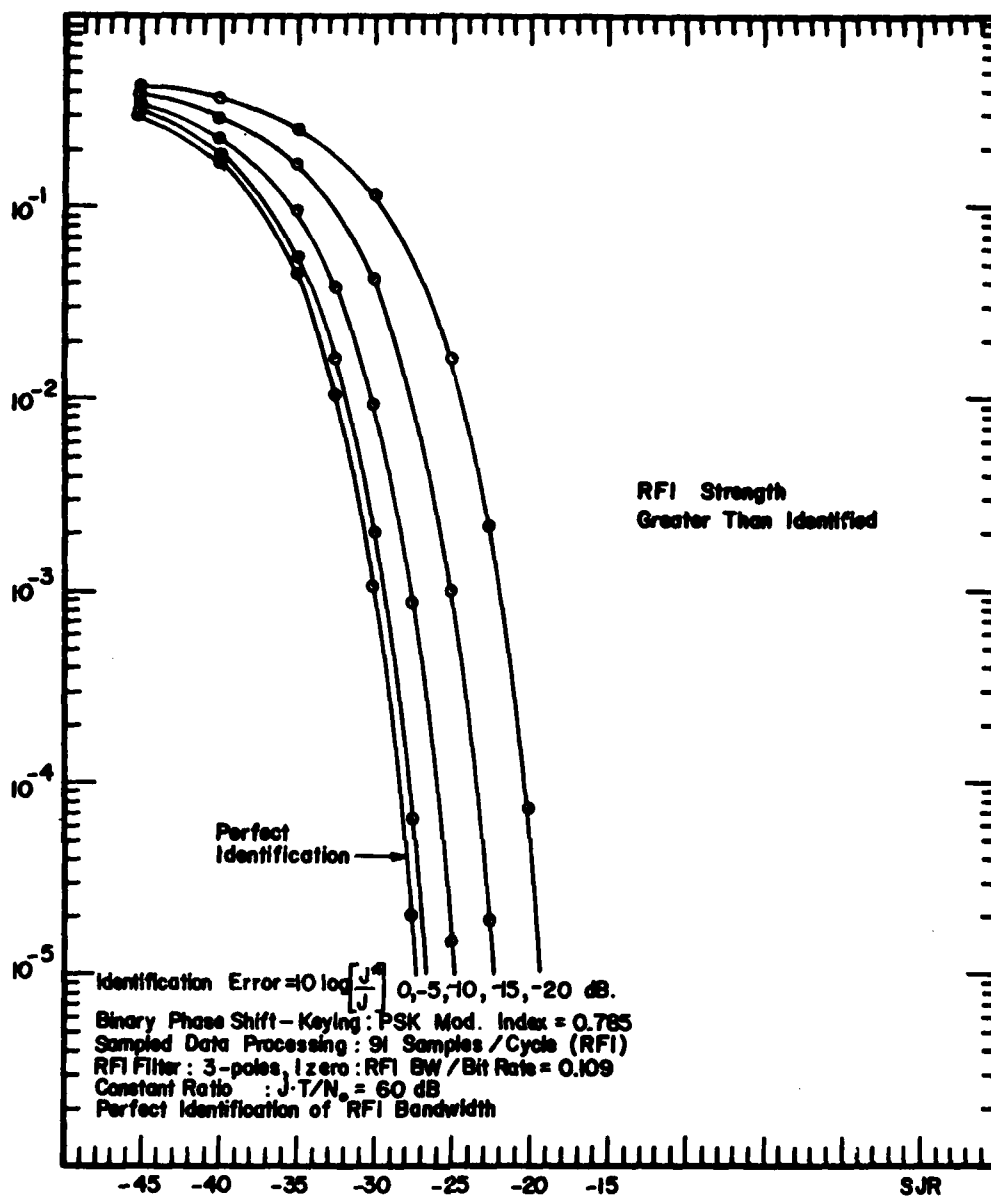


Binary Phase Shift Keying : PSK Mod. Index = 0.785  
 Sampled Data Processing : 91 Samples / Cycle (RFI)  
 Signal / RFI Ratio : SJR = -20 dB :  $E/N_0 = 25$  dB.  
 Ratio of RFI Noise Bandwidth to Bit Rate :  $BW/BR = 0.109$   
 RFI Bandwidth is One-Sided, Low-Pass, Equivalent  
 Perfect Identification of RFI Bandwidth :  $BW^*/BW = 1.0$

DETECTION SNR LOSS VERSUS RFI STRENGTH IDENTIFICATION ERROR

Figure 37. Detection Loss Versus RFI Strength  
 Identification Error,  $E/N_0 = 25$  dB

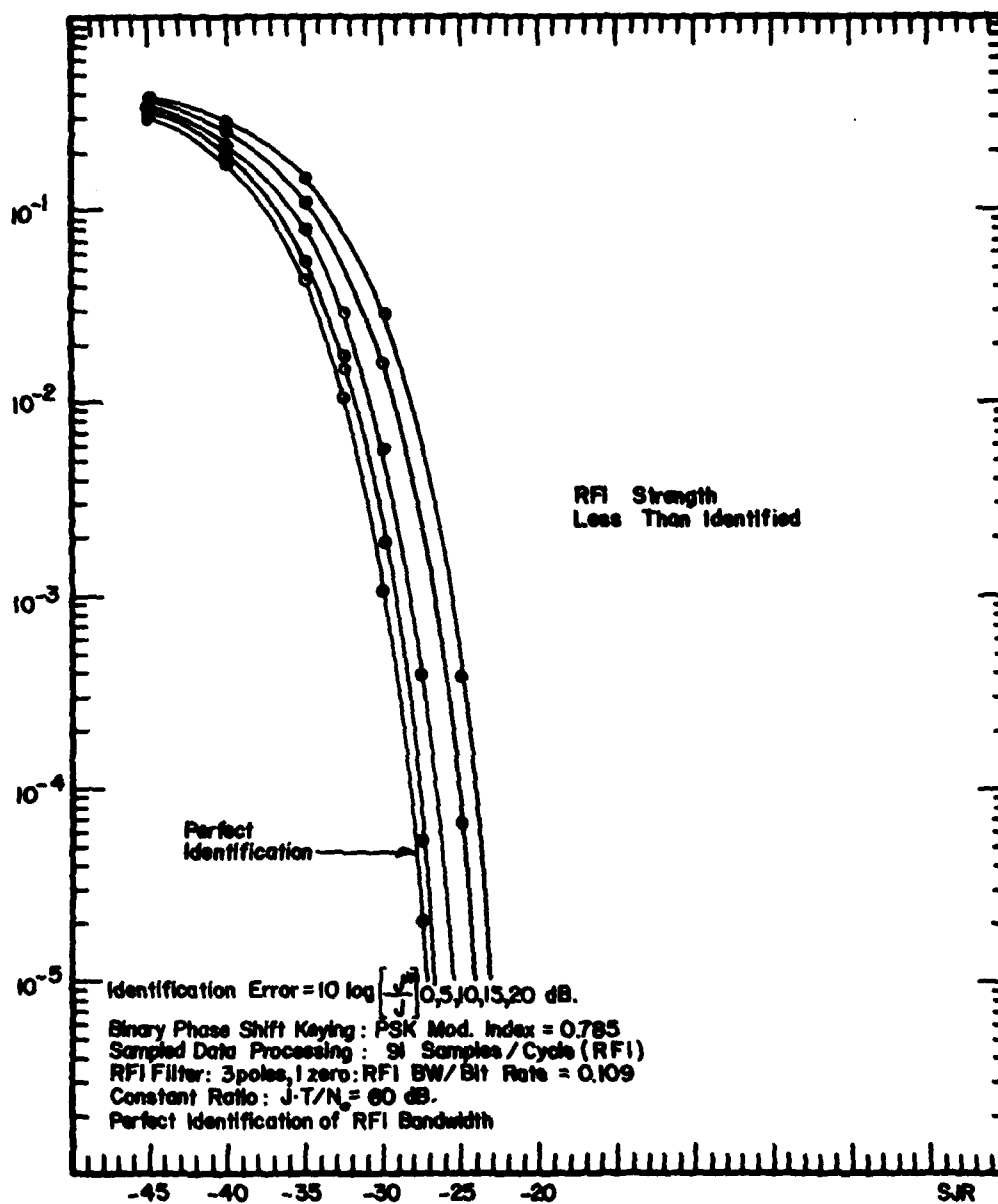




SYMBOL ERROR RATE VERSUS SIGNAL TO RFI RATIO. SENSITIVITY  
TO ERROR IN IDENTIFYING RFI STRENGTH.

Aggie Form No. 2  
P&P Graphics

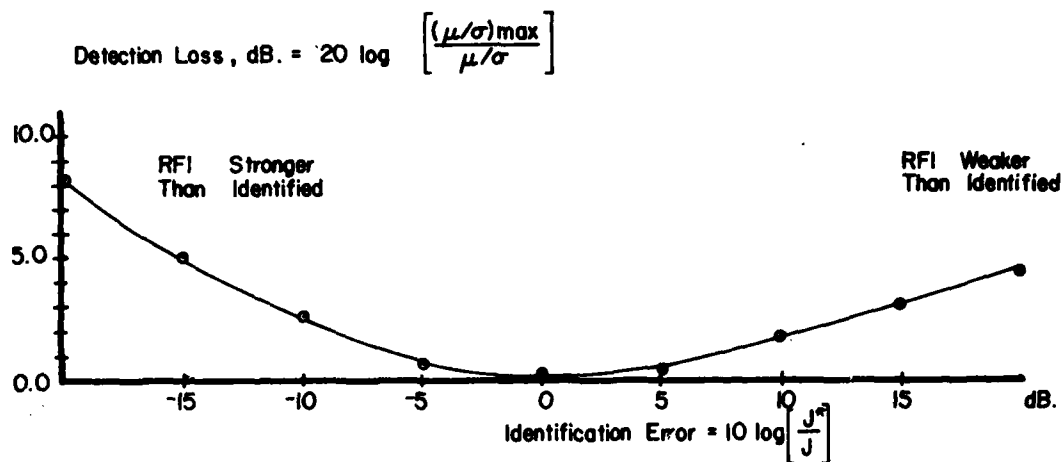
Figure 38. IDEI Error Rate Versus SJR for  
RFI Strength Underestimated,  $JT/N_0 = 60$  dB



SYMBOL ERROR RATE VERSUS SIGNAL TO RFI RATIO, SENSITIVITY  
TO ERROR IN IDENTIFYING RFI STRENGTH

Aggie Form No. 2  
P&P Graphics

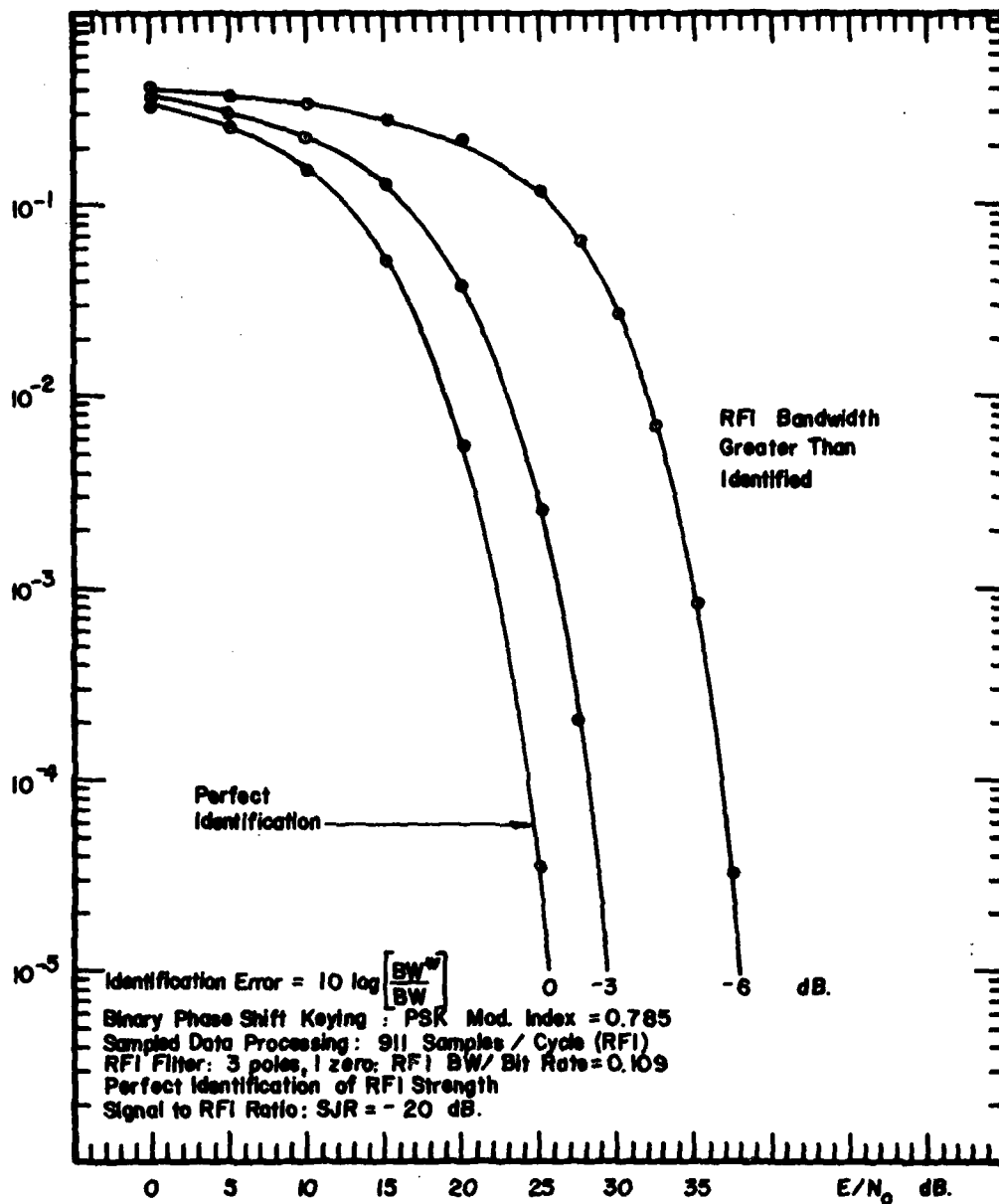
Figure 39. IDEI Error Rate Versus SJR for  
RFI Strength Overestimated,  $JT/N_0 = 60$  dB



Binary Phase Shift Keying : PSK Mod. Index = 0.785  
 Sampled Data Processing : 91 Samples/Cycle (RFI)  
 Signal / RFI Ratio : SJR = -30 dB. :  $E/N_0 = 27$  dB. :  $JT/N_0 = 60$  dB.  
 Ratio of RFI Noise Bandwidth to Bit Rate :  $BW/BR = 0.109$   
 RFI Bandwidth is One-Sided, Low-Pass, Equivalent  
 Perfect Identification of RFI Bandwidth :  $BW/BW = 1.0$

DETECTION SNR LOSS VERSUS RFI STRENGTH IDENTIFICATION ERROR

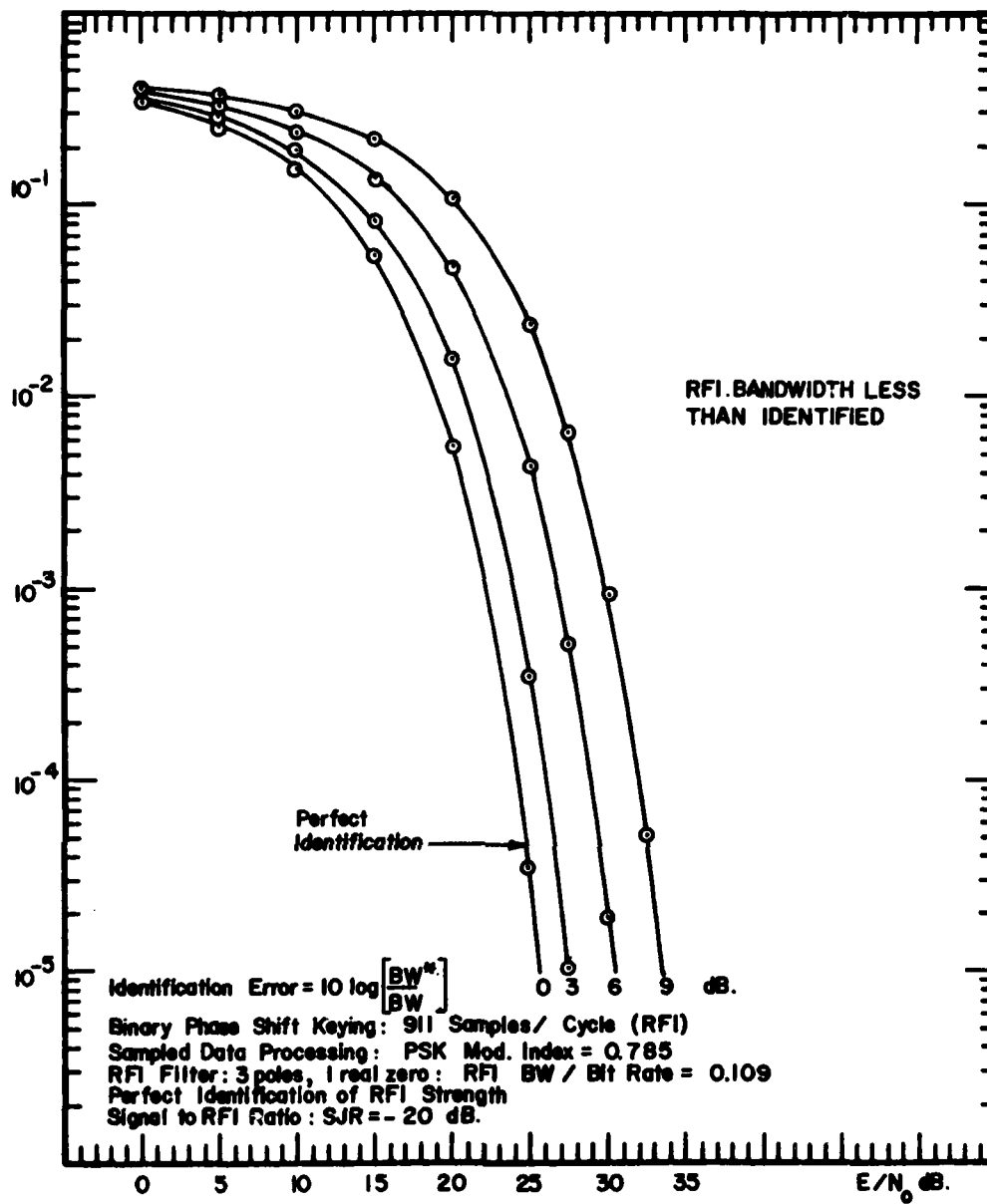
Figure 40. Detection Loss Versus RFI Strength  
 Identification Error,  $JT/N_0 = 60$  dB



SYMBOL ERROR RATE VERSUS  $E/N_0$   
 SENSITIVITY TO ERROR IN IDENTIFYING RFI BANDWIDTH

Aggie Form No. 2  
 P & P Graphics

Figure 41. IDEI Error Rate Versus  $E/N_0$   
 for RFI Bandwidth Underestimated



SYMBOL ERROR RATE VERSUS  $E/N_0$   
 SENSITIVITY TO ERROR IN IDENTIFYING  
 RFI BANDWIDTH

Aggie Form No. 2  
 P&P Graphics

Figure 42. IDEI Error Rate Versus  $E/N_0$  for  
 RFI Bandwidth Overestimated

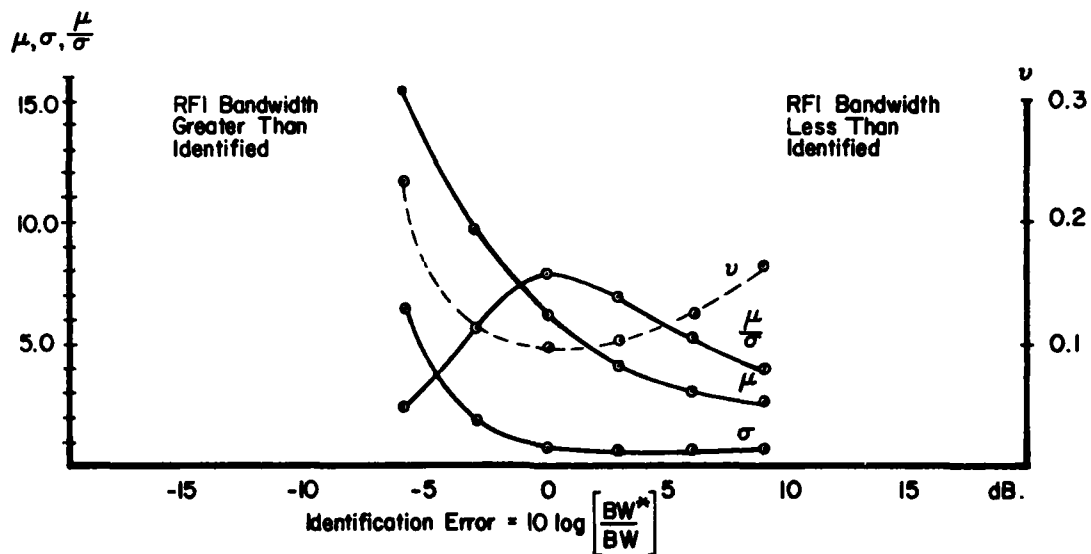
to a scaling error in the bandwidth of the colored noise process, specified by  $BW^*/BW$ . The error rates are again plotted versus  $E/N_0$  for  $SJR = -20$  dB and  $BW/BR = 0.109$ . These two figures show that bandwidth identification error is much more costly if the colored interference bandwidth is underestimated, rather than overestimated. Figure 42 shows that when overestimating the bandwidth the penalty becomes, asymptotically, just that due to the extra white noise which is admitted to the detector.

Figure 43 shows the variation of the error rate argument components, as was done in 36. The same behavior obtains for identifying bandwidth as for strength.

Figure 44 shows a plot of detection loss versus error in bandwidth identification. It is obvious that the margin for error in identifying bandwidth is smaller than that for identifying strength.

Figures 45 and 46 are for the same case as 40 and 41 where, now, the plot is versus  $SJR$  with  $JT/N_0$  held constant at 60 dB. The same conclusions reached previously are also supported by these figures. Figure 47 gives the accompanying plot of detection loss.

Figures 34 through 47, inclusive, have presented an evaluation of the sensitivity of IDEI error rate to error in identifying the strength and bandwidth of the colored interference process. An initial conclusion to be drawn is that the IDEI detector algorithm is reasonably robust in terms of identification error, so long as the filter functions,  $\phi^*$  and  $G^*$  are synthesized in a deterministic manner, based on identification of strength and bandwidth of the colored interfering process. Such an identification-synthesis procedure is ad hoc and not based on a straight-forward application of estimation theory. Before proceeding further with it, it was decided to evaluate a more rigorous approach, that of Maximum-Likelihood Identification.

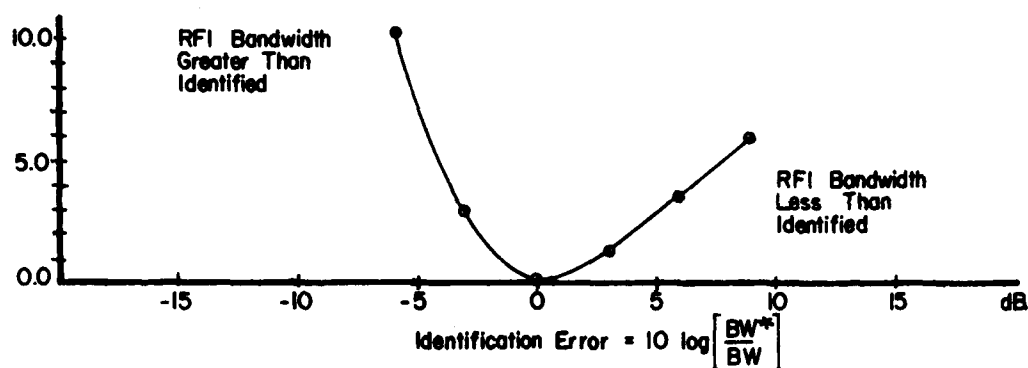


Binary Phase Shift Keying : PSK Mod. Index = 0.785  
 Sampled Data Processing : 911 Samples / Cycle (RFI)  
 Signal / RFI Ratio : SJR = -20 dB :  $E/N_0 = 25$  dB.  
 Ratio of RFI Noise Bandwidth to Bit Rate :  $BW / BR = 0.109$   
 RFI Bandwidth is One-Sided, Low-Pass, Equivalent  
 Perfect Identification of RFI Strength:  $J'/J = 1.0$   
 $\mu$ : Mean ,  $\sigma$ : Std. Dev. ,  $v$ : Tracking Error Variance

VARIANCE OF DETECTION STATISTICS VERSUS RFI BANDWIDTH IDENTIFICATION ERROR

Figure 43. Variation of Detection Statistics Versus RFI Bandwidth Identification,  $E/N_0 = 25$  dB

$$\text{Detection Loss, dB} = 20 \log \left[ \frac{(\mu/\sigma)_{\max}}{\mu/\sigma} \right]$$

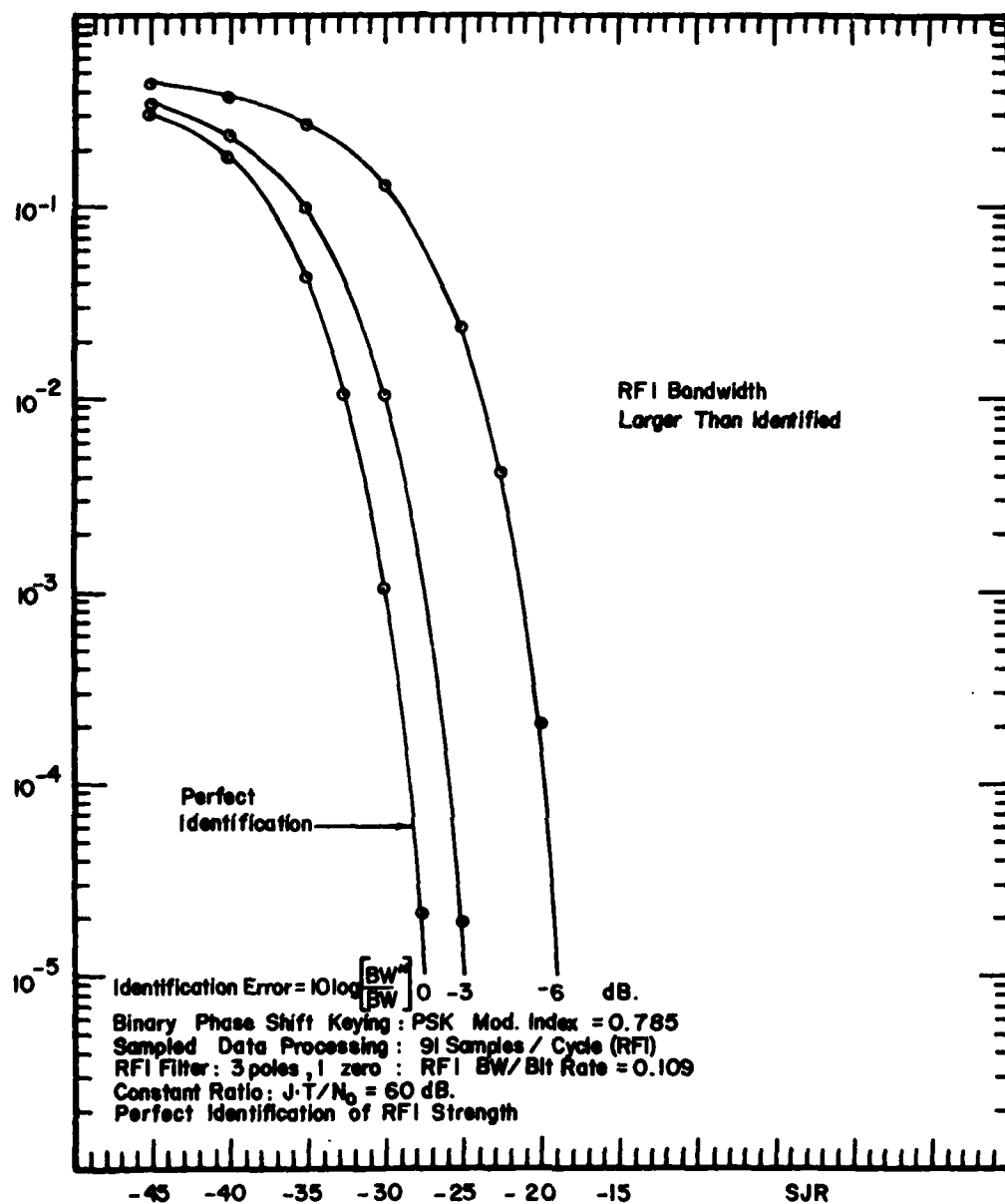


Binary Phase Shift Keying : PSK Mod. Index = 0.785  
 Sampled Data Processing : 911 Samples/Cycle (RFI)  
 Signal / RFI Ratio : SJR = -20dB :  $E/N_0 = 25$  dB  
 Ratio of RFI Noise Bandwidth to Bit Rate :  $BW/BR = 0.109$   
 RFI Bandwidth is One-Sided, Low-Pass, Equivalent  
 Perfect Identification of RFI Strength :  $J^2 J = 1.0$

DETECTION SNR LOSS VERSUS RFI BANDWIDTH IDENTIFICATION ERROR

Figure 44. Detection Loss Versus RFI Bandwidth  
 Identification Error,  $E/N_0 = 25$  dB

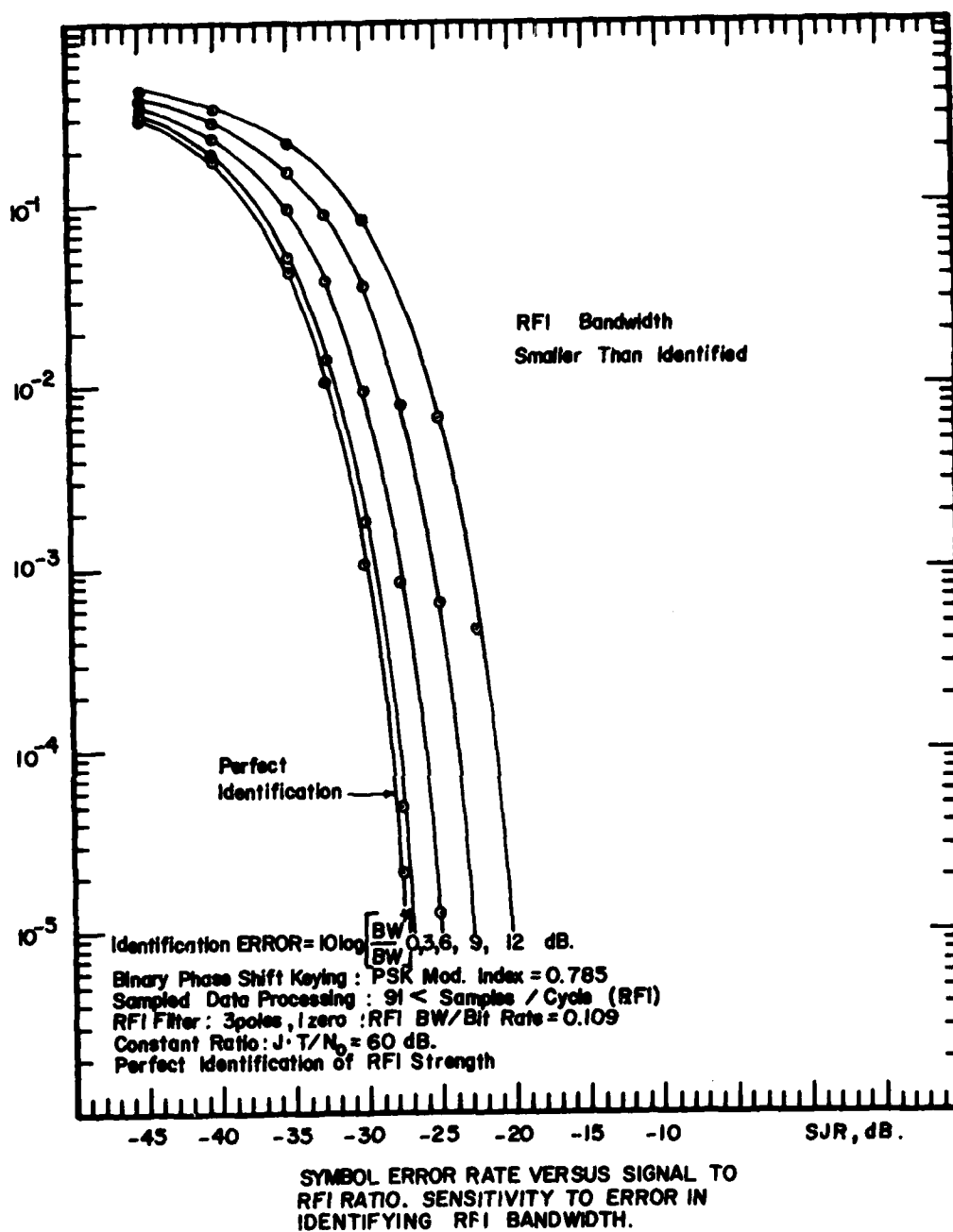




SYMBOL ERROR RATE VERSUS SIGNAL TO RFI RATIO.  
 SENSITIVITY TO ERROR IN IDENTIFYING RFI BANDWIDTH.

Aggie Form No. 2  
 P & P Graphics

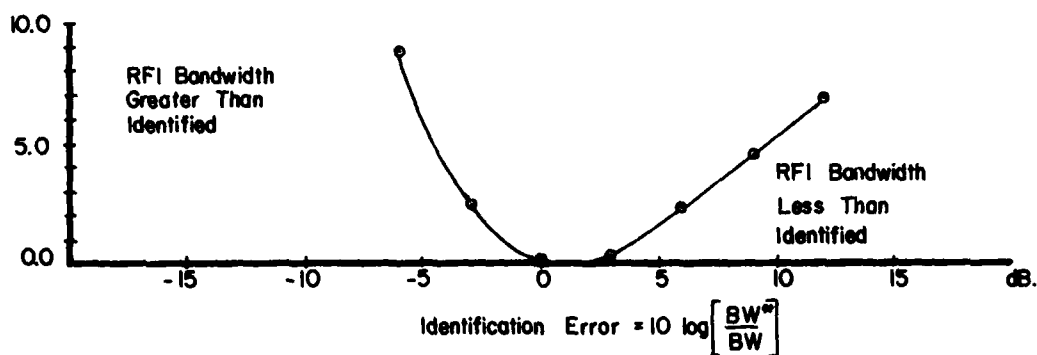
Figure 45. IDEI Error Rate Versus SJR for  
 RFI Bandwidth Underestimated



Aggie Form No. 2  
P&P Graphics

Figure 46. IDEI Error Rate Versus SJR for  
RFI Bandwidth Overestimated

$$\text{Detection Loss, dB} = 20 \log \left[ \frac{(\mu/\sigma)_{\max}}{\mu/\sigma} \right]$$



Binary Phase Shift Keying : PSK Mod. Index = 0.785  
 Sampled Data Processing : 91 < Samples/Cycle (RFI)  
 Signal to RFI Ratio : SJR = -30dB : E/N<sub>0</sub> = 27 dB : JT/N<sub>0</sub> = 60 dB.  
 Ratio of RFI Noise Bandwidth to Bit Rate : BW/BR = 0.109  
 RFI Bandwidth is One-Sided, Low-Pass, Equivalent  
 Perfect Identification of RFI Strength : J\*/J = 1.0

DETECTION SNR LOSS VERSUS RFI BANDWIDTH IDENTIFICATION ERROR

Figure 47. Detection Loss Versus RFI  
 Bandwidth Identification Error,  $\frac{JT}{N_0} = 60$  dB.

#### 4. ERROR-RATE PERFORMANCE OF THE ML IDENTIFICATION ALGORITHMS

In Section III.3., results were given for the performance of the ML identification algorithms in terms of convergence of the estimates of the parameters  $G$  and  $\phi$  of the filter to be identified. However, in the present problem, the filter being identified is embedded in a signal detector. Thus, a further measure of identification performance is the error rate of the associated detector.

The 6x6 example of Section III.3. may be used here. The actual data generator structure is

$$\gamma_1 = 1.11439$$

$$\gamma_2 = -1.40932$$

$$\gamma_3 = 0.303111$$

$$\lambda_1 = \lambda_2 = \lambda_3 = 1.0$$

$$\phi_1 = 0.927374$$

$$\phi_2 = 0.881911$$

$$\phi_3 = 0.777768$$

The above structure results for the following specification of the signal communication problem:

Number of Samples per Symbol (NSPB) : 10

Number of Symbols per Second (BR) :  $25 \times 10^3$

Signal to Colored Interference Ratio (SJRDB) : 0 dB

Colored Interference Bandwidth (BW) : 2743 Hz.

Energy per Symbol : Noise Spectral Density ( $E/N_0$ ) : Variable

Table 5 shows error rate results obtained using identified filter structures, for values of  $E/N_0$  between -15 dB and +25 dB in 5 dB steps. For each value of  $E/N_0$ , identification was performed using 100 data samples and 400 data samples. For both sets of data samples the number of iterations was 100. The filter gains,  $g_1$ ,  $g_2$ , and  $g_3$  were initialized using proper values. The transition parameters,  $\phi_1$ ,  $\phi_2$ , and  $\phi_3$ , were initialized at 0.95, 0.9, and 0.75, respectively.

TABLE 5  
ERROR RATE PERFORMANCE OF SJR = 0

True Data	Estimates $\phi^*$	Estimates $G^*$	Error Rate
$E/N_0 = -15 \text{ dB}$ $r = 8.88786$ $g_1 = .174635 \times 10^{-1}$ $g_2 = -.126974 \times 10^{-1}$ $g_3 = .104189 \times 10^{-2}$ $p(e) = .403394$	$K = 100$ $\phi_1 = .962275$ $\phi_2 = .909611$ $\phi_3 = .749812$ $K = 400$ $\phi_1 = .922637$ $\phi_2 = .905056$ $\phi_3 = .749797$	$g_1 = -.188813 \times 10^{-1}$ $g_2 = .129918 \times 10^{-2}$ $g_3 = .155987 \times 10^{-1}$  $g_1 = .525372 \times 10^{-2}$ $g_2 = -.694674 \times 10^{-2}$ $g_3 = .122717 \times 10^{-1}$	$p(e) = .406673$    $p(e) = .403501$
$E/N_0 = -10 \text{ dB}$ $r = 4.99801$ $g_1 = .501310 \times 10^{-1}$ $g_2 = -.374055 \times 10^{-1}$ $g_3 = .315661 \times 10^{-2}$ $p(e) = .339301$	$K = 100$ $\phi_1 = .933537$ $\phi_2 = .908293$ $\phi_3 = .749640$ $K = 400$ $\phi_1 = .915837$ $\phi_2 = .907796$ $\phi_3 = .750128$	$g_1 = .462744 \times 10^{-1}$ $g_2 = -.404340 \times 10^{-1}$ $g_3 = .306828 \times 10^{-2}$  $g_1 = .407356 \times 10^{-1}$ $g_2 = -.298345 \times 10^{-1}$ $g_3 = .187085 \times 10^{-1}$	$p(e) = .339498$    $p(e) = .339731$
$E/N_0 = -5 \text{ dB}$ $r = 2.81059$ $g_1 = .130345$ $g_2 = -.102093$ $g_3 = .911142 \times 10^{-2}$ $p(e) = .253087$	$K = 100$ $\phi_1 = .922487$ $\phi_2 = .905116$ $\phi_3 = .799720$ $K = 400$ $\phi_1 = .928011$ $\phi_2 = .897036$ $\phi_3 = .800237$	$g_1 = .119131$ $g_2 = -.962566 \times 10^{-1}$ $g_3 = .876633 \times 10^{-2}$  $g_1 = .120169$ $g_2 = -.942549 \times 10^{-1}$ $g_3 = .133610 \times 10^{-1}$	$p(e) = .254793$    $p(e) = .253378$

True Data	Estimates $\phi^*$	Estimates $G^*$	Error Rate
$E/N_0 = 0 \text{ dB}$ $r = 1.58051$ $g_1 = .303158$ $g_2 = -.253838$ $g_3 = .246645 \times 10^{-1}$ $p(e) = .159826$	$K = 100$ $\phi_1 = .931785$ $\phi_2 = .909121$ $\phi_3 = .752618$ $K = 400$ $\phi_1 = .928605$ $\phi_2 = .894738$ $\phi_3 = .754331$	$g_1 = .324643$ $g_2 = -.284925$ $g_3 = .448313 \times 10^{-1}$  $g_1 = .317638$ $g_2 = .278292$ $g_3 = .414739 \times 10^{-1}$	     $p(e) = .161505$        $p(e) = .160246$
$E/N_0 = 5 \text{ dB}$ $r = .888785$ $g_1 = .642817$ $g_2 = -.578550$ $g_3 = .623676 \times 10^{-1}$ $p(e) = .800263 \times 10^{-1}$	$K = 100$ $\phi_1 = .932805$ $\phi_2 = .911643$ $\phi_3 = .749511$ $K = 400$ $\phi_1 = .924907$ $\phi_2 = .886843$ $\phi_3 = .752203$	$g_1 = .664334$ $g_2 = -.556296$ $g_3 = .558376 \times 10^{-1}$  $g_1 = .650377$ $g_2 = -.569073$ $g_3 = .520069 \times 10^{-1}$	     $p(e) = .820992 \times 10^{-1}$        $p(e) = .803929 \times 10^{-1}$
$E/N_0 = 10 \text{ dB}$ $r = .499801$ $g_1 = 1.27345$ $g_2 = -1.22638$ $g_3 = .147568$ $p(e) = .255149 \times 10^{-1}$	$K = 100$ $\phi_1 = .921746$ $\phi_2 = .883289$ $\phi_3 = .765356$ $K = 400$ $\phi_1 = .928777$ $\phi_2 = .888936$ $\phi_3 = .769461$	$g_1 = 1.26826$ $g_2 = -1.18420$ $g_3 = .139419$  $g_1 = 1.25737$ $g_2 = -1.19015$ $g_3 = .136201$	     $p(e) = .263344 \times 10^{-1}$        $p(e) = .257505 \times 10^{-1}$

Table 5. (Continued)

True Data	Estimates $\phi^*$	Estimates $G^*$	Error Rate
$E/N_0 = 15 \text{ dB}$ $r = .281059$ $g_1 = 2.39697$ $g_2 = -2.448$ $g_3 = .3276$ $p(e) = .248033 \times 10^{-2}$	$K = 100$ $\phi_1 = .886738$ $\phi_2 = .831381$ $\phi_3 = .774201$ $K = 400$ $\phi_1 = .938559$ $\phi_2 = .893108$ $\phi_3 = .751622$	$g_1 = 2.27338$ $g_2 = -2.42825$ $g_3 = .259117$  $g_1 = 2.3178$ $g_2 = -2.37971$ $g_3 = .342483$	$p(e) = .346750 \times 10^{-2}$    $p(e) = .261718 \times 10^{-2}$
$E/N_0 = 20 \text{ dB}$ $r = .158051$ $g_1 = 4.32571$ $g_2 = -4.63936$ $g_3 = .683923$ $p(e) = .116825 \times 10^{-4}$	$K = 100$ $\phi_1 = .94344$ $\phi_2 = .894073$ $\phi_3 = .752790$ $K = 400$ $\phi_1 = .942188$ $\phi_2 = .892235$ $\phi_3 = .747709$	$g_1 = 4.1031$ $g_2 = -4.79684$ $g_3 = .50257$  $g_1 = 4.17752$ $g_2 = -4.79354$ $g_3 = .500835$	$p(e) = .468965$    $p(e) = .221338$
$E/N_0 = 25 \text{ dB}$ $r = .888785 \times 10^{-1}$ $g_1 = 7.51162$ $g_2 = -8.38364$ $g_3 = 1.34467$ $p(e) = 0.$	$K = 100$ $\phi_1 = .923291$ $\phi_2 = .875451$ $\phi_3 = .771556$ $K = 400$ $\phi_1 = .918802$ $\phi_2 = .870304$ $\phi_3 = .774477$	$g_1 = 7.36274$ $g_2 = -8.43728$ $g_3 = 1.21118$  $g_1 = 7.36437$ $g_2 = -8.43565$ $g_3 = 1.21267$	$p(e) = 0$    $p(e) = 0$

Table 5. (Continued)

When the filter gains are large, they dominate the Information Matrix. In such cases, the transition matrix values,  $\phi_1, \phi_2, \phi_3$  have lesser effect. The filter gains increase as the ratio of colored noise to white noise increases. Thus for a fixed ratio of signal to colored interference (SJRDB = 0 dB), the filter gains increase with  $E/N_0$ . Since the error rate decreases with  $E/N_0$ , it is for low error rates that good initialization of the filter gain identification is needed.

When  $E/N_0 = 20$  dB, estimates of  $\phi$  and  $G$  closely approximate the true values, and yet the error rate performance is poor. This is because the error rate is determined by  $\phi^*$  and  $G^*$  according to the function  $\Sigma \phi^*(I - G^* \Lambda)$ , as in equations (8) and (9). Thus, when  $|G^*|$  is very large, the error rate is very sensitive to identification error. Conversely, when  $|G^*|$  is quite small, even quite approximate estimates give good error rate performance.

Another example case was examined where the generator structure was

$$\gamma_1 = 11.1439$$

$$\gamma_2 = -14.0932$$

$$\gamma_3 = 3.03111$$

$$\lambda_1 = \lambda_2 = \lambda_3 = 1.0$$

$$\phi_1 = 0.927374$$

$$\phi_2 = 0.881911$$

$$\phi_3 = 0.777768$$

This structure resulted from the following specification of the signal communication problem:

Number of Samples per Symbol (NSPB) : 10

Number of Symbols per Second (BR) :  $25 \times 10^3$

Signal to Colored Interference Ratio (SJRDB) : -20 dB

Colored Interference Bandwidth (BW) : 2743 Hz.

Energy per symbol : Noise Spectral Density ( $E/N_0$ ) : Variable

Table 6 shows the results for two values of  $E/N_0$ , 5 dB and 30 dB. Again, very accurate initialization of the filter gain identification



algorithms is required for convergence. In this case, the ratio of colored interference to white noise is 20 dB greater than in the previous example. Thus, the filter gains are greater by roughly a factor of ten.

TABLE 6  
ERROR-RATE PERFORMANCE FOR SJR = -20 dB

True Data	Estimate $\phi^*$	Estimate $G^*$	Error Rate
$E/N_0 = 5 \text{ dB}$	$K = 200$		
$r = .888785$	$\phi_1 = .923614$	$g_1 = 7.41383$	$p(e) = .286132$
$g_1 = 7.51253$	$\phi_2 = .875887$	$g_2 = -8.43760$	
$g_2 = -8.38495$	$\phi_3 = .770917$	$g_3 = 1.16079$	
$g_3 = 1.34489$	$K = 400$		
$p(e) = .257187$	$\phi_1 = .920892$	$g_1 = 7.41404$	$p(e) = .282038$
	$\phi_2 = .871545$	$g_2 = -8.43599$	
	$\phi_3 = .772184$	$g_3 = 1.16233$	
$E/N_0 = 30 \text{ dB}$	$K = 200$	$g_1 = 60.8014$	$p(e) = .393391 \times 10^{-5}$
$r = .499801 \times 10^{-1}$	$\phi_1 = .944248$	$g_2 = -74.9986$	
$g_1 = 60.4589$	$\phi_2 = .894856$	$g_3 = 15.0013$	
$g_2 = -74.7359$	$\phi_3 = .759842$		
$g_3 = 15.1978$	$K = 400$		
$p(e) = 0.0$	$\phi_1 = .946587$	$g_1 = 60.8012$	$p(e) = .953674 \times 10^{-6}$
	$\phi_2 = .895022$	$g_2 = -74.9988$	
	$\phi_3 = .757249$	$g_3 = 15.0012$	

The previous two examples show that the identification algorithms become more difficult to initialize as the ratio of colored noise to white noise becomes greater. However, these are precisely the conditions under which accurate identification becomes less critical. It has been shown above that so long as all elements in  $G^*$  are increased by the same factor the only effect on the error rate is that of letting additional white noise into the system. Quite large identification errors may be tolerated in this manner.

## SECTION V

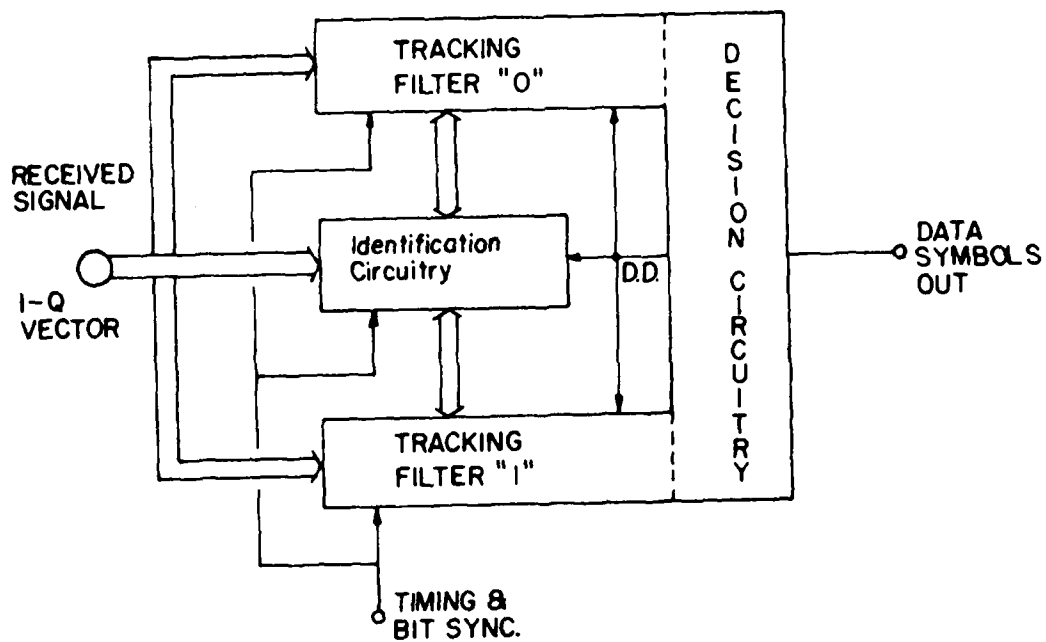
### RECEIVER DESIGN AND PRACTICALITY EVALUATION

#### 1. BASIC RECEIVER SYSTEM DESIGN

Figure 48 shows the basic receiver block diagram. It includes the two decision-directed (D.D.) filters for tracking both additive and multiplicative colored interference. These two filters provide inputs (the tracking error waveforms) to the bit decision circuitry. Also included is the identification circuitry which processes the received signal to provide the constants (perhaps slowly time-varying) for implementing the filters. The identification circuitry is also decision-directed. For this design, it is assumed that timing and bit synchronization references are provided externally. In the final design, bit synchronization will necessarily also be derived directly from the received signal. The method for obtaining bit synchronization was not considered in the present investigation.

The question of feasibility of the present design breaks down into more or less separate questions about the theoretical feasibility and the hardware feasibility. A critical part of the theoretical feasibility question concerns the exact implementation of the identification circuitry. This is dealt with, separately, below. The hardware feasibility question concerns the implementation of both the identification circuitry and the tracking filters. In particular, the hardware question is that of how to implement sampled-data hardware at high sampling rates. This latter question was originally posed in [1].

Another part of the theoretical feasibility question is that of deriving a carrier phase reference for the tracking filters. This question is not critical in the context of multiplicative noise (multipath). In [3] it was shown that a multiplicative noise tracking receiver also tracks out the phase error of a carrier phase-locked loop subjected to the multiplicative noise environment. It is therefore conjectured that a receiver with tracking capability for both multiplicative and additive colored noise will track out the phase error of a carrier phase-locked loop subjected to the additive noise environment. However, the question may be critical for an interfering c.w. carrier which is close enough in frequency to the transmitted carrier to capture the phase-locked loop. The question of the effects of additive interference, c.w. or noise-like, on the carrier tracking loop should be investigated for the IDEI detector.



BASIC RECEIVER BLOCK DIAGRAM

Figure 48. Basic Receiver Block Diagram

## 2. IMPLEMENTATION OF IDENTIFICATION

From [1], the optimum set of required identifying algorithms are those which yield minimum mean-squared-error between the true and identified structure of the colored interference generator. Also, because the IDEI tracking algorithms are sampled-data recursive, memory requirements can be minimized if the identification algorithms are also sampled-data recursive.

The algorithms actually developed during the present investigation were based on the Maximum Likelihood estimation criterion, rather than the Conditional-Mean criterion, called for in [1]. These M.L. algorithms do not necessarily yield minimum-mean-squared-error for estimation of the structure parameters. Neither are they completely recursive, since they operate on batches of received data vector measurements. The reason that batch-M.L. identification was used is that there existed previous well documented theoretical work in the general area. The previous work was extended to the specific case of a coupled I-Q data vector, using the Minimum Canonical Form for the interference generator which was originally derived under this investigation.

The results of Sections III.3 and IV.4 showed several interesting facts. First, when the colored interference vector,  $y(k)$ , was modeled as Markov-1 (the  $\phi$ -matrix is 2x2) the M-L identification algorithm converged nicely to  $\phi^*$  and  $G^*$  with reasonable initialization of the estimates. However, when  $y(k)$  was modeled as Markov-3 (the  $\phi$ -matrix is 6x6) extremely accurate initialization was required for convergence. Secondly, it is possible, even with good convergence, for the resulting error rate to be poor, as for  $E/N_0 = 20$  dB in Table 5 on page 106. Thus it appears that the IDEI tracking detection performance can have great sensitivity to the structure of the filter as identified by the M.L. algorithms, even when the convergence is quite good.

The possible poor error rate under ML identification should be contrasted with the good error rate sensitivity demonstrated in Section IV.3 where the identified filter structure was far removed from the optimum structure. In terms of identification error the filter structure was poor and yet the error rate remained good. What these results imply is that there probably exists an ad hoc identification scheme which will perform much better than the "optimum" M-L identification algorithm, so far as minimizing probability of error is concerned.

One such ad hoc scheme would be to model the possibly Markov-N disturbance,  $y(k)$ , as Markov-1 and use the simple 2x2 identification algorithm to identify a "dominant pole" in the  $\phi$ -matrix and a dominant gain term in the G-matrix. The actual Nth-order  $\phi^*$  and  $G^*$  could then be synthesized using a deterministic filter model such as Butterworth or Chebyshev. Another ad hoc scheme would be to estimate directly the amplitude and bandwidth of the disturbance,  $y(k)$ , and deterministically synthesize a filter for the identified amplitude and bandwidth process using a "design-point" value for  $E/N_0$ .

It is clear that further refinement of the method of implementing identification is required before the IDEI detector can be stated to be theoretically feasible for non-band-limited signals such as PSK and FSK. Such further work should concentrate on a combination of sub-optimal identification of fewer parameters, coupled with deterministic filter synthesis.

### 3. HARDWARE PRACTICALITY

The key question about hardware remains that of fast sampled-data processing. The tracking filters need not be overly complex, having, perhaps, from one to three states per In-phase and per Quadrature vector element per multiplicative noise tracker and per additive noise tracker. However, the tracking filters must process samples at a much higher rate than the Nyquist rate, at least for non-band-limited PSK and FSK signals. Also, the identification processor must accept samples at the same rate during the interval of time over which it is collecting data. It does not, necessarily, need to process the data at the same rate as the recursive tracking filters. Thus, the practicality of hardware is mainly to be determined by the implementation of the fast tracking filters. The required processing speed is proportional to the bandwidth of the disturbance being tracked. For narrow-band disturbances and symbol rates less than, say, 2400 BPS, the processing speed may be achieved using standard digital hardware. For wide-band disturbances and high data rates, CCD filters may be applicable. A practical hardware design will be completely dependent on the signalling environment and interference scenario.

## SECTION VI

### CONCLUSION

This report has documented the results of a fourteen month effort to determine performance boundaries for Integrated Detection, Estimation, and Identification. The best performance of the IDEI detector for perfect identification has been determined using PSK and FSK signal modulation and the probability of error performance criterion.

It was shown that the IDEI algorithms with perfect identification provide performance which is orders of magnitude better than that of standard detectors optimized for white noise only, when the additive and/or multiplicative interference is colored. Furthermore, it was shown that the optimum performance degrades smoothly with increasing error in identification of the strength and/or bandwidth of the additive colored process.

A most interesting result was that the error-rate performance of the IDEI detector depends not only on the accuracy of identification but also on the exact mechanism of the identification error. This result was dwelt upon in Section V. This result implies that rigorously derived stochastic identification algorithm may not be the best solution for the IDEI detector.

Another interesting result is the apparent better performance of PSK over FSK in heavy additive colored interference. This was shown in Figure 13, 14, 15, and 19. Since both closed form and Monte Carlo results agreed, the result is presumed to be valid. The physical explanation for this result has not been found during the present work.

Based on the results obtained in this investigation, the next steps required for reducing the detector to practice become clear. First, a better method for identifying the structure of the tracking filter is needed. It is recommended that a procedure be used which is partly stochastic and partly deterministic. The stochastic identification would be confined to just the strength and bandwidth of the interfering colored process. The tracking filter would then be deterministically synthesized to match the identified process.

Second, the IDEI detector must be augmented with a carrier phase estimator for obtaining the required carrier phase references. The effects of the multiplicative and/or additive colored processes upon the carrier phase estimate and also upon the detector error rate must be determined

quantitatively. Alternately, it should be determined whether or not the IDEI technique can be applied to incoherent detection wherein the carrier phase dependency is deliberately averaged out of the detection algorithm. An intermediate step between the coherent and incoherent IDEI approaches would be to determine if the coherent IDEI detector can be augmented to obtain carrier phase from symbol to symbol, as in DPSK.

Finally, the method for maintaining bit synchronization and system timing must be determined, implemented, and evaluated. It is felt that this scheme will probably be an "early-late" implementation which is more or less standard.

To summarize, it is felt that the IDEI detector has been shown to possess sufficient performance properties to warrant further analysis, design, and ultimate development. It is hoped that the effort to develop the IDEI detector will be continued to fruition.

## APPENDIX A

### DERIVATION OF THE PSEUDO-INNOVATIONS

#### AUTOCOVARANCE FUNCTION

In Section II, the autocovariance function,  $V_{\xi\xi}(j)$  for  $j = 0, 1, 2, \dots$ , was required to numerically evaluate the closed form expression for error rate of the IDEI detector under mis-identification. The autocovariance function  $V_{\xi\xi}(j)$  is the covariance,  $E\{\underline{\xi}(k)\underline{\xi}^T(k-j)\}$ , where  $\underline{\xi}(k)$  is the pseudo-Innovations process of a Kalman filter whose structure is not optimum for the signal being filtered. Figure 1, below, shows the structure of the actual generating model for the signal process,  $\underline{y}(k)$ , and the Kalman filter using identified structure.

The equations governing the actual data generator are

$$\underline{x}(k+1) = \Phi \underline{x}(k) + \Gamma \underline{w}(k); \quad V_{ww}(k) = I$$

$$\underline{y}(k) = \Lambda \underline{x}(k); \quad V_{nn}(k) = V_{nn}$$

$$\underline{z}(k) = \underline{y}(k) + \underline{n}(k) = \Lambda \underline{x}(k) + \underline{n}(k) \quad A-1$$

The Kalman filter equations are

$$\hat{\underline{x}}(k|k) = \hat{\underline{x}}(k|k-1) + G^* \underline{\xi}(k)$$

$$\hat{\underline{x}}(k|k-1) = \Phi^* \hat{\underline{x}}(k-1|k-1)$$

$$\underline{\xi}(k) = \underline{z}(k) - \Lambda \hat{\underline{x}}(k|k-1) \quad A-2$$

In the data generator, the input driving process may be assumed to be white, Gaussian, zero-mean, with unit variance. Also, the output matrix,  $\Lambda$ , may be assumed known and fixed. Any particular autocovariance for  $\underline{y}(k)$  may be realized through manipulation of only  $\Gamma$ ,  $\Phi$ , and  $N$ , the order of the filter-generator. The additive white (receiver-generated) noise,  $\underline{n}(k)$ , is modeled as having a variance,  $V_{nn}$ , which is not known, a Priori.

Since  $\Lambda$  is known, the only elements of the Kalman filter which need be identified are the gain,  $G^*$ , and transition matrix,  $\Phi^*$ , which, latter, is the counterpart of the  $\Phi$ -matrix in the generator. If  $G^*$  is identified



directly from the data,  $\underline{x}(k)$ , then the white noise variance,  $V_{nn}$ , need not be identified separately.

The state-prediction error is defined as

$$\hat{\underline{x}}(k|k-1) \triangleq \underline{x}(k) - \hat{\underline{x}}(k|k-1) \quad A-3$$

The pseudo-innovations may be written in terms of the prediction error,  $\hat{\underline{x}}(k|k-1)$  as

$$\underline{\xi}(k) = \Lambda \hat{\underline{x}}(k|k-1) + \underline{n}(k) \quad A-4$$

In the steady-state,  $\underline{y}(k)$  and  $\underline{n}(k)$  are zero-mean and so is  $\underline{\xi}(k)$ . Thus, the steady-state auto-covariance function for  $\underline{\xi}(k)$  is given as

$$\begin{aligned} V_{\xi\xi}(j) &= E\{\underline{\xi}(k)\underline{\xi}^T(k-j)\} \\ &= \Lambda E\{\hat{\underline{x}}(k|k-1)\hat{\underline{x}}^T(k-j|k-j-1)\Lambda^T \\ &\quad + \Lambda E\{\hat{\underline{x}}(k|k-1)\underline{n}^T(k-j)\}; \quad 0 < j \end{aligned} \quad A-5$$

where use has been made of the facts that since  $\underline{n}(k)$  is white and independent of  $\underline{w}(k)$ , then

$$\begin{aligned} \underline{n}(k) &\perp \hat{\underline{x}}(k-j|k-j-1); \quad 0 \leq j \\ \underline{n}(k) &\perp \underline{n}(k-j); \quad 0 < j \end{aligned} \quad A-6$$

To evaluate the expectations in A-5 requires, first, the one-stage evolution equation for  $\hat{\underline{x}}(k|k-1)$ , which is obtained as follows.

$$\begin{aligned} \hat{\underline{x}}(k|k-1) &= \Phi^* \hat{\underline{x}}(k-1|k-1) \\ &= \Phi^* [\hat{\underline{x}}(k-1|k-2) + G^* \underline{\xi}(k-1)] \\ &= \Phi^* \hat{\underline{x}}(k-1|k-2) + \Phi^* G^* [\underline{z}(k-1) - \Lambda \hat{\underline{x}}(k-1|k-2)] \\ &= \Phi^* [I - G^* \Lambda] \hat{\underline{x}}(k-1|k-2) + \Phi^* G^* [\Lambda \underline{x}(k-1) + \underline{n}(k-1)] \\ &= \Phi^* [I - G^* \Lambda] \hat{\underline{x}}(k-1|k-2) + \Phi^* G^* \underline{x}(k-1) \\ &\quad + \Phi^* G^* \underline{n}(k-1) \end{aligned} \quad A-7$$

Next, the one-stage evolution equation for  $\underline{x}(k|k-1)$  is obtained as

$$\begin{aligned}
 \tilde{\underline{x}}(k|k-1) &= \underline{x}(k) - \hat{\underline{x}}(k|k-1) \\
 &= \phi \underline{x}(k-1) + \Gamma \underline{w}(k-1) - \phi^* [I - G^* \Lambda] \hat{\underline{x}}(k-1|k-2) \\
 &\quad - \phi^* G^* \Lambda \underline{x}(k-1) - \phi^* G^* \underline{n}(k-1) \\
 &= \phi^* [I - G^* \Lambda] [\underline{x}(k-1) - \hat{\underline{x}}(k-1|k-2)] \\
 &\quad - \phi^* [I - G^* \Lambda] \underline{x}(k-1) + [\phi^* + \Delta \phi] \underline{x}(k-1) \\
 &\quad + \Gamma \underline{w}(k-1) - \phi^* G^* \Lambda \underline{x}(k-1) - \phi^* G^* \underline{n}(k-1) \\
 &= \phi^* [I - G^* \Lambda] \tilde{\underline{x}}(k-1|k-2) + \Delta \phi \underline{x}(k-1) - \phi^* G^* \underline{n}(k-1) \\
 &\quad + \Gamma \underline{w}(k-1) \quad \text{A-8}
 \end{aligned}$$

where  $\phi^* \triangleq \phi - \Delta \phi$

The  $j$ -stage evolution equation follows as

$$\begin{aligned}
 \tilde{\underline{x}}(k|k-1) &= [\phi^* (I - G^* \Lambda)]^j \tilde{\underline{x}}(k-j|k-j-1) + \sum_{i=k-j}^{k-1} [\phi^* (I - G^* \Lambda)]^{k-1-i} \\
 &\quad [\Delta \phi \underline{x}(i) - \phi^* G^* \underline{n}(i) + \Gamma \underline{w}(i)] \quad \text{A-9}
 \end{aligned}$$

It follows that

$$\begin{aligned}
 E\{\tilde{\underline{x}}(k|k-1) \tilde{\underline{x}}^T(k-j|k-j-1)\} &= [\phi^* (I - G^* \Lambda)]^j E\{\tilde{\underline{x}}(k-j|k-j-1) \tilde{\underline{x}}^T(k-j|k-j-1)\} \\
 &\quad + \sum_{i=k-j}^{k-1} [\phi^* (I - G^* \Lambda)]^{k-1-i} \cdot \\
 &\quad E\{[\Delta \phi \underline{x}(i) - \phi^* G^* \underline{n}(i) + \Gamma \underline{w}(i)] \tilde{\underline{x}}^T(k-j|k-j-1)\} \\
 &= [\phi^* (I - G^* \Lambda)]^j E\{\tilde{\underline{x}}(k-j|k-j-1) \tilde{\underline{x}}^T(k-j|k-j-1)\} \\
 &\quad + \sum_{i=k-j}^{k-1} [\phi^* (I - G^* \Lambda)]^{k-1-i} \Delta \phi E\{\underline{x}(i) \tilde{\underline{x}}^T(k-j|k-j-1)\} \quad \text{A-10}
 \end{aligned}$$

wherein use has been made of the fact that

$$\begin{aligned}\tilde{\underline{x}}(k-j|k-j-1) &\perp \underline{w}(i) ; & i = k-j, k-j-1, \dots, k-1 \\ \tilde{\underline{x}}(k-j|k-j-1) &\perp \underline{n}(i) ; & \text{A-11}\end{aligned}$$

Now,

$$\underline{x}(i) = \phi^{i-(k-j)} \underline{x}(k-j) + \sum_{\ell=k-j}^{i-1} \phi^{i-1-\ell} \Gamma \underline{w}(\ell) \quad \text{A-12}$$

and thus

$$\begin{aligned}E\{\underline{x}(i) \tilde{\underline{x}}^T(k-j|k-j-1)\} \\ = \phi^{i-(k-j)} E\{\underline{x}(k-j) \tilde{\underline{x}}^T(k-j|k-j-1)\} + \sum_{\ell=k-j}^{i-1} \phi^{i-1-\ell} \cdot\end{aligned}$$

$$\begin{aligned}& \Gamma E\{\underline{w}(\ell) \tilde{\underline{x}}^T(k-j|k-j-1)\} \\ & = \phi^{i-(k-j)} E\{\underline{x}(k-j) \tilde{\underline{x}}^T(k-j|k-j-1)\}; \\ & \tilde{\underline{x}}(k-j|k-j-1) \perp \underline{w}(\ell) : & k-j \leq \ell & \text{A-13}\end{aligned}$$

Substituting A-13 into A-10 gives

$$\begin{aligned}E\{\tilde{\underline{x}}(k|k-1) \tilde{\underline{x}}^T(k-j|k-j-1)\} &= [\phi^*(I - G^* \Lambda)]^j E\{\tilde{\underline{x}}(k-j|k-j-1) \cdot \\ & \tilde{\underline{x}}^T(k-j|k-j-1)\} + \sum_{i=k-j}^{k-1} [\phi^*(I - G^* \Lambda)]^{k-1-i} \cdot \Delta \phi \cdot \\ & \phi^{i-(k-j)} \cdot E\{\underline{x}(k-j) \tilde{\underline{x}}^T(k-j|k-j-1)\} & \text{A-14}\end{aligned}$$

Now, the cross-variance term between  $\underline{x}(k-j)$  and  $\tilde{\underline{x}}(k-j|k-j-1)$  must be computed.

$$\begin{aligned}E\{\underline{x}(k) \tilde{\underline{x}}^T(k|k-1)\} \\ &= E\{\underline{x}(k) [\phi^*(I - G^* \Lambda) \tilde{\underline{x}}(k-1|k-2) + \Delta \phi \underline{x}(k-1) - \phi^* G^* \underline{n}(k-1) \\ & \quad + \Gamma \underline{w}(k-1)]^T\} \\ &= E\{[\phi \underline{x}(k-1) + \Gamma \underline{w}(k-1)] [\phi^*(I - G^* \Lambda) \tilde{\underline{x}}(k-1|k-2) + \\ & \quad + \Delta \phi \underline{x}(k-1) + \Gamma \underline{w}(k-1)]^T\}\end{aligned}$$

(continued)

$$\begin{aligned}
&= \phi E\{\underline{x}(k-1)\underline{\hat{x}}^T(k-1|k-2)\}(I - G^*\Lambda)^T \phi^*{}^T + \phi E\{\underline{x}(k-1) \cdot \\
&\quad \underline{x}^T(k-1)\} \Delta \phi^T + \Gamma \Gamma^T
\end{aligned}
\tag{A-15}$$

where use has been made of the facts that

$$\begin{aligned}
\underline{x}(k) &\perp \underline{n}(k-1) \\
\underline{x}(k-1) &\perp \underline{w}(k-1) \\
\underline{\hat{x}}(k-1|k-2) &\perp \underline{w}(k-1)
\end{aligned}
\tag{A-16}$$

Similarly,

$$\begin{aligned}
&E\{\underline{\hat{x}}(k|k-1)\underline{x}^T(k)\} \\
&= \phi^*(I - G^*\Lambda) E\{\underline{\hat{x}}(k-1|k-2)\underline{x}^T(k-1)\} \phi^T \\
&\quad + \Delta \phi E\{\underline{x}(k-1)\underline{x}^T(k-1)\} \phi^T + \Gamma \Gamma^T
\end{aligned}
\tag{A-17}$$

Equations A-15 and A-17 are recursive. Now define

$$\begin{aligned}
E\{\underline{x}(k)\underline{\hat{x}}^T(k|k-1)\} &\triangleq V_{\underline{x}\underline{\hat{x}}}^{\sim}(k) \quad ; \text{ with steady-state solution, } V_{\underline{x}\underline{\hat{x}}}^{\sim} \\
E\{\underline{\hat{x}}(k|k-1)\underline{x}^T(k)\} &\triangleq V_{\underline{\hat{x}}\underline{x}}^{\sim}(k) \quad ; \text{ with steady-state solution, } V_{\underline{\hat{x}}\underline{x}}^{\sim} \\
E\{\underline{x}(k)\underline{x}^T(k)\} &\triangleq V_{\underline{x}\underline{x}}(k) \quad ; \text{ with steady-state solution, } V_{\underline{x}\underline{x}}
\end{aligned}
\tag{A-18}$$

Then, it follows that

$$\begin{aligned}
V_{\underline{x}\underline{x}}(k) &= \phi V_{\underline{x}\underline{x}}(k-1) \phi^T + \Gamma \Gamma^T \\
V_{\underline{x}\underline{\hat{x}}}^{\sim}(k) &= \phi V_{\underline{x}\underline{\hat{x}}}^{\sim}(k-1) \cdot (I - G^*\Lambda)^T \phi^*{}^T + \phi V_{\underline{x}\underline{x}}(k-1) \Delta \phi^T + \Gamma \Gamma^T \\
V_{\underline{\hat{x}}\underline{x}}^{\sim}(k) &= \phi^*(I - G^*\Lambda) V_{\underline{\hat{x}}\underline{x}}^{\sim}(k-1) \phi^T + \Delta \phi V_{\underline{x}\underline{x}}(k-1) \phi^T + \Gamma \Gamma^T
\end{aligned}
\tag{A-19}$$

Next, define

$$\begin{aligned} E\{\tilde{x}(k|k-1)\tilde{x}^T(k|k-1)\} &\triangleq V_{xx}(k|k-1) \\ E\{\tilde{x}(k|k-1)\tilde{x}^T(k-j|k-j-1)\} &= V_{xx}(k, k-j|k-1, k-j-1) \quad A-20 \end{aligned}$$

Then becomes

$$\begin{aligned} V_{xx}(k, k-j|k-1, k-j-1) &= [\phi^*(I - G^*\Lambda)]^j V_{xx}(k-j|k-j-1) + \\ &+ \sum_{i=k-j}^{k-1} [\phi^*(I - G^*\Lambda)]^{k-1-i} \cdot \Delta\phi \cdot \phi^{i-(k-j)} V_{xx}(k-j) \end{aligned} \quad A-21$$

where  $V_{xx}(k-j)$  is the steady-state value defined by the recursion of A-19 and  $V_{xx}(k-j|k-j-1)$  is the steady-state defined by the following recursion

$$\begin{aligned} V_{xx}(k|k-1) &= E\{\tilde{x}(k|k-1)\tilde{x}^T(k|k-1)\} \\ &= E\{[\phi^*(I - G^*\Lambda)\tilde{x}(k-1|k-2) + \Delta\phi x(k-1) - \phi^*G^*\underline{n}(k-1) \\ &\quad + \Gamma w(k-1)] \cdot [-]^T\} \\ &= \phi^*(I - G^*\Lambda)E\{\tilde{x}(k-1|k-2)\tilde{x}^T(k-1|k-2)\} \cdot (I - G^*\Lambda)^T \phi^{*T} \\ &\quad + \phi^*(I - G^*\Lambda)E\{\tilde{x}(k-1|k-2)x^T(k-1)\Delta\phi^T \\ &\quad + \Delta\phi E\{x(k-1)\tilde{x}^T(k-1|k-2)\} \cdot (I - G^*\Lambda)^T \phi^{*T} + \Delta\phi E\{x(k-1) \cdot \\ &\quad x^T(k-1)\}\Delta\phi^T + \phi^*G^*V_{nn}G^{*T}\phi^{*T} + \Gamma\Gamma^T \end{aligned} \quad A-22$$

which reduces to

$$\begin{aligned} V_{xx}(k|k-1) &= \phi^*(I - G^*\Lambda)V_{xx}(k-1|k-2)(I - G^*\Lambda)^T \phi^{*T} \\ &\quad + \Delta\phi V_{xx}(k-1)\Delta\phi^T + \phi^*(I - G^*\Lambda)V_{xx}(k-1)\Delta\phi^T \\ &\quad + \Delta\phi V_{xx}(k-1)(I - G^*\Lambda)^T \phi^{*T} + \phi^*G^*V_{nn}G^{*T}\phi^{*T} + \Gamma\Gamma^T \end{aligned} \quad A-23$$

There remains to be evaluated the term

$$\begin{aligned}
E\{\tilde{x}(k|k-1)\tilde{n}^T(k-j)\} &= [\phi^*(I - G^*\Lambda)]^j E\{\tilde{x}(k-j|k-j-1)\tilde{n}^T(k-j)\} \\
&+ \sum_{i=k-j}^{k-1} [\phi^*(I - G^*\Lambda)]^{k-1-i} E\{[\Delta\phi\tilde{x}(i) - \phi^*G^*\tilde{n}(i) \\
&+ \Gamma\tilde{w}(i)]\tilde{n}^T(k-j)\} \\
&= -[\phi^*(I - G^*\Lambda)]^{j-1} \phi^*G^*V_{nn} ; \quad 0 < j \quad A-24
\end{aligned}$$

The computational steps are now enumerated as

$$\begin{aligned}
i) \quad V_{\xi\xi}(j) &= \Lambda V_{xx}^{\sim}(k, k-j|k-1, k-j-1)\Lambda^T \\
&- \Lambda[\phi^*(I - G^*\Lambda)]^{j-1} \phi^*G^*V_{nn} \\
ii) \quad V_{xx}^{\sim}(k, k-j|k-1, k-j-1) &= [\phi^*(I - G^*\Lambda)]^j V_{xx}^{\sim}(k-j|k-j-1) \\
&+ \sum_{i=k-j}^{k-1} [\phi^*(I - G^*\Lambda)]^{k-1-i} \cdot \Delta\phi \cdot \phi^{i-(k-j)} \cdot V_{xx}^{\sim}(k-j) \\
iii) \quad V_{xx}^{\sim}(k|k-1) &= \phi^*(I - G^*\Lambda)V_{xx}^{\sim}(k-1|k-2)(I - G^*\Lambda)^T \phi^{*T} + \\
&+ \Delta\phi V_{xx}(k-1)\Delta\phi^T + \phi^*(I - G^*\Lambda)V_{xx}^{\sim}(k-1)\Delta\phi^T + \\
&+ \Delta\phi V_{xx}^{\sim}(k-1)(I - G^*\Lambda)^T \phi^{*T} + \phi^*G^*V_{nn}G^{*T} \phi^{*T} + \Gamma\Gamma^T \\
iv) \quad V_{xx}^{\sim}(k) &= \phi V_{xx}^{\sim}(k-1) \cdot (I - G^*\Lambda)^T \phi^{*T} + \phi V_{xx}(k-1)\Delta\phi^T + \Gamma\Gamma^T \\
v) \quad V_{xx}^{\sim}(k) &= \phi^*(I - G^*\Lambda)V_{xx}^{\sim}(k-1)\phi^T + \Delta\phi V_{xx}(k-1)\phi^T + \Gamma\Gamma^T \\
vi) \quad V_{xx}(k) &= \phi V_{xx}(k-1)\phi^T + \Gamma\Gamma^T ; \quad 0 < j \\
vii) \quad V_{\xi\xi}(j) &= \Lambda V_{xx}^{\sim}(k|k-1)\Lambda^T + V_{nn} ; \quad j=0 \quad A-25
\end{aligned}$$

Now, let  $V_{xx}$ ,  $V_{xx}^{\sim}$ ,  $V_{xx}^{\sim}$ , and  $V_{xx}^{\sim}$  be the steady-state solutions of A-25.

Then the auto-covariance function of the pseudo-Innovations is

$$\begin{aligned}
V_{\xi\xi}(j) &= \Lambda[\Phi^*(I - G^*\Lambda)]^j \tilde{V}_{xx} + \sum_{i=1}^j [\Phi^*(I - G^*\Lambda)]^{j-i} \cdot \\
&\quad \Delta\Phi \cdot \Phi^{j-i} \tilde{V}_{xx} \Lambda^T - \Lambda[\Phi^*(I - G^*\Lambda)]^{j-1} \Phi^* G^* V_{nn} ; \quad 0 < j \\
&= \Lambda \tilde{V}_{xx} \Lambda^T + V_{nn} ; \quad j = 0
\end{aligned} \tag{A-26}$$

Equation A-26 may be put in a more informative form as

$$\begin{aligned}
V_{\xi\xi}(j) &= \Lambda[\Phi^*(I - G^*\Lambda)]^{j-1} \Phi^* [\tilde{V}_{xx} \Lambda^T - G^* (\Lambda \tilde{V}_{xx} \Lambda^T + V_{nn})] \\
&\quad + \Lambda \sum_{i=1}^j [\Phi^*(I - G^*\Lambda)]^{j-i} \cdot \Delta\Phi \cdot \Phi^{j-i} \cdot \tilde{V}_{xx} \Lambda^T ; \quad 0 < j \\
&= \Lambda \tilde{V}_{xx} \Lambda^T + V_{nn} ; \quad j = 0
\end{aligned} \tag{A-27}$$

Note that from A-27, the conditions for  $\xi(k)$  to be white (or for the pseudo-innovations to be the Innovations) is for

$$\begin{aligned}
G^* &= \tilde{V}_{xx} \Lambda^T (\Lambda \tilde{V}_{xx} \Lambda^T + V_{nn})^{-1} = G_{opt} \\
\Delta\Phi &= 0
\end{aligned} \tag{A-28}$$

$G^*$  in A-28 is the value for the Kalman (optimum) gain,  $G_{opt}$ .

## APPENDIX B

### STRUCTURE OF THE PSEUDO-INNOVATIONS AUTOCOVARIANCE FUNCTION FOR A GENERAL IN-PHASE/QUADRATURE PROCESS

#### Statement of the Results

The covariance of the 2-vector stationary Pseudo-Innovations Process,  $\xi(k)$ , is

$$V_{\xi\xi}(j) = \Lambda[\Phi^*(I - G^*\Lambda)]^{j-1} \Phi^* [V_{xx} \Lambda^T - G^*(\Lambda V_{xx} \Lambda^T + V_{nn})] \\ + \Lambda \left\{ \sum_{i=1}^j [\Phi^*(I - G^*\Lambda)]^{i-1} \Delta \Phi \Phi^{j-1} \right\} V_{xx} \Lambda^T \dots$$

for  $0 < j$

where

$$V_{xx} = \Phi^*(I - G^*\Lambda) V_{xx} (I - G^*\Lambda)^T \Phi^{*T} \\ + \Delta \Phi V_{xx} (I - G^*\Lambda)^T \Phi^{*T} + \Phi^*(I - G^*\Lambda) V_{xx} \Delta \Phi^T \\ + \Delta \Phi V_{xx} \Delta \Phi^T + \Gamma \Gamma^T + \Phi^* G^* V_{nn} G^{*T} \Phi^{*T}$$

$$V_{xx} = \Phi V_{xx} (I - G^*\Lambda) \Phi^{*T} + \Phi V_{xx} \Delta \Phi^T + \Gamma \Gamma^T$$

$$V_{xx} = V_{xx}^T$$

$$V_{xx} = \Phi V_{xx} \Phi^T + \Gamma \Gamma^T$$

It will be shown that

$$(I - G^*\Lambda) = \begin{bmatrix} S_{II} & S_{IQ} \\ S_{QI} & S_{QQ} \end{bmatrix} = \begin{bmatrix} S & S' \\ -S' & S \end{bmatrix}$$

$$\Phi^*(I - G^*\Lambda) = \begin{bmatrix} \Phi & \Phi' \\ -\Phi' & \Phi \end{bmatrix} \begin{bmatrix} S & S' \\ -S' & S \end{bmatrix} = \begin{bmatrix} \Phi S - \Phi' S' & \Phi S' + \Phi' S \\ -\Phi' S - \Phi S' & -\Phi' S' + \Phi S \end{bmatrix}$$

$$\Delta \begin{bmatrix} f & f' \\ -f' & f \end{bmatrix} \triangleq F \dots \quad (a)$$



From (a) and Lemma 1, it will be shown by induction that

$$V_{XX} = \begin{bmatrix} V_{XX} & V_{XX}^d \\ -V_{XX}^d & V_{XX} \end{bmatrix} \quad V_{XX} = \begin{bmatrix} V_{XX} & V_{XX}^d \\ -V_{XX}^d & V_{XX} \end{bmatrix} \quad V_{XX} = \begin{bmatrix} V_{XX} & V_{XX}' \\ -V_{XX}' & V_{XX} \end{bmatrix}$$

It will finally be shown that

$$V_{XX}^T \triangleq \begin{bmatrix} u_h & u_h' \\ -u_h' & u_h \end{bmatrix}$$

$$G^*(\Lambda V_{XX}^T + V_{nn}) \triangleq \begin{bmatrix} g_r & g_r' \\ -g_r' & g_r \end{bmatrix}$$

whence

$$V_{XX}^T - G^*(\Lambda V_{XX}^T + V_{nn}) = \begin{bmatrix} \theta & \theta' \\ -\theta' & \theta \end{bmatrix}$$

It is also easily seen that if the In-phase and Quadrature processes are independent (uncorrelated), then the off diagonal terms are null for  $\phi^*(I - G^*\Lambda)$ ,  $\phi^*$ ,  $V_{XX}$ ,  $V_{XX}^d$ ,  $G^*$ ,  $\Delta\phi$ , and  $[V_{XX}^T - G^*(\Lambda V_{XX}^T + V_{nn})]$ . Thus, for the uncorrelated case

$$V_{\xi\xi}(0) = u_{\xi\xi}(0) \begin{bmatrix} 1 & 0 \\ 0 & 1 \end{bmatrix} : u_{\xi\xi}(0) \text{ scalar}$$

For the correlated I-Q case, in general,

$$V_{\xi\xi}(j) = \begin{bmatrix} u_{\xi\xi}(j) & u_{\xi\xi}'(j) \\ -u_{\xi\xi}'(j) & u_{\xi\xi}(j) \end{bmatrix}$$

### Supporting Lemmas and Theorems

#### Lemma 1

A and B are (nxm), (mxl) partitioned matrix respectively.

$$A = \begin{bmatrix} A_1 & A_2 \\ -A_2 & A_1 \end{bmatrix} \quad B = \begin{bmatrix} B_1 & B_2 \\ -B_2 & B_1 \end{bmatrix}$$

Then the resultant matrix  $C = AB$  is also

$$C = \begin{bmatrix} C_1 & C_2 \\ -C_2 & C_1 \end{bmatrix}$$

proof

$$\begin{aligned} AB &= \begin{bmatrix} A_1 & A_2 \\ -A_2 & A_1 \end{bmatrix} \cdot \begin{bmatrix} B_1 & B_2 \\ -B_2 & B_1 \end{bmatrix} = \begin{bmatrix} A_1 B_1 - A_2 B_2 & A_1 B_2 + A_2 B_1 \\ -A_2 B_1 - A_1 B_2 & -A_2 B_2 + A_1 B_1 \end{bmatrix} \\ &= \begin{bmatrix} C_1 & C_2 \\ -C_2 & C_1 \end{bmatrix} \end{aligned}$$

Lemma 2

$$\begin{aligned} [e_1, e_2] \begin{bmatrix} b & b' \\ -b' & b \end{bmatrix} \begin{bmatrix} e_1 \\ e_2 \end{bmatrix} &= [e_1 b - e_2 b', e_1 b' + e_2 b] \begin{bmatrix} e_1 \\ e_2 \end{bmatrix} \\ &= e_1 b e_1 - e_2 b' e_1 + e_1 b' e_2 + e_2 b e_2 = (e_1^2 + e_2^2) b \\ &= b [e_1, e_2] \begin{bmatrix} e_1 \\ e_2 \end{bmatrix} \end{aligned}$$

Lemma 3

$$\begin{aligned}
& \begin{bmatrix} e_1 & e_2 \end{bmatrix} \begin{bmatrix} b & -b' & u_\xi & u'_\xi \\ b' & b & -u'_\xi & u_\xi \end{bmatrix} \begin{bmatrix} b & b' \\ -b' & b \end{bmatrix} \begin{bmatrix} e_1 \\ e_2 \end{bmatrix} \\
&= \begin{bmatrix} e_1 & e_2 \end{bmatrix} \begin{bmatrix} bu_\xi + b'u'_\xi & bu'_\xi - b'u_\xi \\ b'u_\xi - bu'_\xi & b'u'_\xi + bu_\xi \end{bmatrix} \begin{bmatrix} b & b' \\ -b' & b \end{bmatrix} \begin{bmatrix} e_1 \\ e_2 \end{bmatrix} \\
&= \begin{bmatrix} e_1 & e_2 \end{bmatrix} \begin{bmatrix} bu_\xi + b'b'u'_\xi b - bu'_\xi b' + b'u_\xi b' & bu_\xi b' + b'u'_\xi b' + bu'_\xi b - b'u_\xi b \\ b'u_\xi b - bu'_\xi b - b'u_\xi b' - bu_\xi b' & b'u_\xi b' - bu'_\xi b' + b'u'_\xi b + bu_\xi b \end{bmatrix} \begin{bmatrix} e_1 \\ e_2 \end{bmatrix} \\
&= \begin{bmatrix} e_1 & e_2 \end{bmatrix} \begin{bmatrix} (b^2 + b'^2)u_\xi & (b^2 + b'^2)u'_\xi \\ -(b^2 + b'^2)u'_\xi & (b^2 + b'^2)u_\xi \end{bmatrix} \begin{bmatrix} e_1 \\ e_2 \end{bmatrix} \\
&= (b^2 + b'^2)u_\xi \begin{bmatrix} e_1 \\ e_2 \end{bmatrix}
\end{aligned}$$

Behavior of Kalman filter

$$\begin{bmatrix} x_I(k) \\ x_Q(k) \end{bmatrix} = \begin{bmatrix} \phi_1 & 0 & \phi'_1 & 0 \\ 0 & \phi_N & 0 & \phi'_N \\ -\phi'_1 & 0 & \phi_1 & 0 \\ 0 & -\phi'_N & 0 & \phi_N \end{bmatrix} \begin{bmatrix} x_I(k-1) \\ x_Q(k-1) \end{bmatrix} + \begin{bmatrix} \gamma_1 & \gamma'_1 \\ \gamma_2 & \gamma'_2 \\ \gamma_N & \gamma'_N \\ -\gamma'_1 & \gamma_1 \\ -\gamma'_N & \gamma_N \end{bmatrix} \begin{bmatrix} w_1(k-1) \\ w_2(k-1) \end{bmatrix} \quad \text{B-1}$$

$$\begin{bmatrix} z_I(k) \\ z_Q(k) \end{bmatrix} = \begin{bmatrix} \lambda_1 & \lambda_N & 0 & 0 \\ 0 & 0 & \lambda_1 & \lambda_N \end{bmatrix} \begin{bmatrix} x_I(k) \\ x_Q(k) \end{bmatrix} + \begin{bmatrix} n_1(k) \\ n_2(k) \end{bmatrix} \quad \text{B-2}$$

$$x_{Ij}(k) = \phi_j x_{Ij}(k-1) + \phi'_j x_{Qj}(k-1) + \gamma_j w_1(k-1) + \gamma'_j w_2(k-1) \quad \text{B-3}$$

$$X_{Qj}(k) = -\phi_j', X_{Ij}(k-1) + \phi_j X_{Qj}(k-1) - \gamma_j' w_1(k-1) + \gamma_j w_2(k-1)$$

B-4

$$j = 1, 2, \dots, N$$

where  $2 \times N$  is the order of the system

$$1. \quad \hat{X}(k|k-1) = \phi \hat{X}(k-1|k-1)$$

B-5

$$\hat{X}_{Ij}(k|k-1) = \phi_j \hat{X}_{Ij}(k-1|k-1) + \phi_j' \hat{X}_{Qj}(k-1|k-1)$$

B-6.

$$\hat{X}_{Qj}(k|k-1) = -\phi_j \hat{X}_{Ij}(k-1|k-1) + \phi_j \hat{X}_{Qj}(k-1|k-1)$$

B-7

$$2. \quad V_{\hat{X}\hat{X}}(k|k-1) = \phi V_{\hat{X}\hat{X}}(k-1|k-1) \phi^T + \Gamma \Gamma^T$$

B-8

Define

$$V_{II}(\cdot) = E\{\tilde{X}_I(\cdot) \tilde{X}_I^T(\cdot)\}$$

$$V_{QQ}(\cdot) = E\{\tilde{X}_Q(\cdot) \tilde{X}_Q^T(\cdot)\}$$

$$V_{IQ}(\cdot) = E\{\tilde{X}_I(\cdot) \tilde{X}_Q^T(\cdot)\}$$

$$V_{QI}(\cdot) = E\{\tilde{X}_Q(\cdot) \tilde{X}_I^T(\cdot)\}$$

$$\tilde{X}_I(k|k-1) = X_I(k) - \hat{X}_I(k|k-1)$$

B-9

$$\tilde{X}_Q(k|k-1) = X_Q(k) - \hat{X}_Q(k|k-1)$$

B-10

More detailed expression is given

$$\tilde{X}_{Ij}(k|k-1) = \phi_j \tilde{X}_{Ij}(k-1|k-1) + \phi_j' \tilde{X}_{Qj}(k-1|k-1) + \gamma_j w_1(k-1) + \gamma_j' w_2(k-1)$$

B-11

$$\tilde{X}_{Qj}(k|k-1) = -\phi_j \tilde{X}_{Ij}(k-1|k-1) + \phi_j \tilde{X}_{Qj}(k-1|k-1) - \gamma_j' w_1(k-1) + \gamma_j w_2(k-1)$$

B-12

$$V_{\hat{X}\hat{X}}(k|k-1) = \begin{bmatrix} V_{II}(k|k-1) & V_{IQ}(k|k-1) \\ V_{QI}(k|k-1) & V_{QQ}(k|k-1) \end{bmatrix}$$

B-13

$[V^{i,j}(\cdot)]$  denotes the  $i$ th row  $j$ th column of  $V(\cdot)$  matrix

$$V_{II}(k|k-1) = E \left\{ \begin{bmatrix} X_{I1}(k|k-1) \\ \vdots \\ X_{Ii}(k|k-1) \\ \vdots \\ X_{IN}(k|k-1) \end{bmatrix} [X_{Ij}(k|k-1), \dots, X_{Ij}(k|k-1), \dots, X_{IN}(k|k-1)] \right\}$$

B-14

therefore

$$\begin{aligned} [V_{II}^{i,j}(k|k-1)] &= E\{\phi_i \tilde{X}_{Ii}(k-1|k-1) + \phi_i' \tilde{X}_{Qi}(k-1|k-1) + \gamma_i w_1(k-1) + \\ &+ \gamma_i' w_2(k-1)\} [\phi_j \tilde{X}_{Ij}(k-1|k-1) + \phi_j' \tilde{X}_{Qj}(k-1|k-1) + \gamma_j w_1(k-1) + \gamma_j' w_2(k-1)] \\ &= \phi_i \phi_j E\{\tilde{X}_{Ii}(k-1|k-1) \tilde{X}_{Ij}(k-1|k-1)\} + \phi_i \phi_j' E\{\tilde{X}_{Ii}(k-1|k-1) \tilde{X}_{Qj}(k-1|k-1)\} \\ &+ \phi_i' \phi_j E\{\tilde{X}_{Qi}(k-1|k-1) \tilde{X}_{Ij}(k-1|k-1)\} + \phi_i' \phi_j' E\{\tilde{X}_{Qi}(k-1|k-1) \tilde{X}_{Qj}(k-1|k-1)\} \\ &+ \gamma_i \gamma_j + \gamma_i' \gamma_j' \\ &= \phi_i \phi_j [V_{II}^{i,j}(k-1|k-1)] + \phi_i \phi_j' [V_{IQ}^{i,j}(k-1|k-1)] \\ &+ \phi_i' \phi_j [V_{QI}^{i,j}(k-1|k-1)] + \phi_i' \phi_j' [V_{QQ}^{i,j}(k-1|k-1)] + \gamma_i \gamma_j + \gamma_i' \gamma_j' \end{aligned}$$

B-15

Similarly

$$\begin{aligned} [V_{IQ}^{i,j}(k|k-1)] &= E\{\phi_i \tilde{X}_{Ii}(k-1|k-1) + \phi_i' \tilde{X}_{Qi}(k-1|k-1) + \gamma_i w_1(k-1) + \\ &+ \gamma_i' w_2(k-1)\} [-\phi_j' \tilde{X}_{Ij}(k-1|k-1) + \phi_j \tilde{X}_{Qj}(k-1|k-1) - \gamma_j' w_1(k-1) + \gamma_j w_2(k-1)] \\ &= -\phi_i \phi_j' [V_{II}^{i,j}(k-1|k-1)] + \phi_i \phi_j [V_{IQ}^{i,j}(k-1|k-1)] - \phi_i' \phi_j' [V_{QI}^{i,j}(k-1|k-1)] + \\ &+ \phi_i' \phi_j [V_{QQ}^{i,j}(k-1|k-1)] - \gamma_i \gamma_j' + \gamma_i' \gamma_j \end{aligned}$$

B-16

$$\begin{aligned} [V_{QI}^{i,j}(k|k-1)] &= E\{-\phi_i' \tilde{X}_{Ii}(k-1|k-1) + \phi_i \tilde{X}_{Qi}(k-1|k-1) - \gamma_i' w_1(k-1) + \\ &+ \gamma_i w_2(k-1)\} [\phi_j \tilde{X}_{Ij}(k-1|k-1) + \phi_j' \tilde{X}_{Qj}(k-1|k-1) + \gamma_j w_1(k-1) + \gamma_j' w_2(k-1)] \\ &= -\phi_i' \phi_j [V_{II}^{i,j}(k-1|k-1)] - \phi_i' \phi_j' [V_{IQ}^{i,j}(k-1|k-1)] + \phi_i \phi_j [V_{QI}^{i,j}(k-1|k-1)] + \\ &+ \phi_i \phi_j' [V_{QQ}^{i,j}(k-1|k-1)] - \gamma_i' \gamma_j + \gamma_i \gamma_j' \end{aligned}$$

B-17

$$\begin{aligned}
[V_{QQ}^{i,j}(k|k-1)] &= E\{[-\phi_i^i \tilde{X}_{Ii}(k-1|k-1) + \phi_i^i \tilde{X}_{Qi}(k-1|k-1) - \gamma_i^i w_1(k-1) + \\
&+ \gamma_i w_2(k-1)][-\phi_j^j \tilde{X}_{Ij}(k-1|k-1) + \phi_j^j \tilde{X}_{Qj}(k-1|k-1) - \gamma_j^j w_1(k-1) + \gamma_j w_2(k-1)]\} \\
&= \phi_i^i \phi_j^i [V_{II}^{i,j}(k-1|k-1)] - \phi_i^i \phi_j^j [V_{IQ}^{i,j}(k-1|k-1)] - \phi_i^i \phi_j^i [V_{QI}^{i,j}(k-1|k-1)] + \\
&+ \phi_i^i \phi_j^j [V_{QQ}^{i,j}(k-1|k-1)] + \gamma_i^i \gamma_j^i + \gamma_i \gamma_j
\end{aligned}$$

B-18

$$3. \quad G(k) = V_{xx}(k|k-1) \Lambda^T [V_{nn} + \Lambda V_{xx}(k|k-1) \Lambda^T]^{-1}$$

$$\begin{aligned}
V_{xx}(k|k-1) \Lambda^T &= \begin{bmatrix} V_{II}(k|k-1) & V_{IQ}(k|k-1) \\ V_{QI}(k|k-1) & V_{QQ}(k|k-1) \end{bmatrix} \begin{bmatrix} \lambda_1 & 0 \\ \lambda_N & 0 \\ 0 & \lambda_1 \\ 0 & \lambda_N \end{bmatrix} \\
&= \begin{bmatrix} \sum_{j=1}^N V_{II}^{i,j}(k|k-1) \lambda_j & \sum_{j=1}^N V_{IQ}^{i,j}(k|k-1) \lambda_j \\ \sum_{j=1}^N V_{QI}^{i,j}(k|k-1) \lambda_j & \sum_{j=1}^N V_{QQ}^{i,j}(k|k-1) \lambda_j \end{bmatrix} \quad i = 1, 2, \dots, N
\end{aligned}$$

B-19

$$\begin{aligned}
\Lambda V_{xx}(k|k-1) \Lambda^T &= \begin{bmatrix} \lambda_1 & \lambda_N & 0 & 0 \\ 0 & 0 & \lambda_1 & \lambda_N \end{bmatrix} \begin{bmatrix} \sum_{j=1}^N V_{II}^{i,j}(k|k-1) \lambda_j & \sum_{j=1}^N V_{IQ}^{i,j}(k|k-1) \lambda_j \\ \sum_{j=1}^N V_{II}^{N,j}(k|k-1) \lambda_j & \sum_{j=1}^N V_{IQ}^{N,j}(k|k-1) \lambda_j \\ \sum_{j=1}^N V_{QI}^{i,j}(k|k-1) \lambda_j & \sum_{j=1}^N V_{QQ}^{i,j}(k|k-1) \lambda_j \\ \sum_{j=1}^N V_{QI}^{N,j}(k|k-1) \lambda_j & \sum_{j=1}^N V_{QQ}^{N,j}(k|k-1) \lambda_j \end{bmatrix}
\end{aligned}$$

$$= \begin{bmatrix} \sum_{i=1}^N \lambda_i \sum_{j=1}^N V_{II}^{i,j}(k|k-1) \lambda_j & \sum_{i=1}^N \lambda_i \sum_{j=1}^N V_{IQ}^{i,j}(k|k-1) \lambda_j \\ \sum_{i=1}^N \lambda_i \sum_{j=1}^N V_{QI}^{i,j}(k|k-1) \lambda_j & \sum_{i=1}^N \lambda_i \sum_{j=1}^N V_{QQ}^{i,j}(k|k-1) \lambda_j \end{bmatrix}$$

B-20

Equation B-20 can be rewritten as

$$\begin{aligned}
 B(k) &= \Lambda V_{XX}(k|k-1) \Lambda^T \\
 &= \begin{bmatrix} \sum_{i=1}^N \sum_{j=1}^N \lambda_i \lambda_j v_{II}^{i,j}(k|k-1) & \sum_{i=1}^N \sum_{j=1}^N \lambda_i \lambda_j v_{IQ}^{i,j}(k|k-1) \\ \sum_{i=1}^N \sum_{j=1}^N \lambda_i \lambda_j v_{QI}^{i,j}(k|k-1) & \sum_{i=1}^N \sum_{j=1}^N \lambda_i \lambda_j v_{QQ}^{i,j}(k|k-1) \end{bmatrix} \\
 &\triangleq \begin{bmatrix} b_{II} & b_{IQ} \\ b_{QI} & b_{QQ} \end{bmatrix}
 \end{aligned}
 \tag{B-21}$$

$$B^{-1}(k) = \frac{1}{\det(B)} = \frac{1}{b_{II}b_{QQ} - b_{IQ}b_{QI}} \begin{bmatrix} b_{II} & -b_{IQ} \\ -b_{QI} & b_{QQ} \end{bmatrix}$$

where  $\det(B) = b_{II}b_{QQ} - b_{IQ}b_{QI}$

B-22

Combining equations B-19 and B-22, it is easily obtained

$$\begin{aligned}
 G(K) &= V_{XX}(k|k-1) \Lambda^T B^{-1}(K) \\
 &= \frac{1}{\det(B)} \begin{bmatrix} \underline{G}_{II} & \underline{G}_{IQ} \\ \underline{G}_{QI} & \underline{G}_{QQ} \end{bmatrix} = \\
 &\frac{1}{\det(B)} \begin{bmatrix} \sum_{j=1}^N v_{II}^{i,j}(k|k-1) \lambda_j & \sum_{j=1}^N v_{IQ}^{i,j}(k|k-1) \lambda_j \\ \sum_{j=1}^N v_{II}^{N,j}(k|k-1) \lambda_j & \sum_{j=1}^N v_{IQ}^{N,j}(k|k-1) \lambda_j \\ \sum_{j=1}^N v_{QI}^{i,j}(k|k-1) \lambda_j & \sum_{j=1}^N v_{QQ}^{i,j}(k|k-1) \lambda_j \\ \sum_{j=1}^N v_{QI}^{N,j}(k|k-1) \lambda_j & \sum_{j=1}^N v_{QQ}^{N,j}(k|k-1) \lambda_j \end{bmatrix} \begin{bmatrix} b_{II} \\ -\sum_{i=1}^N \sum_{j=1}^N \lambda_i \lambda_j v_{II}^{i,j}(k|k-1) \\ -\sum_{i=1}^N \sum_{j=1}^N \lambda_i \lambda_j v_{QI}^{i,j}(k|k-1) \\ -b_{IQ} \\ -\sum_{i=1}^N \sum_{j=1}^N \lambda_i \lambda_j v_{IQ}^{i,j}(k|k-1) \\ -\sum_{i=1}^N \sum_{j=1}^N \lambda_i \lambda_j v_{QQ}^{i,j}(k|k-1) \\ b_{QQ} \end{bmatrix}
 \end{aligned}
 \tag{B-23}$$

$$\underline{G}_{II} = \begin{bmatrix} \left( \sum_{j=1}^N v_{II}^{i,j}(k|k-1)\lambda_j \right) b_{II} - \left( \sum_{j=1}^N v_{IQ}^{i,j}(k|k-1)\lambda_j \right) b_{QI} \\ \left( \sum_{j=1}^N v_{II}^{N,j}(k|k-1)\lambda_j \right) b_{II} - \left( \sum_{j=1}^N v_{IQ}^{N,j}(k|k-1)\lambda_j \right) b_{QI} \end{bmatrix} \quad B-24$$

$$\underline{G}_{IQ} = \begin{bmatrix} -\left( \sum_{j=1}^N v_{II}^{i,j}(k|k-1)\lambda_j \right) b_{IQ} + \left( \sum_{j=1}^N v_{IQ}^{i,j}(k|k-1)\lambda_j \right) b_{QQ} \\ -\left( \sum_{j=1}^N v_{II}^{N,j}(k|k-1)\lambda_j \right) b_{IQ} + \left( \sum_{j=1}^N v_{IQ}^{N,j}(k|k-1)\lambda_j \right) b_{QQ} \end{bmatrix} \quad B-25$$

$$\underline{G}_{QI} = \begin{bmatrix} \left( \sum_{j=1}^N v_{QI}^{i,j}(k|k-1)\lambda_j \right) b_{II} - \left( \sum_{j=1}^N v_{QQ}^{i,j}(k|k-1)\lambda_j \right) b_{QI} \\ \left( \sum_{j=1}^N v_{QI}^{N,j}(k|k-1)\lambda_j \right) b_{II} - \left( \sum_{j=1}^N v_{QQ}^{N,j}(k|k-1)\lambda_j \right) b_{QI} \end{bmatrix} \quad B-26$$

$$\underline{G}_{QQ} = \begin{bmatrix} -\left( \sum_{j=1}^N v_{QI}^{i,j}(k|k-1)\lambda_j \right) b_{IQ} + \left( \sum_{j=1}^N v_{QQ}^{i,j}(k|k-1)\lambda_j \right) b_{QQ} \\ -\left( \sum_{j=1}^N v_{QI}^{N,j}(k|k-1)\lambda_j \right) b_{IQ} + \left( \sum_{j=1}^N v_{QQ}^{N,j}(k|k-1)\lambda_j \right) b_{QQ} \end{bmatrix} \quad B-27$$

4. Now calculate  $\hat{V}_{xx}(k|k) = [I - G(K)\Lambda] \hat{V}_{xx}(k|k-1)$

$$\begin{aligned} [I - G\Lambda] &= \begin{bmatrix} \underline{G}_{II} & \underline{G}_{IQ} \\ \underline{G}_{QI} & \underline{G}_{QQ} \end{bmatrix} \begin{bmatrix} \lambda_1, \dots, \lambda_N, 0, \dots, 0 \\ 0, \dots, 0, \lambda_1, \dots, \lambda_N \end{bmatrix} \\ &= [I - G\Lambda] = \begin{bmatrix} S_{II}(k) & S_{IQ}(k) \\ S_{QI}(k) & S_{QQ}(k) \end{bmatrix} \end{aligned}$$

$$\hat{V}_{xx}(k|k) = \begin{bmatrix} S_{II}(k) & S_{IQ}(k) \\ S_{QI}(k) & S_{QQ}(k) \end{bmatrix} \begin{bmatrix} \hat{V}_{II}(k|k-1) & \hat{V}_{IQ}(k|k-1) \\ \hat{V}_{QI}(k|k-1) & \hat{V}_{QQ}(k|k-1) \end{bmatrix} \quad B-28$$



$$V_{II}(k|k) = S_{II}(k)V_{II}(k|k-1) + S_{IQ}(k)V_{QI}(k|k-1)$$

$$V_{IQ}(k|k) = S_{II}(k)V_{IQ}(k|k-1) + S_{IQ}(k)V_{QQ}(k|k-1)$$

$$V_{QI}(k|k) = S_{QI}(k)V_{II}(k|k-1) + S_{QQ}(k)V_{QI}(k|k-1)$$

$$V_{QQ}(k|k) = S_{QQ}(k)V_{QQ}(k|k-1) + S_{QI}(k)V_{IQ}(k|k-1)$$

B-29

$$S_{II}(k) = \begin{bmatrix} 1 - \underline{G}_{II}(1)\lambda_1, & -\underline{G}_{II}(1)\lambda_2, & \dots & -\underline{G}_{II}(1)\lambda_N \\ -\underline{G}_{II}(2)\lambda_1, & 1 - \underline{G}_{II}(2)\lambda_2, & \dots & -\underline{G}_{II}(2)\lambda_N \\ \vdots & \vdots & \ddots & \vdots \\ -\underline{G}_{II}(N)\lambda_1, & -\underline{G}_{II}(N)\lambda_2, & \dots & 1 - \underline{G}_{II}(N)\lambda_N \end{bmatrix}$$

B-30

$$[S_{IQ}^{i,j}(k)] = -\underline{G}_{IQ}(i)\lambda_j$$

B-31

$$[S_{QI}^{i,j}(k)] = -\underline{G}_{QI}(i)\lambda_j$$

B-32

$$S_{QQ}(k) = \begin{bmatrix} 1 - \underline{G}_{QQ}(1)\lambda_1, & -\underline{G}_{QQ}(1)\lambda_2, & \dots & -\underline{G}_{QQ}(1)\lambda_N \\ -\underline{G}_{QQ}(2)\lambda_1, & 1 - \underline{G}_{QQ}(2)\lambda_2, & \dots & -\underline{G}_{QQ}(2)\lambda_N \\ \vdots & \vdots & \ddots & \vdots \\ -\underline{G}_{QQ}(N)\lambda_1, & -\underline{G}_{QQ}(N)\lambda_2, & \dots & 1 - \underline{G}_{QQ}(N)\lambda_N \end{bmatrix}$$

B-33

Summary

$$1. \quad \underline{V}_{XX}(k|k-1) = \Phi \underline{V}_{XX}(k-1|k-1) \Phi^T + \Gamma \Gamma^T$$

$$2. \quad G(k) = \underline{V}_{XX}(k|k-1) \Lambda^T B^{-1}(k)$$

$$3. \quad \underline{V}_{XX}(k|k) = [I - G(k)\Lambda] \underline{V}_{XX}(k|k-1)$$

when

$$\underline{k} = 1$$

Initialize  $\underline{V}_{XX}(0|0) = \underline{0}$ .

$$\begin{aligned}
 \text{a. } [v_{II}^{i,j}(1|0)] &= \gamma_i \gamma_j + \gamma_i' \gamma_j' \\
 [v_{IQ}^{i,j}(1|0)] &= -\gamma_i \gamma_j' + \gamma_i' \gamma_j \\
 [v_{QI}^{i,j}(1|0)] &= -\gamma_i' \gamma_j + \gamma_i \gamma_j' \\
 [v_{QQ}^{i,j}(1|0)] &= \gamma_i \gamma_j + \gamma_i' \gamma_j'
 \end{aligned}
 \quad \text{Note } \begin{aligned} v_{II}^{i,j}(1|0) &= v_{QQ}^{i,j}(1|0) \\ v_{IQ}^{i,j}(1|0) &= -v_{QI}^{i,j}(1|0) \end{aligned}$$

b.

$$\begin{aligned}
 B(1) &= \begin{bmatrix} \sum_{i=1}^N \sum_{j=1}^N \lambda_i \lambda_j (\gamma_i \gamma_j + \gamma_i' \gamma_j') & \sum_{i=1}^N \sum_{j=1}^N \lambda_i \lambda_j (-\gamma_i \gamma_j' + \gamma_i' \gamma_j) \\ \sum_{i=1}^N \sum_{j=1}^N \lambda_i \lambda_j (-\gamma_i' \gamma_j + \gamma_i \gamma_j') & \sum_{i=1}^N \sum_{j=1}^N \lambda_i \lambda_j (\gamma_i \gamma_j + \gamma_i' \gamma_j') \end{bmatrix} \\
 &= \begin{bmatrix} b & b' \\ -b' & b \end{bmatrix} \quad \text{Note } B^{-1}(1) = \frac{1}{b^2 - b'^2} \begin{bmatrix} b & -b' \\ b' & b \end{bmatrix} \\
 G_{II}(1) &= \begin{bmatrix} \left( \sum_{j=1}^N (\gamma_i \gamma_j + \gamma_i' \gamma_j') \lambda_j \right) b - \left( \sum_{j=1}^N (-\gamma_i \gamma_j' + \gamma_i' \gamma_j) \lambda_j \right) (-b') \\ \left( \sum_{j=1}^N (\gamma_N \gamma_j + \gamma_N' \gamma_j') \lambda_j \right) b - \left( \sum_{j=1}^N (-\gamma_N \gamma_j' + \gamma_N' \gamma_j) \lambda_j \right) (-b') \end{bmatrix} \frac{1}{b^2 - b'^2} \\
 G_{IQ}(1) &= \begin{bmatrix} \left( \sum_{j=1}^N (\gamma_i \gamma_j + \gamma_i' \gamma_j') \lambda_j \right) b' + \left( \sum_{j=1}^N (-\gamma_i \gamma_j' + \gamma_i' \gamma_j) \lambda_j \right) b \\ \left( \sum_{j=1}^N (\gamma_N \gamma_j + \gamma_N' \gamma_j') \lambda_j \right) b' + \left( \sum_{j=1}^N (-\gamma_N \gamma_j' + \gamma_N' \gamma_j) \lambda_j \right) b \end{bmatrix} \frac{1}{b^2 - b'^2} \\
 G_{QI}(1) &= \begin{bmatrix} \left( \sum_{j=1}^N (-\gamma_i' \gamma_j + \gamma_i \gamma_j') \lambda_j \right) b - \left( \sum_{j=1}^N (\gamma_i \gamma_j + \gamma_i' \gamma_j') \lambda_j \right) b' \\ \left( \sum_{j=1}^N (-\gamma_N' \gamma_j + \gamma_N \gamma_j') \lambda_j \right) b - \left( \sum_{j=1}^N (\gamma_i \gamma_j + \gamma_i' \gamma_j') \lambda_j \right) b' \end{bmatrix} \frac{1}{b^2 - b'^2}
 \end{aligned}$$

$$G_{QQ}(1) = \left[ \begin{array}{c} -(\sum_{j=1}^N (-\gamma_i' \gamma_j + \gamma_i \gamma_j') \lambda_j) (-b') + (\sum_{j=1}^N (\gamma_i \gamma_j + \gamma_i' \gamma_j') \lambda_j) b \\ -(\sum_{j=1}^N (-\gamma_N' \gamma_j + \gamma_N \gamma_j') \lambda_j) (-b') + (\sum_{j=1}^N (\gamma_N \gamma_j + \gamma_N' \gamma_j') \lambda_j) b \end{array} \right] \frac{1}{b^2 - b'^2}$$

Note  $G_{II}(1) = G_{QQ}(1)$        $G_{IQ}(1) = -G_{QI}(1)$

c.  $S_{II}(1) = S_{QQ}(1)$        $V_{II}(1|0) = V_{QQ}(1|0)$   
 $S_{IQ}(1) = -S_{QI}(1)$        $V_{IQ}(1|0) = -V_{QI}(1|0)$

$$V_{II}(1|1) = S_{II}(1)V_{II}(1|0) + S_{IQ}(1)V_{QI}(1|0)$$

$$V_{IQ}(1|1) = S_{II}(1)V_{IQ}(1|0) + S_{IQ}(1)V_{QQ}(1|0)$$

$$V_{QI}(1|1) = S_{QI}(1)V_{II}(1|0) + S_{QQ}(1)V_{QI}(1|0)$$

$$V_{QQ}(1|1) = S_{QQ}(1)V_{QQ}(1|0) + S_{QI}(1)V_{IQ}(1|0)$$

$$V_{II}(1|1) = V_{QQ}(1|1)$$

$$V_{IQ}(1|1) = -V_{QI}(1|1)$$

k = 2

a.  $[V_{II}^{i,j}(2|1)] = (\phi_i \phi_j + \phi_i' \phi_j') [V_{II}^{i,j}(1|1)] + (\phi_i \phi_j' - \phi_i' \phi_j) [V_{IQ}^{i,j}(1|1)]$   
 $[V_{IQ}^{i,j}(2|1)] = (-\phi_i \phi_j' + \phi_i' \phi_j) [V_{II}^{i,j}(1|1)] + (\phi_i \phi_j + \phi_i' \phi_j') [V_{IQ}^{i,j}(1|1)]$   
 $\quad - \gamma_i \gamma_j' + \gamma_i' \gamma_j$   
 $[V_{QI}^{i,j}(2|1)] = (-\phi_i' \phi_j + \phi_i \phi_j') [V_{II}^{i,j}(1|1)] - (\phi_i' \phi_j' + \phi_i \phi_j) [V_{IQ}^{i,j}(1|1)]$   
 $\quad - \gamma_i' \gamma_j' + \gamma_i \gamma_j$   
 $[V_{QQ}^{i,j}(2|1)] = (\phi_i \phi_j + \phi_i' \phi_j') [V_{II}^{i,j}(1|1)] + (\phi_i \phi_j' - \phi_i' \phi_j) [V_{IQ}^{i,j}(1|1)]$

Note  $V_{II}(2|1) = V_{QQ}(2|1)$   
 $V_{IQ}(2|1) = -V_{QI}(2|1)$

$$b. \quad B(2) = \Lambda V_{xx}(2|1) \Lambda^T$$

$$= \begin{bmatrix} b & b' \\ -b' & b \end{bmatrix}$$

$$G = \begin{bmatrix} g & g' \\ -g' & g \end{bmatrix}$$

$$c. \quad S = \begin{bmatrix} S_{II} & S_{IQ} \\ S_{QI} & S_{QQ} \end{bmatrix} \quad \begin{aligned} S_{II} &= S_{QQ} \\ S_{IQ} &= -S_{QI} \end{aligned}$$

$$V(3|3) = \begin{bmatrix} V_{II}(3|3) & V_{IQ}(3|3) \\ V_{QI}(3|3) & V_{QQ}(3|3) \end{bmatrix}$$

$$V_{II}(3|3) = V_{QQ}(3|3)$$

$$V_{IQ}(3|3) = -V_{QI}(3|3)$$

$$\underline{k = k}$$

From (15), (16), (17) and (18)

$$V_{II}(k|k-1) = V_{QQ}(k|k-1)$$

$$V_{IQ}(k|k-1) = -V_{QI}(k|k-1)$$

From (21)

$$B(k) = \begin{bmatrix} b & b' \\ -b' & b \end{bmatrix}$$

From (24), (25), (26) and (27)

$$\underline{G}_{II}(k) = \underline{G}_{QQ}(k) = \underline{g}$$

$$\underline{G}_{IQ}(k) = -\underline{G}_{QI}(k) = \underline{g}'$$

From (29)

$$V_{II}(k|k) = V_{QQ}(k|k)$$

$$V_{IQ}(k|k) = -V_{QI}(k|k)$$

$k = k+1$

Remark:

When the initialization  $V_{II}(1|0) = V_{QQ}(1|0)$  and  $V_{IQ}(1|0) = -V_{QI}(1|0)$  is given it follows for arbitrary  $k$  that the diagonal elements of the partitioned matrices are identical and the off diagonal elements are identical but different in sign for  $V_{\tilde{X}\tilde{X}}(k|k-1)$ ,  $B(k)$ ,  $G(k)$  and  $V_{\tilde{X}\tilde{X}}(k|k)$ . Thus are the initial results proved.

## REFERENCES

1. "Low Cost Anti-Jam Digital Data-Links Techniques Investigation," Final Report for Phase I - Contract F 33615-75-C-1011, AD-A048181, Technical Report, AFAL-TR-77-104, Air Force Avionics Laboratory, Wright-Patterson AFB, Ohio, 1 June 1977.
2. Painter, J. H. and Gupta, S. C., "Recursive Ideal Observer Detection of Known M-ary Signals in Multiplicative and Additive Gaussian Noise," IEEE Trans. on Comm., Vol. COM-21, pp. 948-953, August 1973.
3. Painter, J. H. and Wilson, L. R., "Simulation Results for the Decision-directed MAP Receiver for M-ary Signals in Multiplicative and Additive Gaussian Noise," IEEE Trans. on Comm., Vol. COM-22, pp. 649-660, May 1974.
4. Sage, A. P. and Melsa, J. L., Estimation Theory With Applications to Communications and Control, pp. 303-321, McGraw-Hill Book Co., 1971.
5. Van Trees, H. L., Detection, Estimation and Modulation Theory, Part I, pp. 91-96, John Wiley and Sons, Inc., 1968.
6. Schwartz, S. C., "The Estimator-Correlator for Discrete-Time Problems," IEEE Trans. on Info. Theory, Vol. IT-23, No. 1, pp. 93-100, January 1977.
7. Blachman, N. M., Noise and its Effect on Communication, pp. 127, 140, and 190, McGraw-Hill Book Co., 1966.
8. Wozencraft, J. M. and Jacobs, I. M., Principles of Communication Engineering, p. 527, John Wiley and Sons, Inc., 1965.
9. Doelz, M. L., Heald, E. T., and Martin, D. L., "Binary Data Transmission Techniques for Linear Systems," Proc. of the IRE, Vol. 45, No. 5, pp. 656-661, May, 1957.
10. Becker, H. D. and Lawton, J. G., "Theoretical Comparison of Binary Data Transmission Systems," Report #CA-1172-S-1, Contract AF 30(602)-1702, Cornell Aeronautical Laboratory, Inc., pp. 32-40, May 1958.
11. Lindsey, W. C. and Simon, M. K., Telecommunication Systems Engineering, pp. 177-252, Prentice-Hall, 1973.
12. Painter, J. H. and Jones, S. K., "Results on Discrete-Time, Decision-Directed Integrated Detection, Estimation, and Identification," IEEE Trans. on Comm., Vol. COM-25, No. 7, pp. 715-723, July 1977.

13. Spilker, J. J., Jr., Digital Communications by Satellite, pp. 331-335, Prentice-Hall, Inc., 1977.
14. Papoulis, A., Probability, Random Variables, and Stochastic Processes, p. 373, McGraw-Hill Inc., 1965.
15. Painter, J. H., "Applications of Analytic Function Theory to Analysis of Single-Sideband Angle-Modulated Systems, "NASA Technical Note TN D-5446, Wash. D.C., pp. 34-36, September 1969.
16. Yoon, C. J., System Identification for the Stationary Imphase-Quadrature Process, Ph.D. Dissertation, Department of Electrical Engineering, Texas A&M University, 1978.
17. Astrom, K. J., "Numerical Identification of Linear Dynamic Systems From Normal Operating Records," Proceedings of the IFAC Conference on Self-Adaptive Control Systems, 1965.
18. Gupta, N. K. and Mehra, R. K., "Computational Aspects of Maximum Likelihood Estimation and Reduction in Sensitivity Function Calculations," IEEE Trans. on Auto. Control, Vol. AC-19, No. 6, December 1974.
19. Stepner, D. E. and Mehra, R. K., "Maximum Likelihood Identification and Optimal Input Design for Identifying Aircraft Stability and Control Derivatives," NASA Contractor Report, CR-2200, NAS1-10700, Wash. D.C., March 1973.
20. Becker, H. D. and Lawton, J. G., "Theoretical Comparison of Binary Data Transmission Systems," Report #CA-1172-S-1 (Revised), Cornell Aeronautical Laboratory, Inc., RADC-TR-58-91, AD-148803, p. 23, March 1961.